A Study of Sediment Transport in Euphrates River Upstream AL- Ramadi Barrage

A Thesis
Submitted to the College of Engineering of The University of Al-Anbar in Partial Fulfillment of the Requirements for The Degree of Master of Science in Civil Engineering

By
Sadiq Eleiwi Suleiman Al-Fahdawi

(B.Sc., Civil Engineering, 1993)

January-2002 **ذي القعدة – 1422**

DEDICATED TO :

My Parents , Brothers , Sisters and My Wives in appreciation of their patience , Encouragement and help

Sadiq

بِسْمِ ٱللَّهِ ٱلرَّحْمَٰنِ ٱلرَّحِيمِ

((أَنزَلَ مِنَ السَّمَاءِ مَاءً فَسَالَتْ أَوْدِيَةٌ بِقَدَرِهَا
فَاحْتَمَلَ السَّيْلُ زَبَدًا رَابِيًا وَمِمَّا يُوقِدُونَ عَلَيْهِ فِي
النَّارِ ابْتِغَاءَ حِلْيَةٍ أَوْ مَتَاعٍ زَبَدٌ مِثْلُهُ كَذَٰلِكَ
يَضْرِبُ اللَّهُ الْحَقَّ وَالْبَاطِلَ فَأَمَّا الزَّبَدُ فَيَذْهَبُ جُفَاءً
وَأَمَّا مَا يَنفَعُ النَّاسَ فَيَمْكُثُ فِي الْأَرْضِ كَذَٰلِكَ
يَضْرِبُ اللَّهُ الْأَمْثَالَ))

صدق الله العظيم

سورة الرعد (الآية:117)

ACKNOWLEDGEMENT

The author wishes to express his sincere thanks and gratitude to ***DR. ABDUL-KAREEM H.GHAILAN*** *who gave great and continuous efforts and encouragement which helped me to achieve this research.*

Gratitude is due to the faculty members of the Civil Engineering Department for their support and continuous encouragement special thanks to my friends ***ABDUL-KAREEM EL-JAF, TARIQ, MOAYD, THAMER*** *and* ***WASEN*** *who helped me during this research.*

A special word of thanks is also due to staff of Al-Ramadi barrage office.

Finally my thanks are due to those who helped me in away or another throughout the writing of this research .

Table of content (CONt.)

Table of content (CONt.)

LIST OF FIGURES

LIST OF TABLES

LIST OF SYMBOLS

Symbols	Description
$\mathbf{A_e}$	The domain of subregion (element).
$\boldsymbol{B}$	Local width of the channel.
d	Mean practical size of sediment.
$\mathbf{d_{50}}$	The sediment size for which 50% is finer.
F	Coefficient of friction slope.
f_0	Function described the secondary flow distribution.
g	Acceleration due to gravity.
$\boldsymbol{H}$	Surface water level.
$\boldsymbol{h}$	Depth of water.
$\boldsymbol{M_s}$	Static friction factor.
$\boldsymbol{M_K}$	Kinetic friction factor.
$\boldsymbol{N_o}$	Factor (usually =7).
$\boldsymbol{n}$	Manning Roughness Coefficient
N	Linear interpolation (shape) function.
$\mathbf{q_{Bs}}$	Longitudinal volumetric bed load per unit width.
$\mathbf{q}_{Bn}$	Lateral volumetric bed load per unit width.
R	Radius of curvature of the section.
r	Local radius of curvature.
S	Longitudinal axis.
$\boldsymbol{t}$	Time.
u	Velocity in x-direction.
U*	Shear velocity.
$\boldsymbol{V}$	Velocity in y-direction.
$\boldsymbol{x}$	Cartesian coordinate in x-direction.
$\boldsymbol{y}$	Cartesian coordinate in y-direction.
z	Channel bed elevation.
Є	Eddy-viscosity coefficient
$\mathbf{n_o}$	Transverse axis.
λ	The bed porosity.

LIST OF SYMBOLS (CONT.)

Symbols	Description
ρ	Density of sediment.
θ	Direction angle of flow nears the bed.
$\bar{\tau_*}$	Grain shear stress.
τ_{*c}	Critical shear stress.
$\dot{\tau}_*$	Bed shear stress.
l_x	Direction cosine of outward normal vector in X-direction.
l_y	Direction cosine of outward normal vector in Y-direction.
Ω	The domain of subregion (element).
ω	Angular velocity (frequency).
SF	Shape function.
Bx	Shape function derivative with respect to X.
By	Shape function derivative with respect to y.
J	Jacobian matrix.
NQ	No. of Gauss point.
J_x	Element length in X-direction
J_y	Element length in Y-direction
$\bar{v}$	Secondary flow velocity

A Study of Sediment Transport in Euphrates River Upstream AL- Ramadi Barrage

By
Sadiq Eleiwi suleiman AL-Fahdawi
B.Sc., Civil Engineering
College of Engineering
University of AL-Anbar
2002

Supervisor: Ass. Prof. Dr. Abdul-Kerim H. Ghailan

ABSTRACT

Sediment transport induced by flow of alluvial rivers has received increasing attention in recent years, because it has manifested effects on engineering problems. Thus, two models were developed to predict the river behaviour under given flow conditions.

The first model is a two dimensional depth-averaged hydrodynamic model based on the conservation of mass and momentum equations to estimate the velocity field and water depths. The second model is a morphological model based on the dynamic equation of sediment continuity to predict the river bed variations in two dimensions.

The finite element technique was applied to formulate the two models incorporating with weighted residual method. Iterative scheme with a modified Gaussian elimination was used for solving the nonlinear differential equations of hydrodynamic model, whereas the morphological model is linear and it has no need to an iterative fashion.

The two-dimensional hydrodynamic model was applied to an idealized case and verified by comparison with analytical solution. The application gave a good agreement between calculated and analytical

result. Calibration and verification are achieved in study reach using observed data (stage) in selected node.

The two models were coupled together and applied to Euphrates River in AL-Ramadi City. The result of coupled models revealed reasonable outcomes and the variation of the bed elevation reflected the expected tendency in bend region of river when the scour happened at the outer bank and deposition at inner bank.

CHAPTER ONE

Introduction

CHAPTER ONE

Introduction

1.1General

Water flowing in natural river or artificial Channel often has ability to scour or deposit the materials that compose the bed or banks. The scour or deposition process and its control have for along time been one of the most challenging problems confronting the hydraulic engineer.

Deformation in bed morphology of the river, which continuously changes with time, is affected by water discharges and velocities, sediment discharges, and composition of bed and banks. The materials movement by water flow carried as a bed load and suspends load. The estimation of bed loads that is the major factor effects on bed topography of the river.

The neglecting of sediment movement may sometime be acceptable over short periods of flow. But in any long–time evaluation of river behaviour, the deformability of the bed morphology in alluvial river must be considered in spite of the natural condition that rivers rarely reach a state of equilibrium even over short reaches (Petersen 1986).

Alluvial rivers tend to meander or braid. The origin of this tendency has explained successfully in terms of stability analysis, assuming unerodible side banks with a straight alignment. Once rivers begin to meander, alternate area of local scour and deposition are generated. Therefore, flow and bed topography in meandering rivers are important subjects to be investigated from a practical point of view in relation to bank protection, navigation, water intake, etc. (Ikeda 1986).

There are two methods to simulate flow and bed topography of rivers using physical model and using mathematical model.

The physical model is physically representing the system. The verification of this model needs a mathematical relationship between prototype and model dimensions of basic parameters often called the similarity criteria. However, the representation of the situation cannot achieve the same degree of accurate representation gained by the mathematical expressions. Moreover, physical models are always a problem-specific models. That is to say, models of particular problems cannot be employed to investigate different problems, even if both of the problems are governed by the same mathematical expressions (Ghailan, 1982).

Physical model suffers from scale effect (distortion) and the large cost of building of the model, and the difficulties associated with measurement tools needed.

Mathematical models give quicker results with cheapest cost. The increase in computer speed and memory made mathematical models preferable to the other ways.

The present study covers the two dimensional flow and bed topography of Euphrates river reaches between Palestine Bridge on highway road (upstream end) to Ramadi Barrage (downstream end) about (2.8 KM) long. The modelling technique employed in this work is the finite element technique using galerkin weighted residual method with linear triangular element.

In chapter two of this study some of earlier studies are reviewed and the basic equations of the mathematical model derived from the Navier-Stockes equations and dynamic sediment continuity equation by using Galerkin weighted residual approach in finite element. The solution approach is effected by the initial conditions and boundary conditions of river reach under study.

In chapter three the matrix form of Navier-Stockes equations and dynamic sediment continuity equation are descriped. The non-linear partial deffirential equation of hydrodynamic model is solved by using the Newton-Raphson

iteration and the modified Gaussian elimination technique. The programming of mathematical models are expressed as a flowcharts in this chapter.

In chapter four a numerical solution of hydrodynamic model is applied for idealized channel to test the model by comparing with exact solution. Accuracy and stability of numerical model are effected by model parameters such as manning coefficient of friction and model weighting factor, therefore, the calibration and verification of numerical model is an important step made by comparing the calculated result of the hydrodynamic model and morphological model application to Euphrates river reach under study with prototype observed data.

Finally, chapter five sets fourth the conclusions and recommendations.

1.2 Objectives of the study

The main objectives of this study are to achieve the following:

1- To develop a two-dimensional depth averaged hydrodynamic mathematical model to estimate the variations of velocities and water depths.
2- To develop a two dimensional morphological model to simulate the changes in bed river topography.
3- To demonstrate the application of the hydrodynamic and morphological models to Euphrates river in Ramadi city studying the variation of bed profile of river reach in study area.

CHAPTER TWO

Literature Review

Chapter two

Literature Review

It is important in river management to be able to predict water and surface elevation, scour and deposit in alluvial channels under given flow conditions. Mathematical and physical models can be used in designing or planning for improvement of river channels and hydraulic structures. Some of earlier models will be reviewed in this chapter.

2.1 Description of the Euphrates River

Euphrates River is the one of two rivers that fed Iraq. It rises in the mountains between the Black Sea and Lake Van in Turkey. The river is traverse through Syria from Jerablus to reaches Deir El-Zour at (410 km) down stream Jerablus.

The River enters Iraq in Al-Qaim town and from Al-Qaim town to Hit the river length is (320 km). Ramadi Barrage is situated at about (60 km) down stream Hit, the Barrage had been constructed and put into operation since 1956. It is composed of 24 gates each 6 meters wide, navigation locks 6 meter wide and fishes ladder.

Just upstream from Ramadi Barrage the Warrar intake channel and regulator are situated. The Warrar regulator which is composed of (24) gates each 6 meters wide. (Kashif Al-Ghitaa 1959)

2.2 General review

Engelund (1974) presented an analytical work for mutual interaction between flow and bed topography. The stable bed topography was calculated by integrating numerically the equation of continuity of bed material transport as

bed load. The secondary flow, which is known to be quite influential in defining the bed topography, was taken into account implicitly via a formula, which expresses the later bed load rate. Due to the secondary flow, the direction of shear stress may, however, deviate from the direction of the mean flow by angle δ. Because of the gravity, a migrating sediment particle will tend to move downhill along the transverse slope, which makes an angle α_o with the horizontal plane. The transverse component of the bed load $\{q_{Bn}\}$ to the longitudinal component of bed load, $\{q_{Bs}\}$, is expressed as:

$$\frac{q_{Bn}}{q_{Bs}} = \frac{v}{u} - 7\frac{y}{r} + \frac{\tan\alpha_o}{\tan\phi} \qquad \text{.....(2.1)}$$

Where:

u, v : Velocity components in the longitudinal and transverse direction.
y : Local depth.
r :Local radius of curvature
ϕ :Dynamic friction angle, and

From above equation the three reasons for the deviation of sediment particle from the longitudinal direction are:

1.Convection due to transverse velocity component.
2.The secondary flow,and
3.The transverse slope of the bed ($\frac{\partial y}{\partial n_o}$; n_o=transverse direction).

The agreement between experimental data and predicted result was not attained because the bed elevation in the flume always covered by ripples, which must be smoothed out by hand before measuring the elevation when this is done, uncertainty of the measured elevation was expected.

Su and Wang (1980) modeled river flow using a two-dimensional depth-averaging model. By integrating the properties vertically from the bed to free surface, the averaged properties become a function of two spatial coordinates in plane.

They assumed that:

1. The bed is rigid and no bed variation occur with time
2. Neither slip nor seepage are allowed at channel boundaries
3. The wind stress on the free surface is neglected, which implies that the maximum velocity occurs at free surface.

The coefficient of eddy-viscosity,ε ,is related to the mean flow properties with an adjustable eddy-viscosity parameter, E

$$\varepsilon = Eh\sqrt{u^2 + v^2} \qquad \text{...(2.2)}$$

where

h =depht of water

u,v = the velocity component in x and y direction respectively.

An admissible value for E equal to 0.1-0.25 was proposed for the upper Mississippi river without generating a considerable difference in flow field. Typical finite element system was used to discretize the continuos domain with isoparametric interpolation functions to relate the properties at any point within an element to those at nodal points of the same element.

The Galerkin weighted residual method was applied and the quadrilateral with four nodes at the corners was chosen. The finite difference operator using third order Taylor expansion replaced the time derivative. The boundary conditions on solid walls were imposed to eliminate the equations at the boundaries where the conditions is known.

Howard and change (1985) developed a mathematical model for water and sediment routing through a curved channel with non-erodible banks to simulate time and spatial variation in water level, sediment transport, and bed topography as the spiral motion or transverse circulation in which the space domain was represented by discretizing the cross section. The time domain was represented by discrete time step and were computed by an iterative procedure.

The model used analytical equation governing the flow and sediment processes has the following four major interactive components:

1- water routing.

2- evaluation of changing flow curvature.

3- computation of sediment transport; and

4- prediction of streambed profile change.

In the prediction of streambed profile changes, aggradation and degradation was tide in with the effect of transverse flow under the changing channel curvature. Changes in streambed profile at each time step due to longitudinal and transverse variation in sediment load. Simulated, aggradation and degradation were tide in with the effect of transverse flow under the changing channel curvature and which were computed using the continuity equation for sediment movement in the longitudinal, then, the continuity equation for sediment movement was expressed as:

$$\frac{\partial z}{\partial t} + \frac{1}{1-\lambda}.\frac{1}{r}.(rq_s') = o \quad \text{..... (2.3)}$$

Where:

λ = Porosity.

r = Radius of curvature.

q_s' = Transverse bed material load per unit channel length.

Simulating flow and bed profile changes in the San-Lorenzo River tested the model. Simulated result showed that increasing transverse bed sloped and scour near the concave bank in the down stream direction consistent with the growth in flow curvature (i.e.) a gradual decrease in transverse bed slope and scour depth with the decrease in flow curvature.

Chaudhry (1987) introduced a beam and warming implicit finite difference schemes for hyperbolic system in conservation-law form to integrate

the equations. It describes the two-dimensional unsteady free-surface flows if both sub- critical and supercritical flows are presented simultaneously (in different parts of channel) or in sequence (at the same location at different time).

The linearization of the nonlinear terms of governing equations carried out at the unknown time level (implicit linearization). These schemes were second-order accurate in time and can be made second or fourth order accurate in space and they were split-flux schemes (implicit-split-flux factoring).

Then a flux splitting was used to incorporate in the approximate –factored algorithm using an alternating direction implicit (ADI) procedure

They assumed that:

1. hydrostatic pressure distribution
2. small channel bottom slopes
3. uniform velocity distribution in vertical direction and
4. slope of friction in x-and y- directions are determined from the steady-state Manning's formula was written as

$$Sf_x = \frac{n^2 u}{h^{4/3}}\sqrt{u^2+v^2} \quad ; \quad sf_y = \frac{n^2 v}{h^{4/3}}\sqrt{u^2+v^2} \qquad \text{.....(2.4)}$$

Where:

Sf_x, sf_y : slope of friction in x-and y- directions respectively.

n : Manning's roughness coefficient.

The boundary conditions for the solid wall is the normal velocity is zero, i.e. no flow through the wall and the longitudinal velocity and the depth were assumed as an values are equal to those near the wall.

Shimizu and Itakura (1989), applied a two dimensional model to calculate the bed variation in alluvial channels. The depth averaged flow field is obtained from a steady state two-dimensional shallow water flow model, and the bed variation is calculated by a continuity equation for bed load transport. The equations are solved using a finite difference method on a computational grid.

The equations for flow are computed implicitly, while the continuity equation for sediment transport is computed explicitly. A steady state solution is obtained through an iteration process.

They assumed that channel width and radius of curvature large compared with flow depth thus, the vertical component of velocity is negligible and the pressure is hydrostatic.

Continuity of the flow rate is checked at each point on the computational grid. The numerical calculations are performed for zigzag channel to investigate the characteristics of migration of alternating bars.

In alluvial rivers, the interactions between hydraulic conditions and plan's geometry result in different kinds of bed configurations that are highly dependent on formation, cessation, and migration of bars. The two dimensional model demonstrates that it can predict these phenomena for given hydraulic and geometric conditions, which may be useful in practical engineering work.

Jin and Kranenburg (1993) presented a quasi three-dimensional numerical model of shallow water circulation (an intersection between the depth-averaged flow and vertical distribution of horizontal velocities). This model composed of two coupled models has been developed for computing the circulation in shallow waters.

In one of the models, the depth-averaged shallow water equations are solved by using an alternating direction implicit (ADI) algorithm (Booj, 1989). In the second model, the vertical distribution of horizontal velocities is determined using the water surface gradient computed in the first model. In this model, a non slip bottom boundary condition with a roughness height is used and simple parabolic distribution is used for the vertical eddy viscosity (i.e.) at bottom the velocity components vanish and algorithmic velocity distribution (i.e.) constant stress near the bottom.

Computations using one-dimensional model showed that for the flow case considered and generalized Crank-Nicolson scheme to solve the parabolic partial-differential equations with a large time step.

In this model, firstly, the depth-averaged flow and the free surface level are computed in the first model in a two-dimensional horizontal grids based on continuity and momentum equation for the depth averaged flow. The non-linear terms are treated explicitly in the numerical scheme. Then in second model, continuity and equations for shallow water flow are solved to compute the vertical distribution of velocities and the bottom shear stress separately for each vertical in that grid.

Majeed (1994) developed a hydrodynamic and morphological models, the first model developed by using an alternating direction implicit (ADI) finite difference technique to simulate the velocity field and water level, while the second using the macCormack scheme, it consists of a predictor and a corrector steps. In the predictor part, forward finite difference approximation are used for approximating the spatial partial differential terms. In the corrector step, the spatial partial differential terms are approximated by the backward finite differences, but using the predicted valuues. He applied this technique to simulate the bed levels in Tigris River in Baghdad city.

Abed (1998) used Galerkin's weighted residual finite element method to formulated Saint-Vennaut equations for Tigris river within Baghdad city for sixty-six kilometers reach.

Khalaf (1999) constructed three models to predict the river behaviour under certain conditions. The first model was a two dimensional depth-averaged hydrodynamic model to compute the velocity field and water depth, the second one was transport-dispersion model to distribute the suspended sediment concentrations, while the third one was a morphological model to simulate the river bed variation in two dimensions.

A finite element technique was applied to formulate the three models incorporation with the weighted residual method. Iterative Newton-Rhaphson scheme with a modified Gaussian elimination was used for solving the non-linear differential equations of first model, where as the second and the third model are linear and they have no need to an iterative fashion.

Finally, the three models were coupled together and applied for Tigris river within Baghdad city.

AL-Ani (2001) using Galerkin finite element method to develop two models to predict river behaviour under given flow condition. The first model is a two dimensional depth-averaged hydrodynamic model and the second one is a morphological model.

The two models were coupled together and applied for Euphrates River upstream Falluja regulator to study morphological changes at different flow conditions.

2.3 Study Program

In the present study the hydrodynamic and morphological models are developed and applied to the Euphrates River upstream Ramadi Barrage. The purpose is to investigate the morphological changes in this region.

The mathematical model of the hydrodynamic flow composed of three governing equations, they are Navier-Stockes equations, which are continuity equation and momentum equation in two-dimensional form as following:

$$\frac{\partial h}{\partial t}+\frac{\partial (uh)}{\partial x}+\frac{\partial (vh)}{\partial y}=0 \quad \text{……..…..(2.5)}$$

$$\frac{\partial U}{\partial t}+u\frac{\partial u}{\partial x}+V\frac{\partial u}{\partial y}+g\frac{\partial H}{\partial x}+Fu-\mathrm{E}\left[\frac{\partial^2 u}{\partial x^2}+\frac{\partial^2 u}{\partial y^2}\right]=0 \quad \text{……..…..(2.6)}$$

$$\frac{\partial V}{\partial t}+u\frac{\partial V}{\partial x}+V\frac{\partial V}{\partial y}+g\frac{\partial H}{\partial x}+FV-\mathrm{E}\left[\frac{\partial^2 V}{\partial x^2}+\frac{\partial^2 V}{\partial y^2}\right]=0 \quad \text{……....(2.7)}$$

Where

u,v= the depth-averaged velocity component in x and y direction respectively .

h= depth of flow = H-Z

H= surface water level.

Z= channel bed level

x,y= Cartesian coordinates.

t= time.

E = Eddy-Viscosity calculated by: - (Shimizu and I Takura, 1989)

E= 0.1666 KU^* h ……...……(2.8)

In which- :

K=VonKarman constant = 0.4

U*=shear velocity =n$\sqrt{(u^2+V^2)}./h^{1/6}$

g=acceleration of gravity.

n= Manning roughness coefficient.

F= coefficient of friction slopes and is calculated from :

$$F=\frac{n^2}{h^{4/3}}.g.\sqrt{U^2+V^2} \qquad \text{……(2.9)}$$

The basic assumptions employed in the derivation of two-dimensional depth-averaged model are:

1. The pressure distribution in vertical direction is hydrostatics, i.e., vertical acceleration is small enough to be neglected compared with the gravitational acceleration.

2. The channel bottom slope is small .

3. The channel reach isn't sufficiently straight or uniform, therefore, a two-dimensional model is to be considered.

4. The depth is small compared with width in to satisfy the shallow water flows that are prominently two-dimensional.

5.The friction losses can be accounted by using the Manning formulas for steady state.

6. The flow is mainly controlled by friction. I.e. bottom shear stress is dominant while the wind stress and geostropic effects are neglected.

7. The roughness is assumed to remain constant with time and distance.

8. Average values are sufficient to describe the properties that vary over the depth of flow.

9. The transfer velocities caused by secondary flow are computed.

10.Meyer-Peter and Muller type formula is used to compute the local sediment transport.

The mathematical model of morphological form composed of one governing equation. It is the sediment continuity equation which is written in a curvilinear coordinate system. The governing equation is (Shimizu and Itakura, 1989):

$$\frac{\partial Z}{\partial t}+\frac{1}{1-\lambda}\left[\frac{\partial q_{Bs}}{\partial s}+\frac{1}{r}.\frac{\partial\left(r.q_{Bs}\right)}{\partial n_o}\right]=0 \quad \text{.....(2.10)}$$

Where: -

q_{Bs}= longitudinal volumetric bed load per unit width

q_{Bn}= lateral volumetric bed load per unit length

t = time.

r = local radius of curvature at (s,n_o), can be put in term of:

$r=R+n_o$

R= average radius of curvature

n_o= varies from (B/2) at the left bank to (-B/2) at the right bank along the local width of river, B.

λ = porosity of bed material can be written as (Mahmood et al.,1975):

$$\lambda = 0.245 + \frac{0.0864}{d^{0.12}} \quad \text{.....(2.11)}$$

In which (d) is a mean particle size of sediment.

Evaluation of s- and n_o- components of volume rate of bed – load transport per unit width (q_{BS} and q_{Bn}) yield the following Mayer-peter-Muller formula, which can be written as:

$$q_{BS} = 8\sqrt{\frac{\rho s}{\rho - 1} g d^3}\left(\tau'_* - \tau_{*c}\right)^{3/2} \quad \text{.....(2.12)}$$

$$q_{Bn} = q_{BS}\left[tan\theta - \sqrt{\frac{\tau_{*c}}{M_s M_K \tau_*}}\frac{\partial Z}{\partial n_o}\right] \quad \text{.....(2.13)}$$

Where:

ρ_s = specific density of sediment.

τ'_* =Grain shear stress.

τ_{*c} = Critical shear stress can be taken as a constant value of (0.047).

τ_* = Bed shear stress $= \frac{n^2}{h^{2/6}}\sqrt{v^2 + u^2}\frac{1}{d_{so}}\frac{\rho - 1}{\rho_s}$ .....(2.14)

M_s = static friction factor (1.0).

M_k = kinetic friction factor of sediment particle on the bed (0.45).

θ = direction angle of flow velocity near the bed

$\frac{\partial Z}{\partial n}$ = The direction of the flow near the bed

$$\tan\theta = \frac{\bar{v} + \bar{\bar{v}}}{\bar{u}} \quad \text{.....(2.15)}$$

in which $\bar{v}$,$\bar{u}$ is(s,n_o) component of velocity near the bed and are related to the depth-averaged velocity by secondary flow velocity which can be expressed as :

$$v^{=} = -N_o \frac{h}{r} f_o\left(\frac{n_o}{B}\right) \quad \text{.....(2.16)}$$

In above equation, the value of (N_o) will be adopted by (7) as proposed by Engelund (1974).

The (f_o) is a function of (n_o) that describes the distribution of secondary flow near the bed where the (n) is the distance from left bank and (B) is the local width of the channel and (r) is the radius of curvature.

Kikkawa et. al. (1976) has investigate of (f_o) as:

$$f_0\left(\frac{n_o}{B}\right) = -100\left(\frac{n_o}{B}\right)^2 + 20\left(\frac{n_o}{B}\right) \qquad for\left(0 \le \frac{n_o}{B} \le 0.1\right)$$

$$f_0\left(\frac{n_o}{B}\right) = 1 \qquad for\left(0.1 \le \frac{n_o}{B} \le 0.9\right)$$

$$f_0\left(\frac{n_o}{B}\right) = -100\left(1-\frac{n_o}{B}\right)^2 + 20\left(1-\frac{n_o}{B}\right) \qquad for\left(0.9 \le \frac{n_o}{B} \le 1\right) \quad (2.17)$$

Application of above equation and N_o=7 leads to solve the following equation:

$$tan\Theta = \frac{V - \left[N_o \frac{hu}{r} fo\left(\frac{n_o}{B}\right)\right]}{u} \quad \text{.....(2.18)}$$

The finite element model of hydrodynamic flow can be derivated by applying the standard galerkin weighted residual method using green's theorm. Global form representing finite element model of continuity and momentum equations in x- and y- directions, equations (2.5), (2.6) and (2.7) is as following:

$$[A]\{\Psi^{\circ}\}+[C]\{\Psi\}=\{P\} \quad \text{.....(2.19)}$$

Where:

[A] =The diagonal mass matrix.

[C] =The system matrix or non-linear connective matrix.

$\{\Psi^{\circ}\}$=The time derivative of the nodal values.

$\{\Psi\}$=The vector of nodal values of h,u and v respectively; and

{P}=Force vector or prescribed values vector.

The finite element model of morphological form can be derived applying the Galerkin weighted residual approach for equation (2.10) and similary to the hydrodynamic model, the element equation must be assembled over the whole area. The final global matrix equation for dynamic sediment continuity is:

$$[B][Z^{\circ}]+[D][Z]=[F] \quad \text{.....(2.20)}$$

Where:-

[B]=The square mass matrix

$[Z^{\circ}]$=The column vector of the time derivative of the nodal values.

[D]=The system matrix.

[Z]=The column vector of nodal values.

[F]=the column vector of forces.

Discretization of time derivatives in the above two models are achieved using the following forward finite difference scheme (Abed, 1998 and AL-Eoubaidy, 1999):

$$\frac{d\Psi}{dt}=\frac{1}{\Delta t}\left[\Psi^{t+\Delta t}-\Psi^{t}\right] \quad \text{.....(2.21)}$$

t : elapsed time

Δt : time step

CHAPTER THREE

Finite Element Programming

Chapter Three

Finite Element Programming

The finite element programme was developed to treat a hydrodynamic model in two dimensions with morphological Model. The programme was built to stimulate the hydrodynamic behavior with time for any channel or river and it has also a facility as a prediction tool to the morphological changes of river. It is useful to employ a natural coordinate system (local system) in finite element programming than use Cartesian (global) coordinate system (see appendix C) so we will use local system in our program.

This chapter will give a description for steps of model derivation and programming operations.

3.1 Finite Element Hydrodynamic and Morphological Models

By applying the standard Galerkin weighted residual finite element method for equation (2.5), (2.6) and (2.7) using Green's theorem the equations can be written as (see appendix A):

$$\iint \mathrm{N}\mathrm{N}^{\mathrm{t}} \frac{\partial \mathrm{h}}{\partial \mathrm{t}} + \left[-\bar{\mathrm{u}} \iint \frac{\partial \mathrm{N}}{\partial \mathrm{x}} \mathrm{N}^{\mathrm{t}} \mathrm{dxdy} - \bar{\mathrm{V}} \iint \frac{\partial \mathrm{N}}{\partial \mathrm{y}} \mathrm{N}^{\mathrm{t}} \mathrm{dxdy} \right] \mathrm{h}$$

$$\left[-\bar{\mathrm{h}} \iint \frac{\partial \mathrm{N}}{\partial \mathrm{x}} \mathrm{N}^{\mathrm{t}} \mathrm{dxdy} \right] \mathrm{u} + \left[-\bar{\mathrm{h}} \iint \frac{\partial \mathrm{N}}{\partial \mathrm{x}} \mathrm{N}^{\mathrm{t}} \mathrm{dxdy} \right] \mathrm{V} +$$

$$\left[\bar{\mathrm{u}} \int \mathrm{N}\mathrm{N}^{\mathrm{t}} \mathrm{dy} + \bar{\mathrm{V}} \int \mathrm{N}\mathrm{N}^{\mathrm{t}} \mathrm{dx} \right] \mathrm{h} + \left[\bar{\mathrm{h}} \int \mathrm{N}\mathrm{N}^{\mathrm{t}} \mathrm{dy} \right] \mathrm{u} +$$

$$+ \left[\bar{h} \int N N^{t} dx \right] V = 0 \qquad \text{.....(3.1)}$$

$$\iint N N^{t} \frac{\partial u}{\partial t} + \left[-\bar{u} \iint \frac{\partial N}{\partial x} N^{t} dxdy - \bar{V} \iint \frac{\partial N}{\partial y} N^{t} dxdy + \bar{F} \iint N N^{t} dxdy + \right.$$

$$\left. \mathrm{E} \iint \left(\frac{\partial \mathrm{N}}{\partial \mathrm{x}} \right) \left(\frac{\partial \mathrm{N}^{\mathrm{t}}}{\partial \mathrm{y}} \right) + \left(\frac{\partial \mathrm{N}}{\partial \mathrm{y}} \frac{\partial \mathrm{N}^{\mathrm{t}}}{\partial \mathrm{y}} \right) \mathrm{dxdy} \right] \mathrm{u} + \left[-\mathrm{g} \iint \frac{\partial \mathrm{N}}{\partial \mathrm{x}} \mathrm{N}^{\mathrm{t}} \mathrm{dxdy} \right] \mathrm{H} + \mathrm{g} \int \mathrm{N}\mathrm{N}^{\mathrm{t}} \mathrm{dy} \mathrm{H} +$$

$$\left[\bar{u}\int NN^t dy + \bar{V}\int NN^t dx - E\int N^t\left[(\frac{\partial N}{\partial x})\ell_x + (\frac{\partial N}{\partial y})\ell_y\right]ds\right]u = 0 \quad \ldots(3.2)$$

$$\iint \mathrm{NN^t}\frac{\partial \mathrm{V}}{\partial \mathrm{t}} + \left[-\bar{\mathrm{u}}\iint \frac{\partial \mathrm{N}}{\partial \mathrm{x}}\mathrm{N^t dxdy} - \bar{\mathrm{V}}\iint \frac{\partial \mathrm{N}}{\partial \mathrm{y}}\mathrm{N^t dxdy} + \bar{\mathrm{F}}\iint \mathrm{NN^t dxdy} +\right.$$

$$\left. E\iint(\frac{\partial N}{\partial x}\cdot\frac{\partial N^t}{\partial x}) + (\frac{\partial N}{\partial y}\frac{\partial N^t}{\partial y})dxdy\right]V + \left[\bar{u}\int NN^t dy + \bar{V}\int NN^t dx - E\int N^t\left[(\frac{\partial N}{\partial x})\ell_x + (\frac{\partial N}{\partial y})\ell_y\right]ds\right]v$$

$$\iint g\frac{\partial N}{\partial x}N^t dxdyH - g\int NN^t dxH = \ldots\ldots\ldots\ldots\ldots\ldots\ldots\ldots\ldots\ldots\ldots\ldots\ldots\ldots(3.3)$$

Where:

N and N^t = the column and row matrix of the shape function respectively

$\bar{\aleph}$ $\underline{n}$,And $\bar{\nu}$: the average known value of the element depth and velocities evaluated from pervious solution step or initial values (Sharhan, 1986).

$\left\{\frac{\partial h}{\partial t}\right\}$,$\left\{\frac{\partial u}{\partial t}\right\}$ and $\left\{\frac{\partial v}{\partial t}\right\}$ = The column vector of the nodal depth and velocities derivative with time respectively.

$\left\{\frac{\partial N}{\partial x}\right\}$ And $\left\{\frac{\partial N}{\partial y}\right\}$ = The row vector of the derivative of a shape function with respect to the coordinates x and y respectively

h, u and v : The column vector of the unknown nodal values of water depth and velocities over the element area(Ae) .

$\bar{F}$ = The average known value of the coefficient of the friction slope over the element yields the following formula- :

$$\frac{n^2}{\bar{h}^{4/3}}.g.\sqrt{\bar{U}^2 + \bar{V}^2}\ \bar{F} = \ldots\ldots\ldots\ldots\ldots\ldots\ldots\ldots\ldots\ldots\ldots\ldots\ldots\ldots(3.4)$$

ℓx and ℓy = the direction cosines of the outward normal vector in x- and y-direction, respectively.

The forms of equations (3.1), (3.2) and (3.3) are that expression of the three integral equations which solved simultaneously for every element, and they must be arranged in matrix form to contain the total number of elements.

The assembled global matrix equation for equation (3.1), (3.2) and (3.3) are:

$$[A]\{\Psi^{\circ}\}+[C]\{\Psi\}=\{P\} \quad \text{.....(3.5)}$$

Where:

[A] =The diagonal mass matrix.

[C] =The system matrix or non-linear connective matrix.

$\{\Psi^{\circ}\}$=The time derivative of the nodal values.

$\{\Psi\}$=The vector of nodal values of h,u and v respectively; and

{P}=Force vector or prescribed values vector.

Equation (3.5) can be written in a matrix form as:

$$\begin{bmatrix} A_{11} & 0 & 0 \\ 0 & A_{22} & 0 \\ 0 & 0 & A_{33} \end{bmatrix}\begin{bmatrix} h^{\circ} \\ u^{\circ} \\ v^{\circ} \end{bmatrix}+\begin{bmatrix} C_{11} & C_{12} & C_{13} \\ C_{21} & C_{22} & C_{23} \\ C_{31} & C_{32} & C_{33} \end{bmatrix}\begin{bmatrix} h \\ u \\ v \end{bmatrix}=\begin{bmatrix} P_1 \\ P_2 \\ P_3 \end{bmatrix} \quad \text{.....(3.6)}$$

The matrix entries of the [A] matrix are:

$$[A_{11}]=[A_{22}]=[A_{33}]=\iint_{Ae}[N][N^t]dxdy$$

The matrix entries of the [C] matrix and {p} vector are: -

$$[C^{II}]=-\bar{U}\iint_{Ae}\left[\frac{\partial N}{\partial X}\right]\{N^t\}dxdy-\bar{V}\iint_{Ae}[N]\left\{\frac{\partial N^t}{\partial y}\right\}dxdy+\left[\bar{u}\int[N]\{N^t\}dy+\bar{V}\int[N]\{N^t\}dx\right]$$

$$[C_{12}]=-\bar{h}\iint_{Ae}[N]\left\{\frac{\partial N^t}{\partial x}\right\}dxdy+h\int[N]\{N^t\}dy$$

$$[C_{13}]=-\bar{h}\iint_{Ae}[N]\left\{\frac{\partial N^t}{\partial y}\right\}dxdy+h\int[N]\{N^t\}dx$$

$$[C_{21}]=0$$

$$[C_{22}]=\iint_{Ae}\left[\overline{U}\,[N]\left\{\frac{\partial N^t}{\partial x}\right\}+\overline{V}\,[N]\left\{\frac{\partial N^t}{\partial y}\right\}+\overline{F}\,[N][N^t]+\right.$$

$$E\left(\left\{\frac{\partial N}{\partial X}\right\}.\left\{\frac{\partial N^t}{\partial X}\right\}+\left\{\frac{\partial N}{\partial y}\right\}.\left\{\frac{\partial N^t}{\partial y}\right\}\right)\Big]dxdy-\oint_{\Gamma}E[[N]\left\{\frac{\partial N^t}{\partial X}\right\}\ell x+$$

$$[N]\left\{\frac{\partial N^t}{\partial y}\right\}\ell y]\,ds+\left[\overline{u}\int NN^t dy+\overline{V}\int NN^t dx\right]$$

$$[C_{23}]=0$$

$$[C31]=0$$

$$[C_{32}]=0$$

$$[C_{33}]=[C_{22}]$$

$$[p_1]=0$$

$$[P_2]=-g\iint_{Ae}[N]\left\{\frac{\partial N^t}{\partial X}\right\}[H]dxdy-g\int[N]\{N^t\}H\,dy$$

$$[P_3]=-g\iint_{Ae}[N]\left\{\frac{\partial N^t}{\partial y}\right\}[H]\,dxdy-g\int[N]\{N^t\}H\,dx$$

In equation (3.5) the variable (Ψ°) is assumed as function of time. By considering (Δt) and denoted by Ψ^{t} and $\Psi^{t+\Delta t}$. The estimation of these terms yields the following forward difference scheme (Abed, 1998, Al-Eoubaidy, 1999): -

$$\frac{\partial\Psi}{\partial t}=\frac{1}{\Delta t}\left[\text{Ħ}_{\text{ι}+\nabla\text{ι}}-\text{Ħ}_{\text{ι}}\right]\text{……..….(3.7)}$$

A temporal integration scheme, Known as Generalized rule, is based on the assumption that the (Ψ) and (P) vectors have relation as: -

$$\Psi^{t+\Delta t}-\Psi^{t}=\left[(1-\propto)\Psi^{t}+\propto\Psi^{t+\Delta t}\right]\Delta t \quad \text{……...(3.8)}$$

$$P^{t+\Delta t} - P^{t} = \left[(1-\propto)P^{t} + \propto P^{t+\Delta t}\right]\Delta t \quad \ldots\ldots\ldots\ldots\ldots\ldots\ldots\ldots\ldots\ldots(3.9)$$

The value of $\propto$ can be taken from 0 to 1 according to the methods of solution, the common values of $\propto$ are: -

1. $\propto$=1, Fully implicit scheme.
2. $\propto$=0.67, Galerkin scheme.
3. $\propto$=0.5, Crank Nicolson scheme.
4. $\propto$=0, Fully explicit scheme.

By substituting equation (3.7), (3.8) and (3.9) into equation (3.5) yield, after rearranging, the following non-linear algebraic equation: -

$$\left[[A]+\propto \Delta t[C]^{t+\Delta t}\right][\Psi]^{t+\Delta t} = \left[[A]-(1-\propto)\Delta t[C]^{t}\right][\Psi]^{t} + \Delta t\left[(1-\propto)[P]^{t} + \propto [P]^{t+\Delta t}\right] \quad \ldots\ldots\ldots\ldots\ldots\ldots\ldots\ldots\ldots\ldots\ldots\ldots(3.10)$$

The non-linear matrix [C] and force vector {P} must be evaluated at each time step, but matrix [A] need to be assembled only once for the problem.

A nonlinear solution for the equation (3.10) can be carried out by using any iterative schemes, about this, Four iterative schemes are represented by Gartling et al., (1977). Initial velocity, modified initial-velocity, Picard iteration and Newton Raphson methods.

The widely used of iteration methods in finite element analysis are based on classical Newton method is employed.

The equation used in Newton-Raphson method is: -

$$\Psi_{i}^{t+\Delta t} = \Psi_{i-1}^{t+\Delta t} + \Delta\Psi i \quad \ldots\ldots\ldots\ldots\ldots\ldots\ldots\ldots\ldots\ldots\ldots\ldots(3.11)$$

$$[K]_{i-1}^{t+\Delta t}[\Delta\Psi] = [-B]_{i-1} \quad \ldots\ldots\ldots\ldots\ldots\ldots\ldots\ldots\ldots\ldots\ldots\ldots(3.12)$$

Where [K] is linearized Jacobian matrix and [-B] is the column vector of the nodal residual values and (i) indicates the iteration step. Equation (3.12) has shown that the solution at iteration (i-1) must be known, (Bathe, 1996).

About this, equation (3.10) can rewrite in iteration form as: -

$$[[A]+\propto \Delta t[C]]_{i-1}^{t+\Delta t}[\Psi]_{i}^{t+\Delta t}=[[A]-(1-\propto)\Delta t[C]]^{t}[\Psi]^{t}+$$

$$\Delta t\left[(1-\propto)[\text{Ь}]_{\text{ι}}+\propto[\text{Ъ}]_{\text{ι}+\nabla\text{ι}}^{\text{ι}-1}\right]\text{.....(3.13)}$$

Application of the Newton-Raphson solution to equation (3.13) result the linear equation that can be solved directly by using Gaussian elimination method.

The accuracy and convergence for numerical solution are checked for any results obtained from the two subsequent iterations. The basic idea of convergent criteria that which used essentially for checking the accuracy of linearization equations.

A convergence criterion, which can be expressed by the ratio of Euclidian norm of the corrections to that of the updated solutions (Sharhan, 1986). Then, the tolerance ratio, which can be written as: -

$$E=\frac{\left\|\left\{\Psi^{i}-\Psi^{i-1}\right\}_{t+\Delta t}\right\|}{\left\|\left\{\Psi^{i}\right\}_{t+\Delta t}\right\|}\text{.....(3.14)}$$

Now, assuming a tolerance ratio for the depth and velocities with an iteration step makes an indirect measure of accuracy. In this model, the mathematical solution is reduced to accuracy solution at last iteration if the change in water depth and velocity in two subsequent iterations are within (5%).

By applying the Galerkin weighted residual approach for morphological model the equation (2.10) can be written as (see appendix A):

$$\iint[N]\left[N^{t}\left[\frac{\partial Z}{\partial t}\right]dsdn+\frac{1}{1-\lambda}\left[\iint[N]\left[\frac{\partial N^{t}}{\partial S}\right][q_{BS}]dsdn\right]+\frac{1}{1-\lambda}\left[\iint[N]\left[\frac{\partial N^{t}}{\partial n}\right][q_{BS}\quad\tan\theta]dsdn\right]-$$

$$\frac{2}{1-\lambda}\left[\iint[N]\left[\frac{\partial N^{t}}{\partial n}\right]\left[\frac{q_{BS}.K}{R+n}\right]\left[\frac{\partial N^{t}}{\partial n}\right][Z]dsdn\right]+\frac{1}{1-\lambda}\left[\iint[N]\left[\frac{q_{Bs.}\tan\theta}{R+n}\right][N^{t}]dsdn\right]=0\text{ ..(3.15)}$$

Where: -

$\left[\frac{\partial Z}{\partial t}\right]$=The column vector of time derivative of the nodal bed elevation.

$[q_{BSi}]$=The column vector of the Nodal bed load transport in S-direction

$$K = \sqrt{\tau_{*c} / M_s M_k \ \tau_*} \quad \text{.....(3.16)}$$

Similarly to the Navier-Stockes equations, equation (3.15) must be applied over the whole domain flow. The assembled global matrix equation for dynamic sediment continuity is:

$$[B][Z^\circ]+[D][Z]=[F] \quad \text{.....(3.17)}$$

Where:-

[B]=The square mass matrix

$[Z^\circ]$=The column vector of the time derivative of the nodal values.

[D]=The system matrix.

[Z]=The column vector of nodal values.

[F]=the column vector of forces.

The equation (3.17) have a time derivative term, which can be evaluated by using the following forward difference scheme: -

$$\frac{\partial Z}{\partial t} = \frac{1}{\Delta t}\left[Z^{t+\Delta t} - Z^t\right] \quad \text{.....(3.18)}$$

|Where the (Δt) is the length of the time step. Substituting equation (3.18) to equation (3.17) result the linear equation, which can be solved directly by using the Gauss-elimination as: -

$$[[B]+\Delta t[D]\ ][Z]^{t+\Delta t}=[B][Z]^t+\Delta t[F] \quad \text{.....(3.19)}$$

The matrix entries of the [B], [D] and [F] matrixes are: -

$[B]= \iint_A [N][N_t]\, ds\, dn$

$$[D]= - \frac{2}{1-\lambda}\left[\iint[N]\left[\frac{\partial N^t}{\partial n}\right]\left[\frac{q_{Bs}K}{R+n}\right]\left[\frac{\partial N^t}{\partial n}\right]dsdn\right]$$

$$[F]= \frac{1}{1-\lambda}\left[\iint[N]\left[\frac{\partial N^t}{\partial S}\right][q_{BS}]dsdn+\iint[N]\left[\frac{\partial N^t}{\partial n}\right][q_{BS}\tan\theta]dsdn+\iint[N]\left[\frac{q_{BS}\tan\theta}{R+n}\right][N^t]dsdn\right]$$

The linear matrix [D] and Force Vector [F] must be calculated each time step, while the matrix [B] must be assembled only once for the problem.

3.2 Input Data

This part of program is used for preparation of the data necessary for the model working. The data which necessary for define the model was showing in Fig. (3.1) and it include the following:

3.2.1 Geometrical Data

The data entry is a subroutine by which the following data can be read.

- Number of nodes, number of element, number of time steps and time step.
- Manning number (n) and weighting factor (α).
- The Cartesian coordinates for each node.
- Element number, number of nodes for each element and topology array.

3.2.2 Initial and boundary conditions

3.2.2.1 Initial conditions

The initial conditions can be described as the following data:

i) Prescribed velocity component at initial time for each node in the domain.

ii) Prescribe depth of water at initial time for each node.

3.2.2.2 Boundary Conditions

The boundary conditions can be specified in terms of:

i) Velocity component in x-direction: Where the switch (SWU) can be either (1) for nodes with prescribed velocity in x-direction for each time or (0) for nodes with unknown velocity in x-direction.

ii) Velocity component in y-direction: Where the switch (SWV) can be either (1) for nodes with prescribed velocity in y-direction for each time or (0) for nodes with unknown velocity in y-direction.

iii) Depth of water: Where the switch (SWh) can be either (1) for nodes with prescribed depth of water for each time or (0) for nodes with unknown depth of water.

3.3 Element Stiffness Matrix Generator

In this subroutine, the stiffness matrix (C^e) for two dimensional hydrodynamic model will be generated as follows:

From equation (3.6), the building ($\underline{C}^e$) can be done by generate $\underline{C}_{i,j}^{3,3}$ sub matrix where i=1,2,3 and j=1,2,3 So that:

$$\underline{C}_{11}^{e} = \int_0^1 \int_0^1 \left[\underline{BX}^T \, \underline{SF} \left|J\right| UEE + \underline{BY}^T \, \underline{SF} \left|J\right| VEE\right] d\xi \, d\eta \quad \text{.....(3.20)}$$

Where: -

Bx= Shape function derivative with respect to x i.e. $\left\{\frac{\partial N}{\partial X}\right\}$

BY= Shape function derivative with respect to Y i.e. $\left\{\frac{\partial N}{\partial Y}\right\}$

SF= Shape function

J = Jacobian matrix

A numerical integration scheme is used to evaluate this integral, and Gaussian quadrate has provided an efficient procedure that can be adopted as follows: -

$$\underline{C}_{11}^{e} = \sum_{r=1}^{NQ} \sum_{s=1}^{NQ} W_T \, \underline{BX}^T (\xi r, \eta s) * \underline{SF}(\xi r, \eta s) UEE + W_T \, \underline{BY}^T (\xi r, \eta s) * \underline{SF}(\xi r, \eta s) VEE \text{ .(3.21)}$$

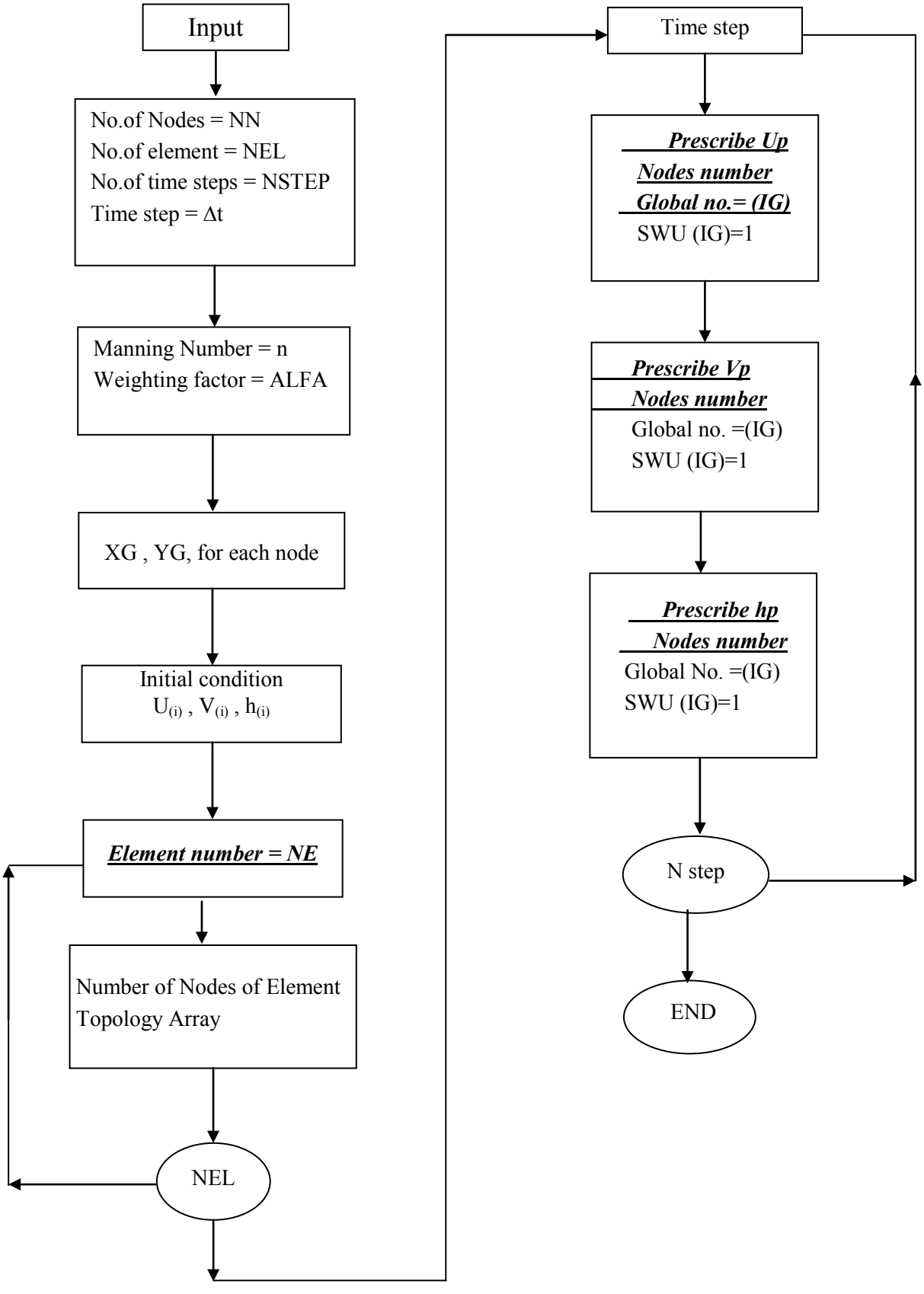

Fig. (3-1) Flowchart of Input Data subroutine

Where

NQ= no. of Gauss point

$W_T = W_r W_s (1-\eta_s)$

Wr, Ws are the gauss points

$$UEE = \sum_{i=1}^{Nc} U_i N_i(\xi r, \eta s)$$

$$VEE = \sum_{i=1}^{Nc} V_i N_i(\xi r, \eta s)$$

And also

$$\underline{C}_{12}^e = \int_0^1 \int_0^1 \underline{BX}(\xi,\eta)\underline{SF}(\xi,\eta,)HEE|J|\,d\xi\,d\eta \quad \text{.....(3.22)}$$

And by using numerical integration

$$\underline{C}_{12}^e = \sum_{r=1}^{NQ} \sum_{s=1}^{NQ} W_T \underline{BX}(\xi r, \eta s)\underline{SF}(\xi r, \eta s)|J|HEE \text{.....(3.23)}$$

HEE = $\sum_{i=1}^{Nc} H_i N_i(\xi r, \eta s)$

The third term

$$\underline{C}_{13}^e = \int_0^1 \int_0^1 \underline{By}(\xi r, \eta s)\underline{SF}(\xi r, \eta s)HEE|J|d\xi d\eta \quad \text{.....(3.24)}$$

$$\underline{C}_{13}^e = \sum_{r=1}^{NQ} \sum_{s=1}^{NQ} W_T \underline{By}(\xi r, \eta s)\underline{SF}(\xi r, \eta s)|\underline{J}|HEE \text{.....(3.25)}$$

$$C_{21}^e = C_{23}^e = C_{31}^e = C_{32}^e = 0$$

The term C_{22}^e can be calculated in the same method for above terms and the term C_{33}^e is equal to C_{22}^e. The matrix C^e is constructed by the terms $C_{i,j}$.

Fig (3.2) shows the main subroutine on the C^e matrix generator.

3.4 Element Mass Matrix Generator

The element mass matrix for two-dimensional hydrodynamic model is to be determinate according to equation (2.14) as follows:

$$\underline{A}_{ii}^{e} = \int_0^1 \int_0^1 NN^T |J| d\xi d\eta$$

$$\underline{A}_{ij}^{e} = \sum_{r=1}^{NQ} \sum_{s=1}^{NQ} W_T \underline{N}(\xi r, \eta s) N^T(\xi, \eta) |J| \qquad \text{i = 1,2,3,…} \qquad \text{……..(3.26)}$$

$$A^e = \begin{vmatrix} \underline{A}_{11} & 0 & 0 \\ 0 & \underline{A}_{22} & 0 \\ 0 & 0 & \underline{A}_{33} \end{vmatrix}$$

The subroutine of element mass matrix is shown in fig (3.2).

3.5 Force vector subroutine

The force vector (P) for two-dimensional hydrodynamic model is to be determined according to equation (3.6) as follows:

$P1 = 0$

$$P_2 = -g \int_0^1 \int_0^1 SF\, BX^t\, H\, d\xi\, d\eta$$

$$P_3 = -g \int_0^1 \int_0^1 SF\, BY^t\, H\, d\xi\, d\eta$$

By using numerical integration

$P1 = 0$

$$P_2 = \sum_{r=1}^{NQ} \sum_{s=1}^{NQ} W_T\, BX(\xi_S, \eta_r) SF(\xi_S, \eta_r) g\, |J| \qquad \text{……(3.27)}$$

$$P_3 = \sum_{r=1}^{NQ} \sum_{s=1}^{NQ} W_T\, BY(\xi_S, \eta_r) SF(\xi_S, \eta_r) g\, |J| \qquad \text{……(3.28)}$$

$$P=\begin{Bmatrix}P_1\\P_2\\P_3\end{Bmatrix}=\begin{Bmatrix}0\\0\\0\\P_2(1)\\P_2(2)\\P_2(3)\\P_3(1)\\P_3(2)\\P_3(3)\end{Bmatrix}$$

Figure (3.2) shows the subroutine of force vector.

3.6 Boundary Element Matrix Generator

In this subroutine the influence of the boundary conditions are considered as an additional matrix where the boundary element is the element that two-node at least from its nodes lie on the boundary.

The subroutine was build to construct the boundary condition matrix that used depend on the boundary. The integration is done numerically by using Gaussian quadratuer to evaluate a more correct result.

$$\underline{C}_b=\begin{vmatrix}C_{b11} & C_{b12} & C_{b13}\\C_{b21} & C_{b22} & C_{b23}\\C_{b31} & C_{b32} & C_{b33}\end{vmatrix}$$

Where

$$\underline{C}_{b11}=\int \underline{SF}\,\underline{SF}^T UCC\left|J\right|d\xi+\int \underline{SF}\,\underline{SF}^T VCC\left|J\right|d\xi \quad \text{.....(3.29)}$$

And by using numerical integration

$$\underline{C}_{b11}=\sum_{r=1}^{NQ} WQ(\xi_r)SF(\xi_r)SF^T(\xi_r)UCC\left|J_x\right|+\sum WQ(\xi_r)SF(\xi_r)SF^T(\xi_r)VCC\left|J_y\right| \text{..(3.30)}$$

The matrix $\underline{C}_{b12}$ can be expressed as:

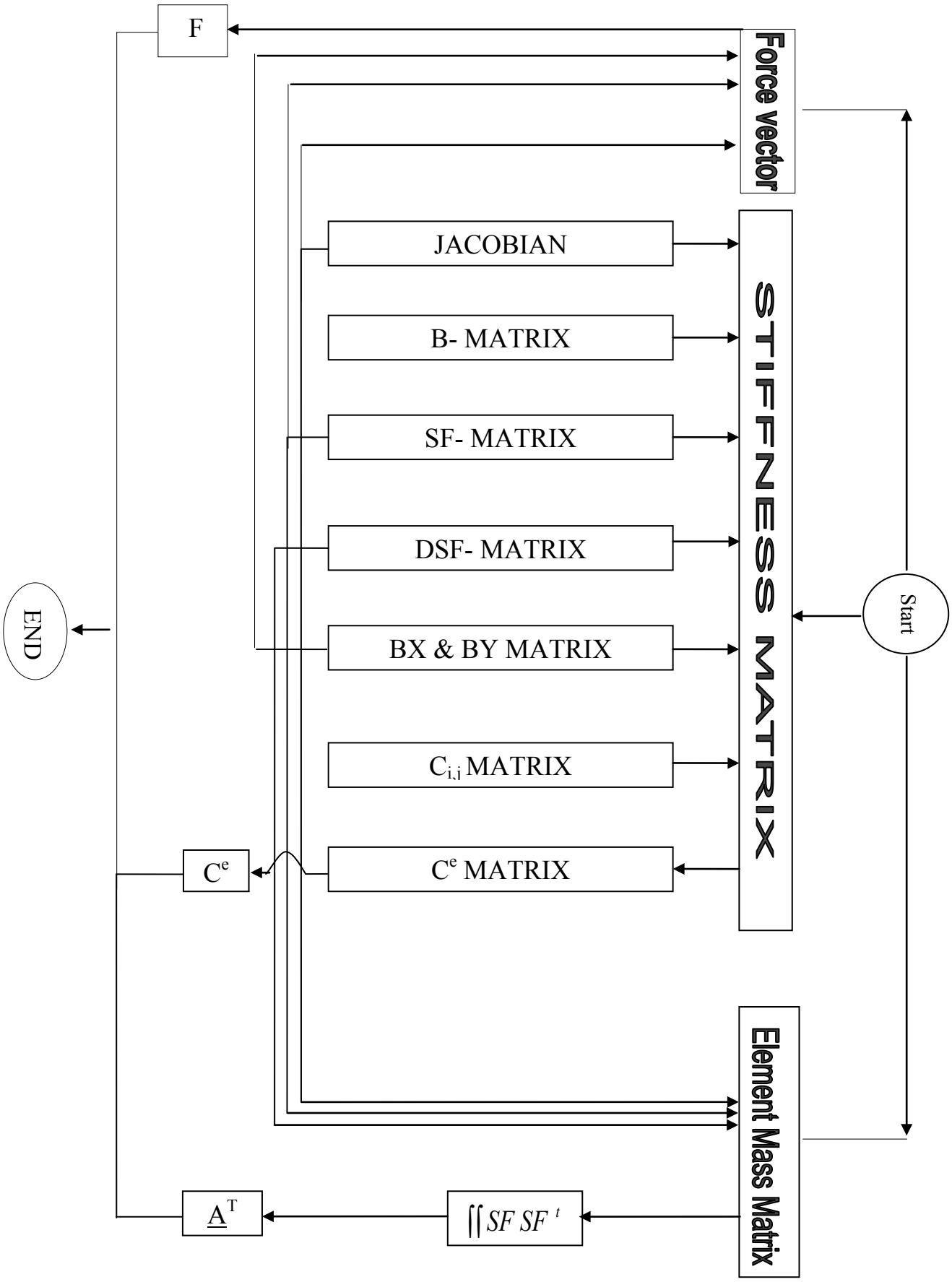

Fig. (3.2) Stiffness Matrix, Mass Matrix and Force vector Generator

$$\underline{C}_{b12} = \int_0^1 SF(\xi) SF^T(\xi) HCC |J_X| d\xi \quad \text{.....(3.31)}$$

It can be written in the form numerical integration as:

$$C_{b12} = \sum_{r=1}^{NQ} WQ(\xi r) SF(\xi r) SF^T(\xi r) HCC |J_X| \quad \text{.....(3.32)}$$

And

$$\underline{C}_{b13} = \sum_{r=1}^{NQ} WQ(\xi r) SF(\xi r) SF^T(\xi r) HCC |J_X| \quad \text{.....(3.33)}$$

And also C_{b22} and C_{b33} as above

$$C_{b21} = C_{b23} = C_{b31} = C_{b32} = 0$$

Where

$|J_X|$ = Element length in x -direction.

$|J_Y|$ = Element length in Y-direction.

HCC, UCC and VCC are the mean value of the element depth and velocities.

WQ = for quadrilateral elements.

The matrix C_b is added to C_e for each element before making the Global Matrix C_G. Figure (3.3) shows the boundary condition calculation.

3.7 Global Element Stiffness Matrix C_G

The global element stiffness matrix C_G is defined as the sum of the domain element stiffness matrix C_e and the boundary element matrix C_b. The domain element stiffness matrix was effected on all nodes of elements, but the boundary element matrix effected on some nodes of the element as shown in fig (3.4).

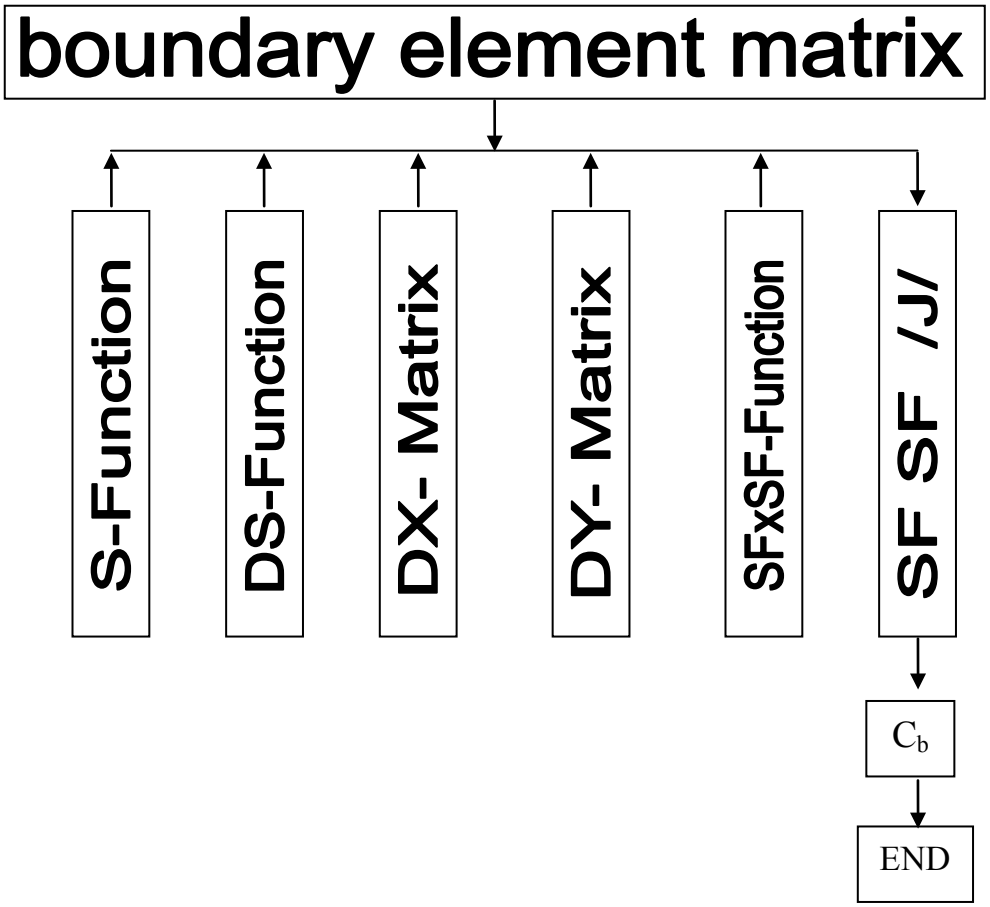

Fig. (3.3) Flowchart of Boundary Element Matrix Generator

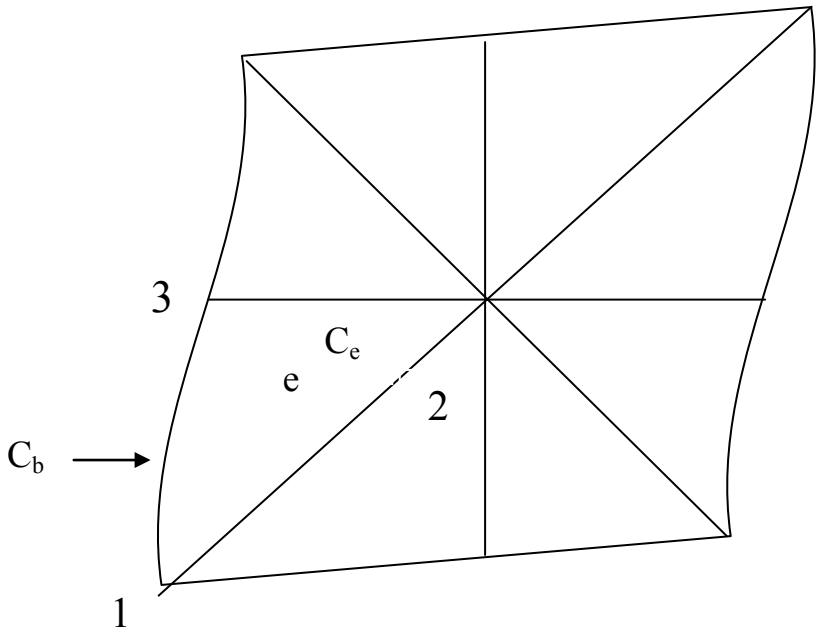

Fig. (3.4) Effect of the Boundary Condition on the Element

The element (e) is affected by the boundary condition on the side (1-3).

The stiffness matrix is written as follows:

$$C_e = \begin{vmatrix} C_{11} & C_{12} & C_{13} & C_{14} & C_{15} & C_{16} & C_{17} & C_{18} & C_{19} \\ C_{21} & C_{22} & C_{23} & C_{24} & C_{25} & C_{26} & C_{27} & C_{28} & C_{29} \\ C_{31} & C_{32} & C_{33} & C_{34} & C_{35} & C_{36} & C_{37} & C_{38} & C_{39} \\ C_{41} & C_{42} & C_{43} & C_{44} & C_{45} & C_{46} & C_{47} & C_{48} & C_{49} \\ C_{51} & C_{52} & C_{53} & C_{54} & C_{55} & C_{56} & C_{57} & C_{58} & C_{59} \\ C_{61} & C_{62} & C_{63} & C_{64} & C_{65} & C_{66} & C_{67} & C_{68} & C_{69} \\ C_{71} & C_{72} & C_{73} & C_{74} & C_{75} & C_{76} & C_{77} & C_{78} & C_{79} \\ C_{81} & C_{82} & C_{83} & C_{84} & C_{85} & C_{86} & C_{87} & C_{88} & C_{89} \\ C_{91} & C_{92} & C_{93} & C_{94} & C_{95} & C_{96} & C_{97} & C_{98} & C_{99} \end{vmatrix}$$

And the boundary element matrix is:

$$C_b = \begin{vmatrix} C_{b11} & C_{b12} & C_{b13} & C_{b14} & C_{b15} & C_{b16} \\ C_{b21} & C_{b22} & C_{b23} & C_{b24} & C_{b25} & C_{b26} \\ C_{b31} & C_{b32} & C_{b33} & C_{b34} & C_{b35} & C_{b36} \\ C_{b41} & C_{b42} & C_{b43} & C_{b44} & C_{b45} & C_{b46} \\ C_{b51} & C_{b52} & C_{b53} & C_{b54} & C_{b55} & C_{b56} \\ C_{b61} & C_{b62} & C_{b63} & C_{b64} & C_{b65} & C_{b66} \end{vmatrix}$$

OR

$$C_b = \begin{vmatrix} C_{b11} & C_{b12} & C_{b13} & 0 & 0 & 0 & C_{b17} & C_{b18} & C_{19} \\ C_{b21} & C_{b22} & C_{b23} & 0 & 0 & 0 & C_{b27} & C_{b28} & C_{29} \\ C_{b31} & C_{b32} & C_{b33} & 0 & 0 & 0 & C_{b37} & C_{b38} & C_{39} \\ 0 & 0 & 0 & 0 & 0 & 0 & 0 & 0 & 0 \\ 0 & 0 & 0 & 0 & 0 & 0 & 0 & 0 & 0 \\ 0 & 0 & 0 & 0 & 0 & 0 & 0 & 0 & 0 \\ C_{b71} & C_{b72} & C_{b73} & 0 & 0 & 0 & C_{b77} & C_{b78} & C_{b79} \\ C_{b81} & C_{b82} & C_{b83} & 0 & 0 & 0 & C_{b87} & C_{b88} & C_{b89} \\ C_{b91} & C_{b92} & C_{b93} & 0 & 0 & 0 & C_{b97} & C_{b98} & C_{b99} \end{vmatrix}$$

The global element matrix C_G is equal to the sum of C_e and C_b .

$$C_G = C_e + C_b$$

$$C_G = \begin{matrix} C_{11}+C_{b11} & C_{12}+C_{b12} & C_{13}+C_{b13} & C_{14} & C_{15} & C_{16} & C_{17}+C_{b17} & C_{18}+C_{b18} & C_{19}+C_{b19} \\ C_{21}+C_{b21} & C_{22}+C_{b22} & C_{23}+C_{b23} & C_{24} & C_{25} & C_{26} & C_{27}+C_{b27} & C_{28}+C_{b28} & C_{29}+C_{b29} \\ C_{31}+C_{b31} & C_{32}+C_{b32} & C_{33}+C_{b33} & C_{34} & C_{35} & C_{36} & C_{37}+C_{b37} & C_{38}+C_{b38} & C_{39}+C_{b39} \\ C_{41} & C_{42} & C_{43} & C_{44} & C_{45} & C_{46} & C_{47} & C_{48} & C_{49} \\ C_{51} & C_{52} & C_{53} & C_{54} & C_{55} & C_{56} & C_{57} & C_{58} & C_{59} \\ C_{61} & C_{62} & C_{63} & C_{64} & C_{65} & C_{66} & C_{67} & C_{68} & C_{69} \\ C_{71}+C_{b71} & C_{72}+C_{b72} & C_{73}+C_{b73} & C_{74} & C_{75} & C_{76} & C_{77}+C_{b77} & C_{78}+C_{b78} & C_{79}+C_{b79} \\ C_{81}+C_{b81} & C_{82}+C_{b82} & C_{83}+C_{b83} & C_{84} & C_{85} & C_{86} & C_{87}+C_{b87} & C_{88}+C_{b88} & C_{89}+C_{b89} \\ C_{91}+C_{b91} & C_{92}+C_{b92} & C_{93}+C_{b93} & C_{94} & C_{95} & C_{96} & C_{97}+C_{b97} & C_{98}+C_{b98} & C_{99}+C_{b99} \end{matrix}$$

For non-surrounded element $C_G = C_e$ only.

3.8 Subroutine of Assembly

In this subroutine the element stiffness matrix (C_G) and the time dependent matrix (A^e) and force vector (F) that calculates in pervious subroutine used in equation (3.13) as following:

$$\left[\underline{A}^e + \alpha\,\Delta t\left[\ C_G\ \right]^{t+\Delta t}\right]\Psi^{t+\Delta t} = \left[A^e - (1-\alpha)\Delta t\left[\ C_G\ \right]^t\right]\Psi^t + \Delta t(1-\alpha)P^t + \alpha\,\Delta t\,P^{t+\Delta t}$$

The right hand side is all known and it can be assumed as $\underline{CM}$ except $\Delta t\,\alpha P^{t+\Delta t}$.

$$\underline{CM} = \left[\underline{A}^e - (1-\alpha)\Delta t\left[\ C_G\ \right]^t\right]\Psi^t + \Delta t(1-\alpha)P^t \quad \text{.....(3.34)}$$

And

$$\underline{AM} = \left[\underline{A}^e + \alpha\,\Delta t\left[\ \underline{C}_G\ \right]^{t+\Delta t}\right] \quad \text{.....(3.35)}$$

$$\Psi e^{t+\Delta t} = \underline{AM}^{-1}\underline{CM} + \underline{AM}^{-1}\Delta t\,\alpha P^{t+\Delta t}$$

$$= \underline{AC} + AE\,P^{t+\Delta t} \quad \text{.....(3.36)}$$

Where $\underline{AC} = \underline{AM}^{-1}\ \underline{CM}$

And $\underline{AE} = \Delta t\,\alpha\,\underline{AM}^{-1}$

The matrix (CM) was calculated only once in every time step but the matrix (AM) was calculated in every iteration. The concept of topology array can be employed to find the global matrix of AC and AE.

$$\underline{AC}_G(I_G, J_G) = \sum_A \underline{AC}^{(I,J)}\Big/_{nrpt}$$

$$\underline{AE}_G(I_G, J_G) = \sum_A \underline{AE}^{(I,J)}\Big/_{nrpt} \quad \text{.....(3.37)}$$

Where

$\underline{AC}_G, \underline{AE}_G$: Are matrices for whole domain.

$I_G = TA(e,I)$: Is the global number i[th] node in e [th] elements.

$J_G = TA(e,J)$: Is the global number j[th] node in e [th] elements.

nrpt : is the number of the repeating condition.

i,j = 1,2,3,…….n is the local number of e th element.

n = number of element nodes *3 .

Figure (3.5) showing the assembly subroutine.

3.9 Reducer Module

The equation of the hydrodynamic model may be written as follows:

$$AE_G P^{t+\Delta t} = \Psi^{t+\Delta t} - AC_G \quad \text{……..(3.38)}$$

In this model, the equations of prescribed (P^{n+1}) will be eliminated from the above equation. When some of the (P^{n+1}) are prescribed this vector can be split to : $\underline{P}^{t+\Delta t} = \{P_u . P_p\}$

where

P_u : Is the unknown.

P_p : is the prescribed.

Hence, the corresponding matrix equations can be partitioned as follows:

$$\begin{vmatrix} AE_{Guu} & AE_{Gup} \\ AE_{Gpu} & AE_{Gpp} \end{vmatrix} \begin{vmatrix} P_u \\ P_p \end{vmatrix} = \begin{vmatrix} \Psi_u^{t+\Delta t} \\ \Psi_p^{t+\Delta t} \end{vmatrix} - \begin{vmatrix} AC_G \\ AC_G \end{vmatrix}$$

i.e.

$$AE_{Guu} P_u + AE_{Gup} P_p = \Psi_u^{t+\Delta t} - AC_G$$

$$AE_{Gup} P_u + AE_{Gpp} P_p = \Psi_p^{n+1} - AC_G \quad \text{……(3.39)}$$

Hence,

$$AE_{Guu} P_u = \Psi_u - AC_G - AE_{Gup} P_p$$

Represents the reduced system of equation

$$\Psi_p = AE_{Gup} P_u + AE_{Gpp} P_p + AC_G \quad \text{……..(3.40)}$$

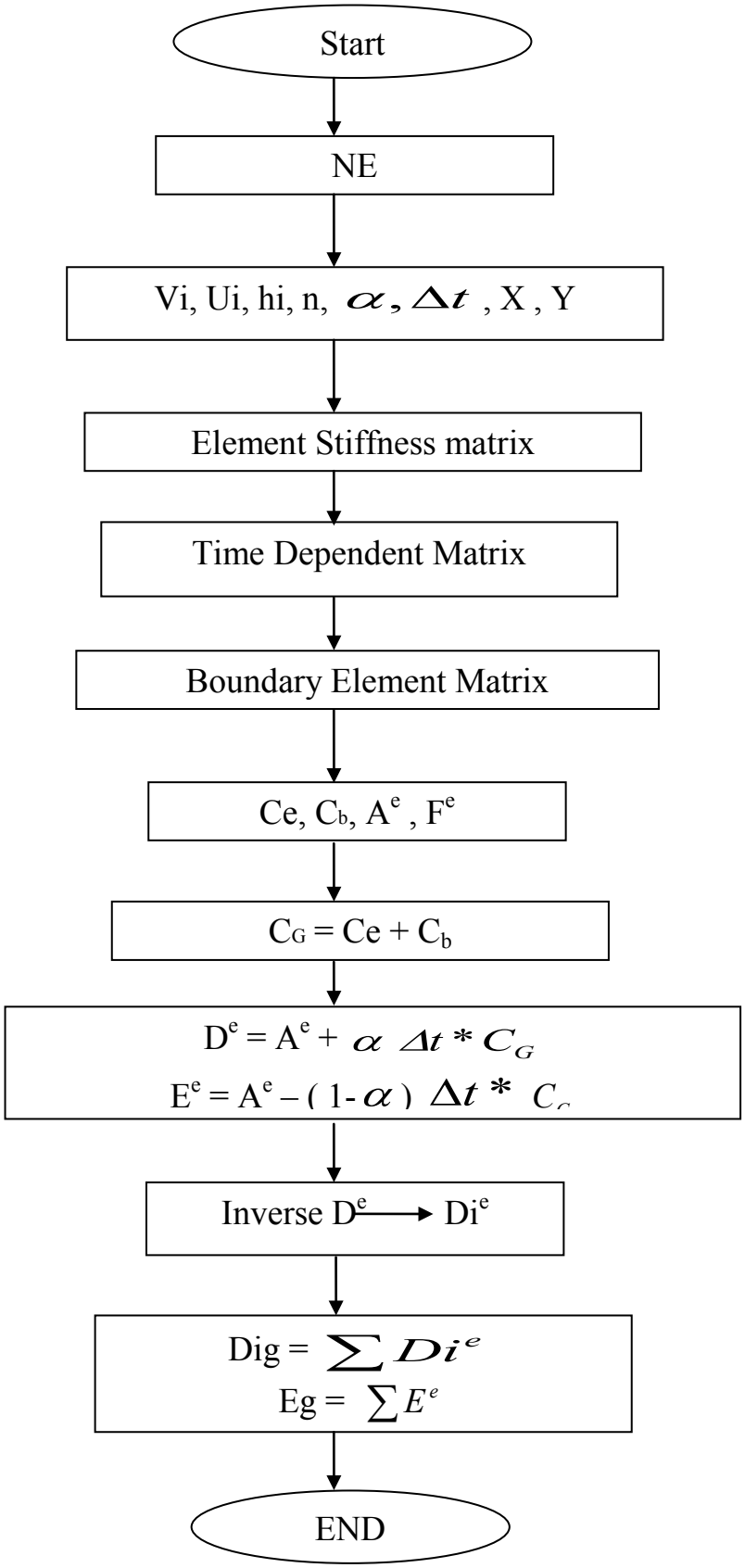

FIG. (3.5) FLOWCHART OF ASSEMPLY SUBROUTINE

3.10 Equation Solver Subroutine

The solver that used here is using the Newton-Raphson method. It is iteration method for solving equations f (x)=0, where (f) is differentiable.

The matrix equation can be written as:

$$AE_{Guu}\,F_u - \Psi_u + \underline{AC}_G + AE_{Gup}\,F_p = 0 \quad \text{.....(3.41)}$$

$$AE_{Guu}\,F_u + B = 0$$

Where

$$B = -\Psi_u + AC_G + AE_{Gup}\,F_p$$

And by using the equation

$$P_{u\ i+1}(I) = P_{u\ i}(I) - \frac{AE_{Guu\ i}(I,I)\,P_{u\ i}(I) + B}{AE_{Guu}(I,I)} \quad \text{.....(3.42)}$$

This method is giving always the convergence in the solution at least time.

3.11 Main Program of Hydrodynamic Model

Fig (3.6) shows the output of the scheme of the main program of hydrodynamic model. In this main program for each time step the old values where used to give a new value for the iteration method this repeat until it gives a convergent new values then call a new time step and so on.

The equation of finite element method in this study is non-linear and it is linearized to make the solution easier and using Newton-Raphson method make the convergence of solution become fast.

3.12 Main Program of Morphological Model

The morphological model is run after we have a new values for (u,v,h) by using the hydrodynamic model . The morphological model depends on the equation (3.19) as following:

$$\left\| B \right| + \Delta t\left[D \right]\left[Z \right]^{t+\Delta t} = \left[B \right]\left[Z \right]^{t} + \Delta t\left[F \right]$$

The matrix entries of the [B], [D], and [F] matrices are:

$$[B] = \iint_{A} [N][N]^{T} \, ds \, dn$$

$$[B] = \sum_{r=1}^{NQ} \sum_{s=1}^{NQ} Wt \, N \, N^{T} / J / \quad \text{.....(3.43)}$$

$$[D] = \frac{-2}{1-\lambda} [\iint [N][\frac{\partial N^{T}}{\partial n}][\frac{q_{Bs} K}{R+n}][\frac{\partial N^{T}}{\partial n}] ds \, dn$$

$$[D] = \frac{-2}{1-\lambda} \sum_{r=1}^{NQ} \sum_{s=1}^{NQ} Wt \, [N.\frac{\partial N^{T}}{\partial n}][\frac{q_{Bs} K}{R+n}.\frac{\partial N^{T}}{\partial n}] \; / J / \quad \text{.....(3.44)}$$

$$[F] = \frac{1}{1-\lambda} [\iint [N][\frac{\partial N^{T}}{\partial s}][q_{Bs}] \, ds \, dn + \iint [N][\frac{\partial N^{T}}{\partial n}][q_{Bs} TAN\theta] \, ds \, dn + \iint [N][\frac{q_{qBs} TAN\theta}{R+n}][N^{T}] \, ds \, dn]$$

$$[F] = \sum_{r=1}^{NQ} \sum_{s=1}^{NQ} Wt / J / \frac{1}{1-\lambda} [N \frac{\partial N^{T}}{\partial s} q_{Bs} + N \frac{\partial N^{T}}{\partial n} q_{Bs} TAN\theta + N \frac{q_{Bs} TAN\theta}{R+n} N^{T}]$$

.....(3.45)

The linear matrix [D] and force vector [F] must be calculated at each time step while the matrix [B] will be assembled only once for the problem.

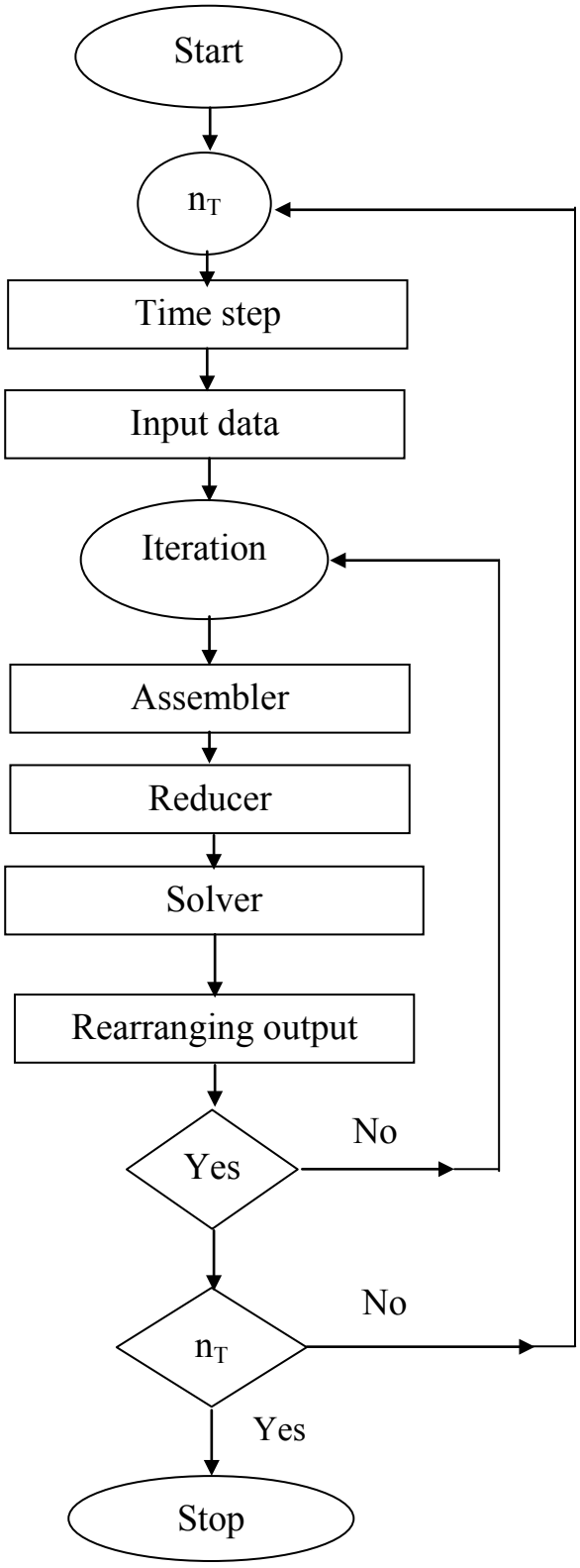

FIG. (3.6) FLOWCHART OF MAIN PROGRAM FOR HYDRODYNAMIC MODEL

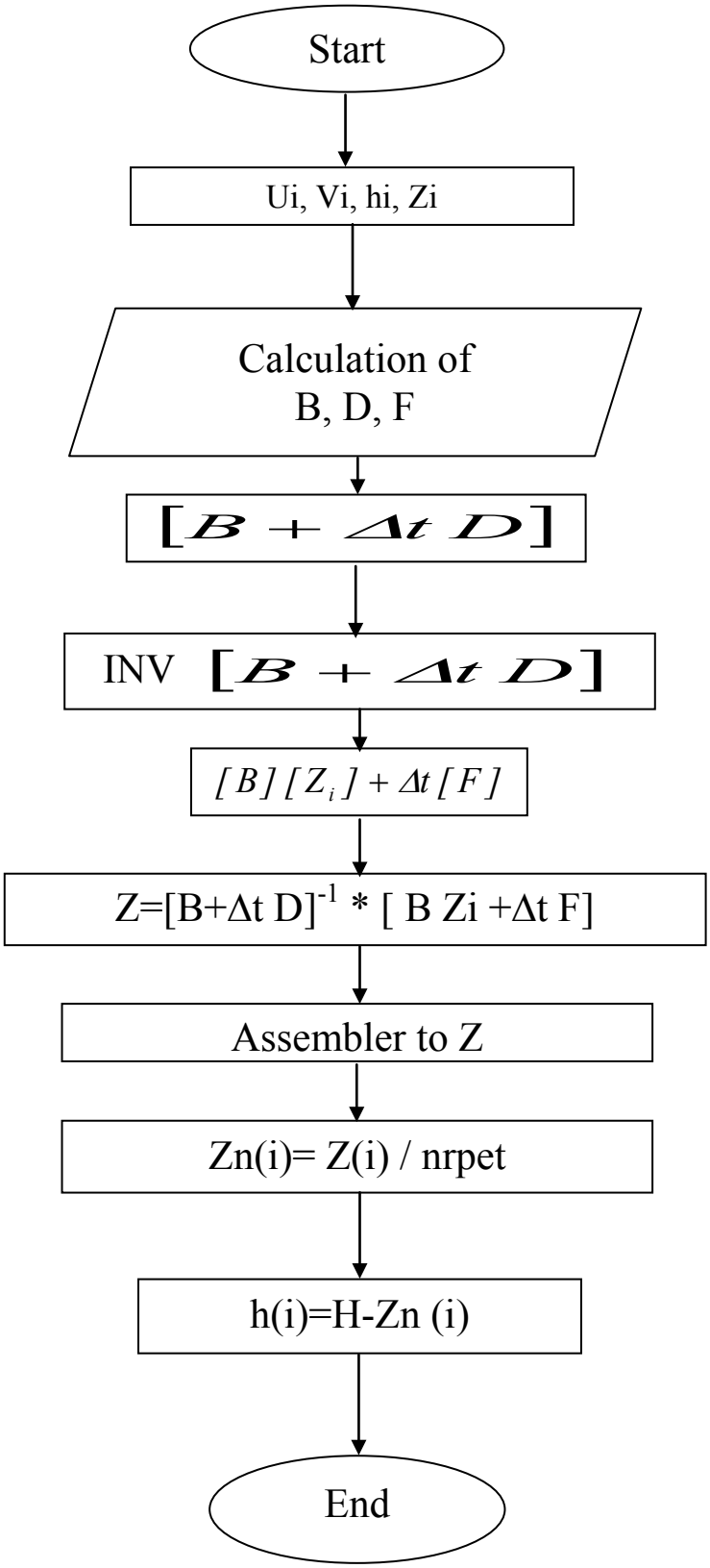

FIG. (3.7) FLOWCHART OF MAIN PROGRAM FOR MORPHOLOGICAL MODEL

CHAPTER FOUR

Applications, Results and Discussion

CHAPTER FOUR

Applications, Results and Discussion

4.1 General

The two dimensional hydrodynamic model that developed in pervious chapter was applied to Euphrates river within AL-Ramadi City .The input data required to run the model are based on the unsteady nature of flow, the cross sections under consideration are irregular and changes in width from one location to another.

Calibration and verification of the numerical model are important in applying the model to the field problems.

4.2 Application of Hydrodynamic Model to Idealized channel

Before specifying the success of any model, the numerical solution of finite element model should be tested relatively to other solution. This can be verified by comparing the numerical solution with analytical solution and then applied to natural case.

The tidal wave in an idealized channel is a good example of which an analytical solution exists. The reference model was taken from Ippen (1966). The configuration of the system is a typical rectangular channel 160m long and 40m wide having a downstream closed end at and open end at upstream.

The grid system was developed using 16 triangular elements divided along channel centerline. Ippen (1966) gives an analytical solution can be taken as: -

$$Y=h+ [a/\{\cos (kL)\}] \cos [k (L-x)] \sin (\omega t) \quad \ldots\ldots\ldots\ldots\ldots\ldots\ldots\ldots (4.1)$$

$$V=-[a\, Ce /\{h \cos (kL)\}] \sin [k (L-x)] \cos (\omega t) \quad \ldots\ldots\ldots\ldots\ldots\ldots\ldots\ldots (4.2)$$

Where: -

Y= depth of flow

h= mean depth of flow in channel

a= maximum amplitude of the imposed wave.

ω=2Л /T ,angular velocity

T= time period

t= the time

V= the channel velocity

L= length of channel

K=ω/Ce =2Л /Lo, the wave number

Ce= (g h) ½, the wave celerity, and

Lo= the wave length

The initial velocities were set as: -

$$V=-[a\ Ce / \{h \cos (kL)\}] \sin [k (L-k)] \quad \ldots\ldots (4.3)$$

The initial depths were set a constant and equal to mean depth of flow in channel. This channel is a frictionless tidal channel with: -

a=0.2

h=2m

L=160m

Lo=886m

The upstream and downstream boundary conditions can be established by substituting (x=0) and (x=L) respectively as: -

$$Y=h+a \sin (\omega t) \quad \ldots\ldots (4.4)$$

V=0

The fluctuation of depth and velocities at mid section represented by using the fully implicit (α=1) and Crank-Nicolson (α=0.5) with t=20 second and T=200 second.

Figure (4.1) and Figure (4.2) shows a comparison between the analytical data and the hydrodynamic model results, it is clear from figures (4.1) and (4.2).

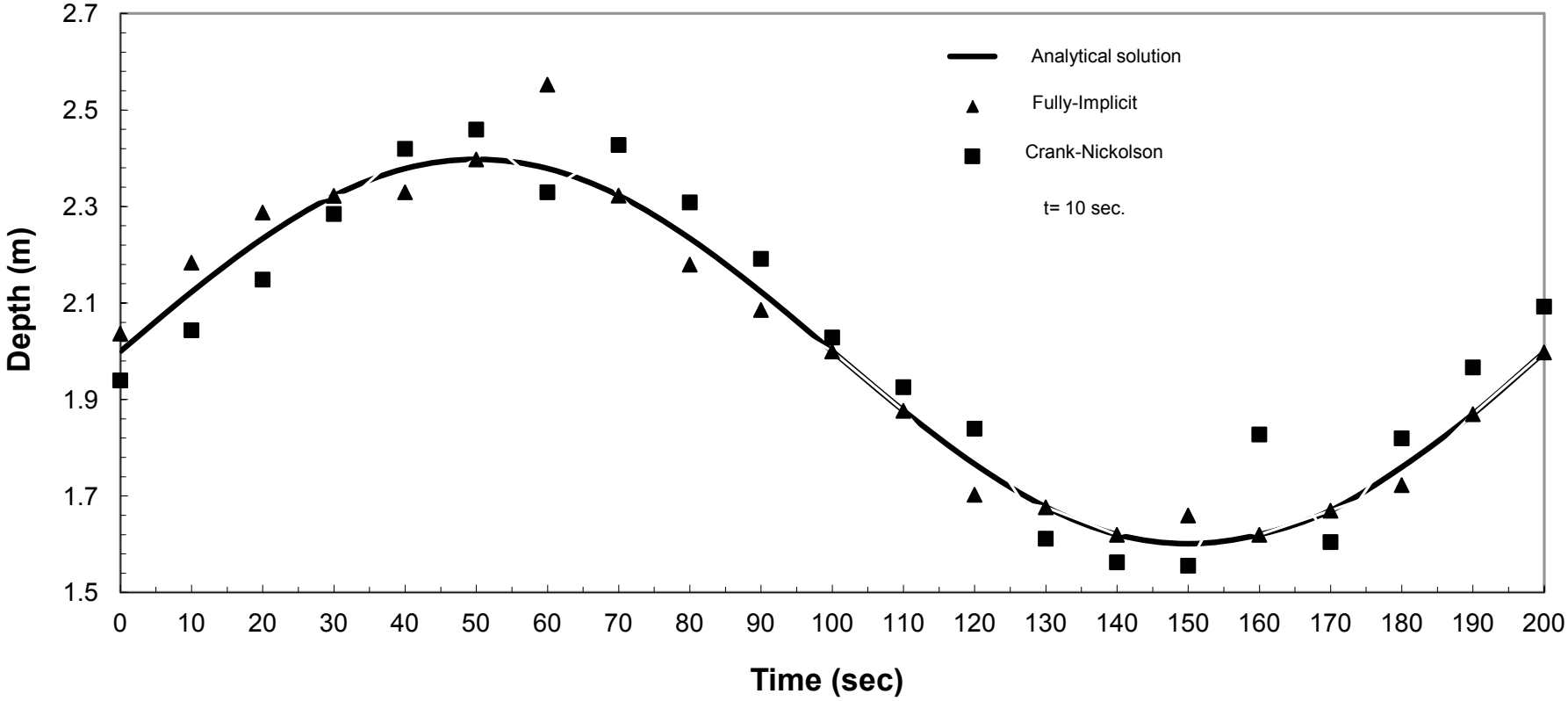

FIG. (4.1) TYPICAL MID SECTION DEPTH FLUCTUATION FOR FRICTIONLESS TIDAL CHANNEL AT ONE END CLOSED

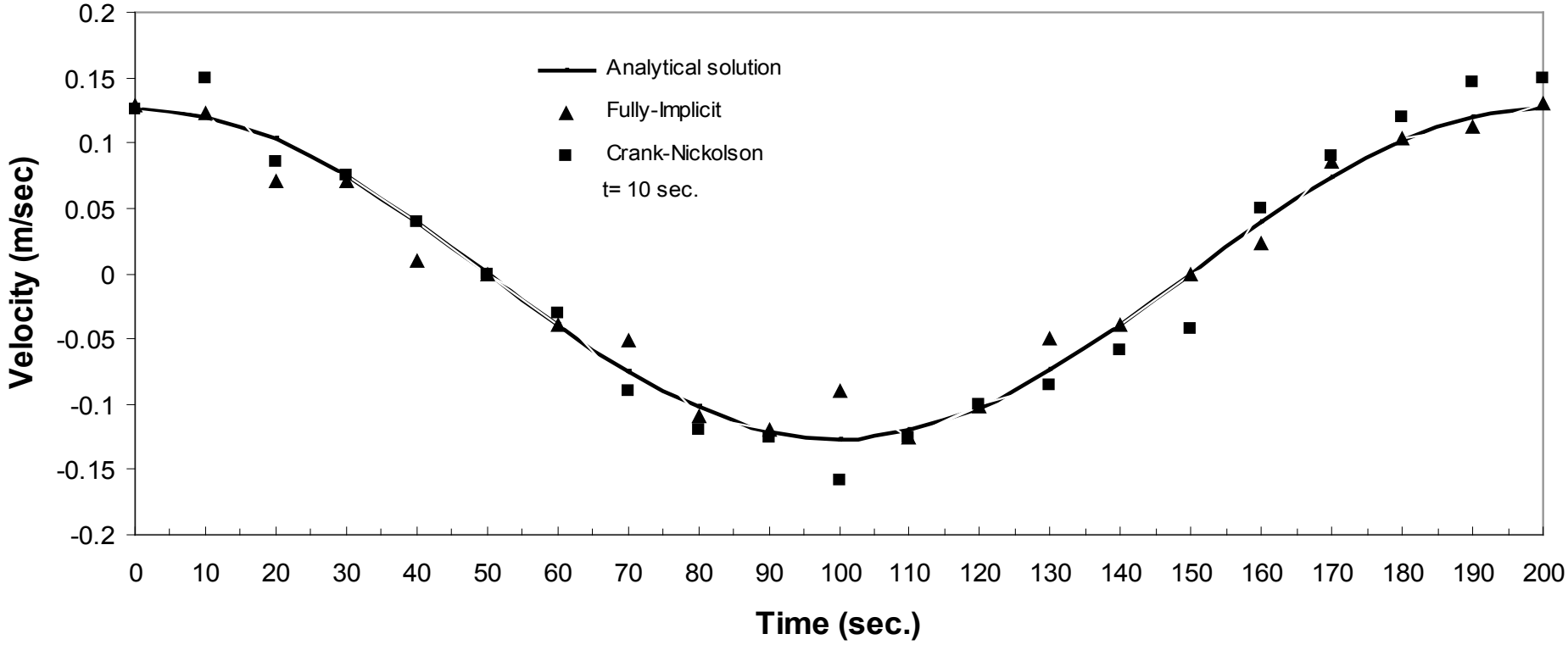

FIG. (4.2) TYPICAL MID SECTION VELOCITY FLUCTUATION FOR FRICTIONLESS TIDAL CHANNEL AT ONE END CLOSED.

that the fully implicit scheme gives more acceptable results than that of Crank-Nicolson.

4.3 Application of Morphological Model

The simulation of morphological changes in river bed can be achieved after the hydrodynamic model was coupled with the morphological model. The block diagram shown in figure (4.3) represents the linked models in a systematic mode. For the first run of the hydrodynamic model to Euphrates River in study reach, it took (54) iterations for convergence to the required solution. After maintaining the steady state condition of the hydrodynamic model, the morphological model was run by using (u, v, h) and the initial bed level of river to estimate new bed level of river.

After new bed level of river was formed with correction for depth of water values, the two-dimensional hydrodynamic model was run again.

4.4 Euphrates River Application

The two-dimensional hydrodynamic model which developed in chapter three was applied to Euphrates River study reaches upstream Ramadi barrage.

4.4.1 Description of the Study Reach

The study reach under consideration is (2.8 km long) and lies between Ramadi barrage to Palestine Bridge on highway road as showing in fig. (4.4). The region of study was divided to (20) cross-sections and this region was divided to (239) of triangular elements with (147) nodes as shown in fig. (4.5) (see appendix B). The data of bed elevation of river in study region was obtained from the data of General Committee of Surveying in 3/10/1999 as shown in cross-sections, figures (4.6-A), (4.6-B), (4.6-C), (4.6-D), (4.6-E), (4.6-F), and (4.6-G).

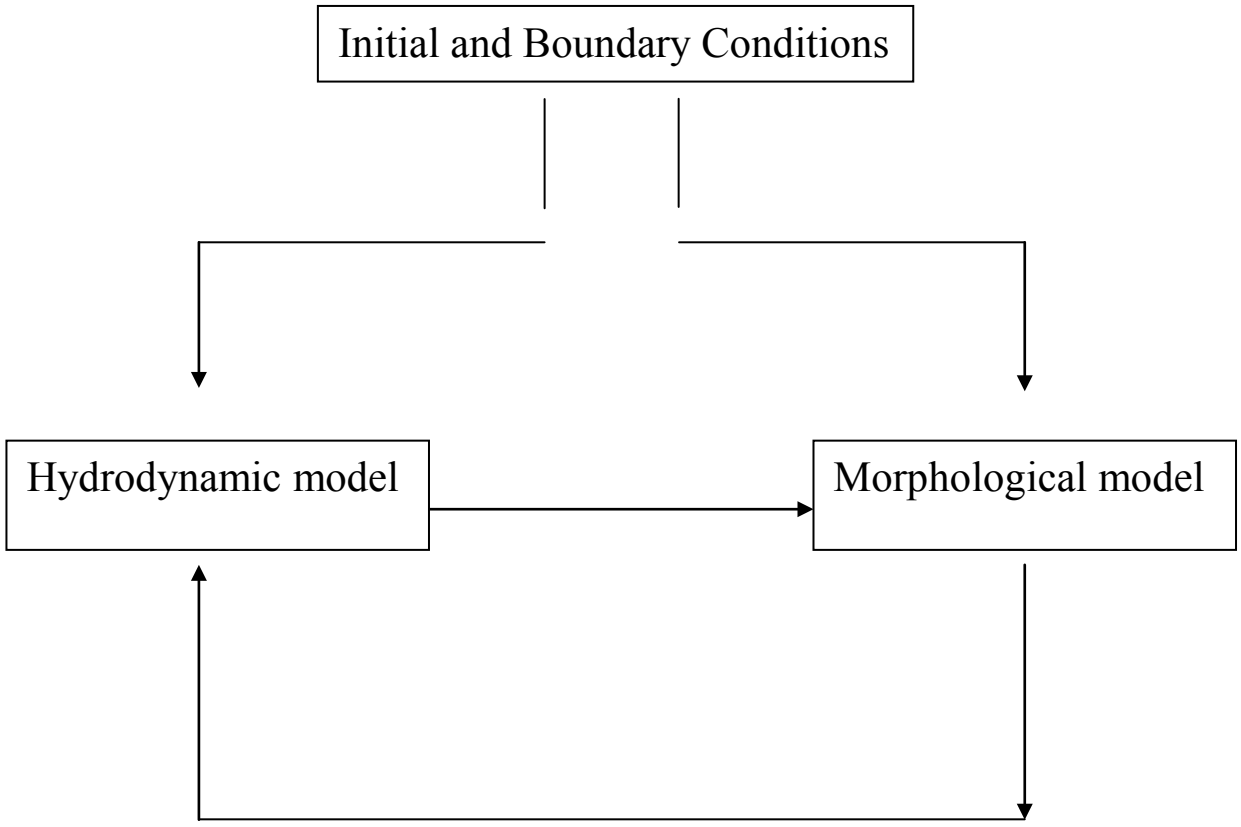

FIG (4.3) LINKED BLOCK DIAGRAM

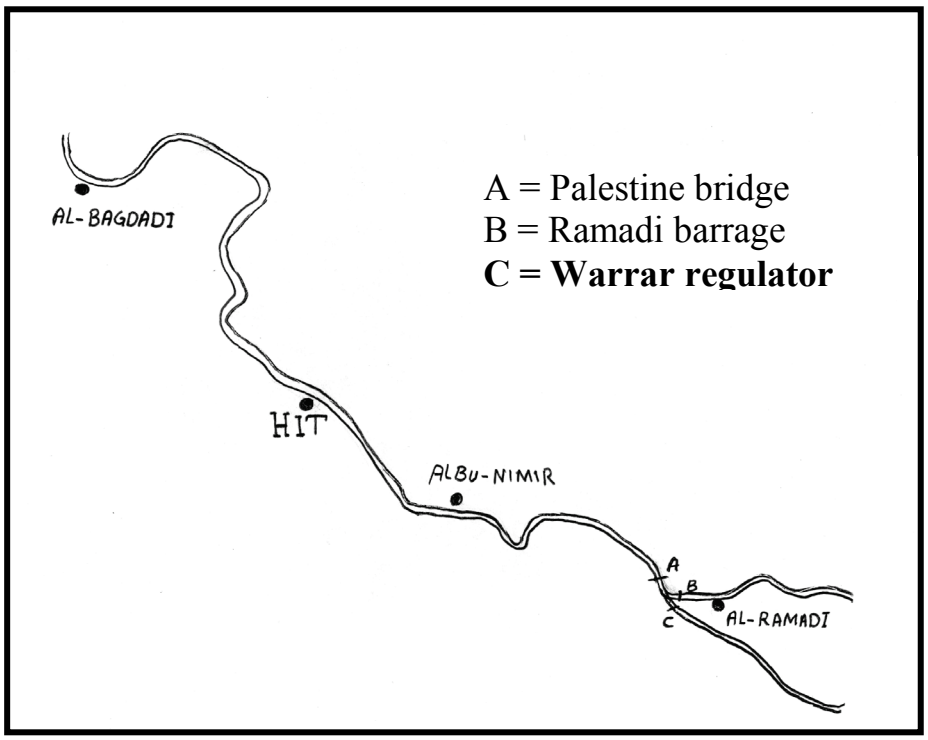

FIG. (4.4) GENERAL LAYOUT OF EUPHRATES RIVER REGION UPSTREAM OF RAMADI BARRAGE

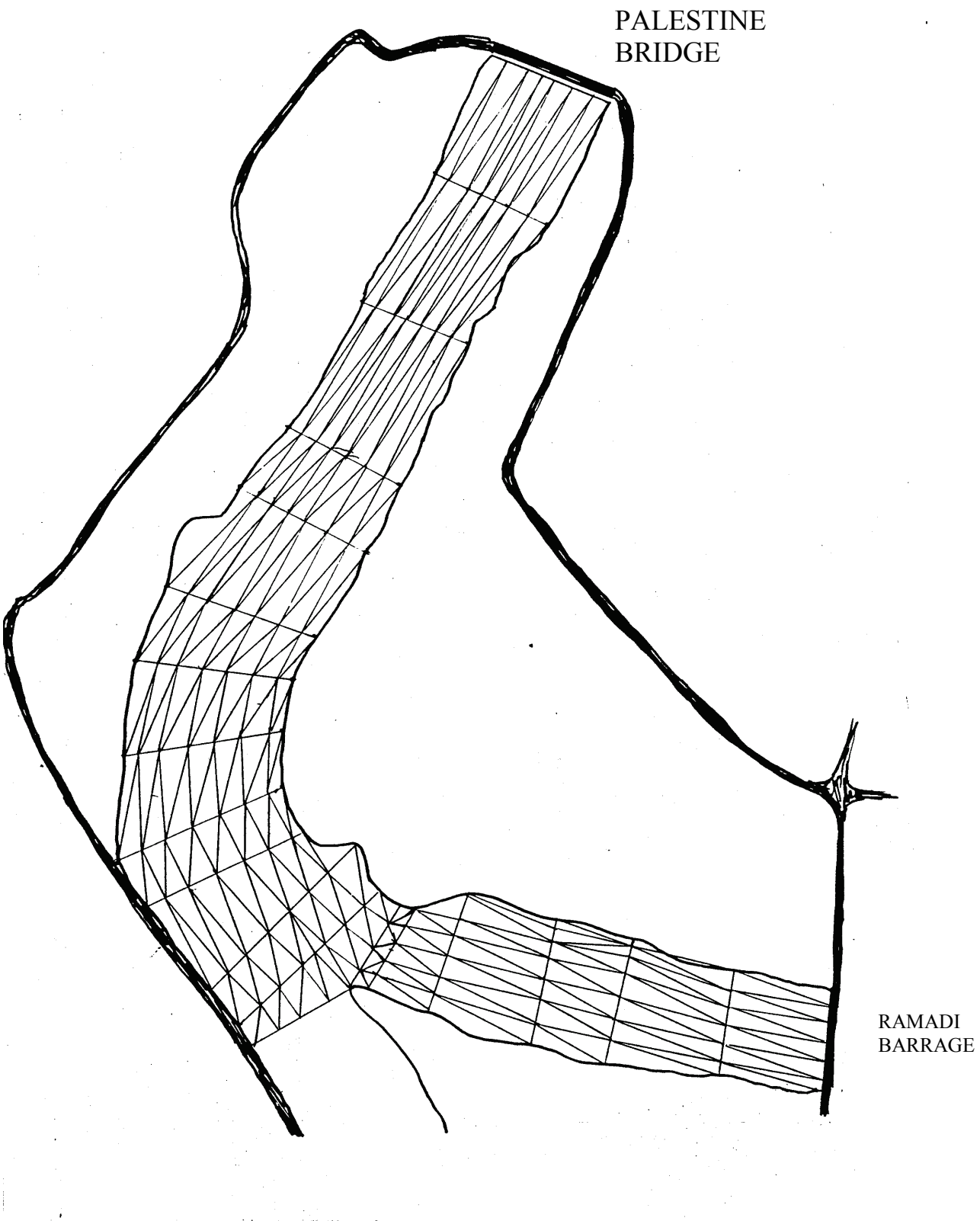

FIG. (4.5) FINITE ELEMENT DISCRETIZATION

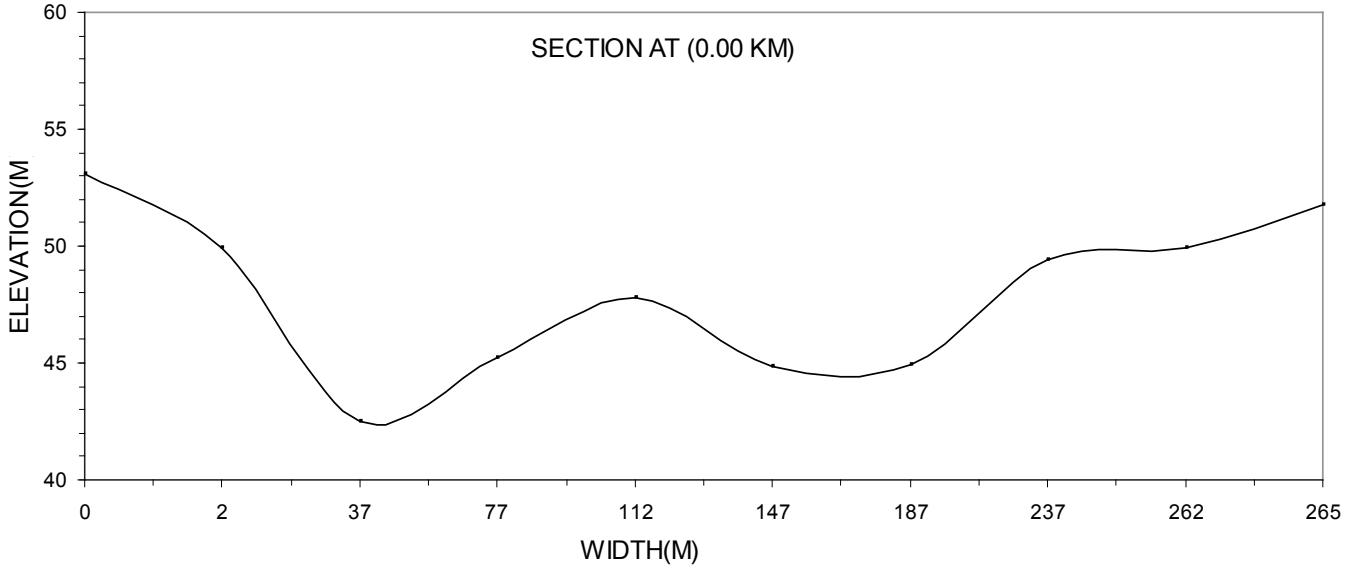

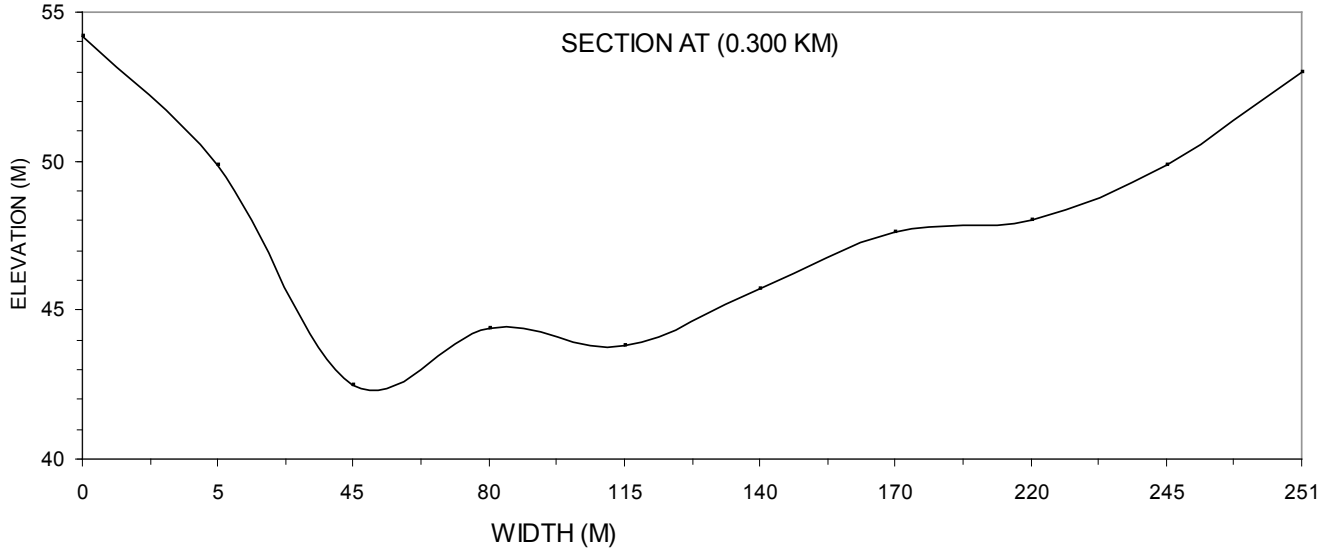

FIG. (4.6-A) INITIAL BED ELEVATIONS FOR EUPHRATES RIVER

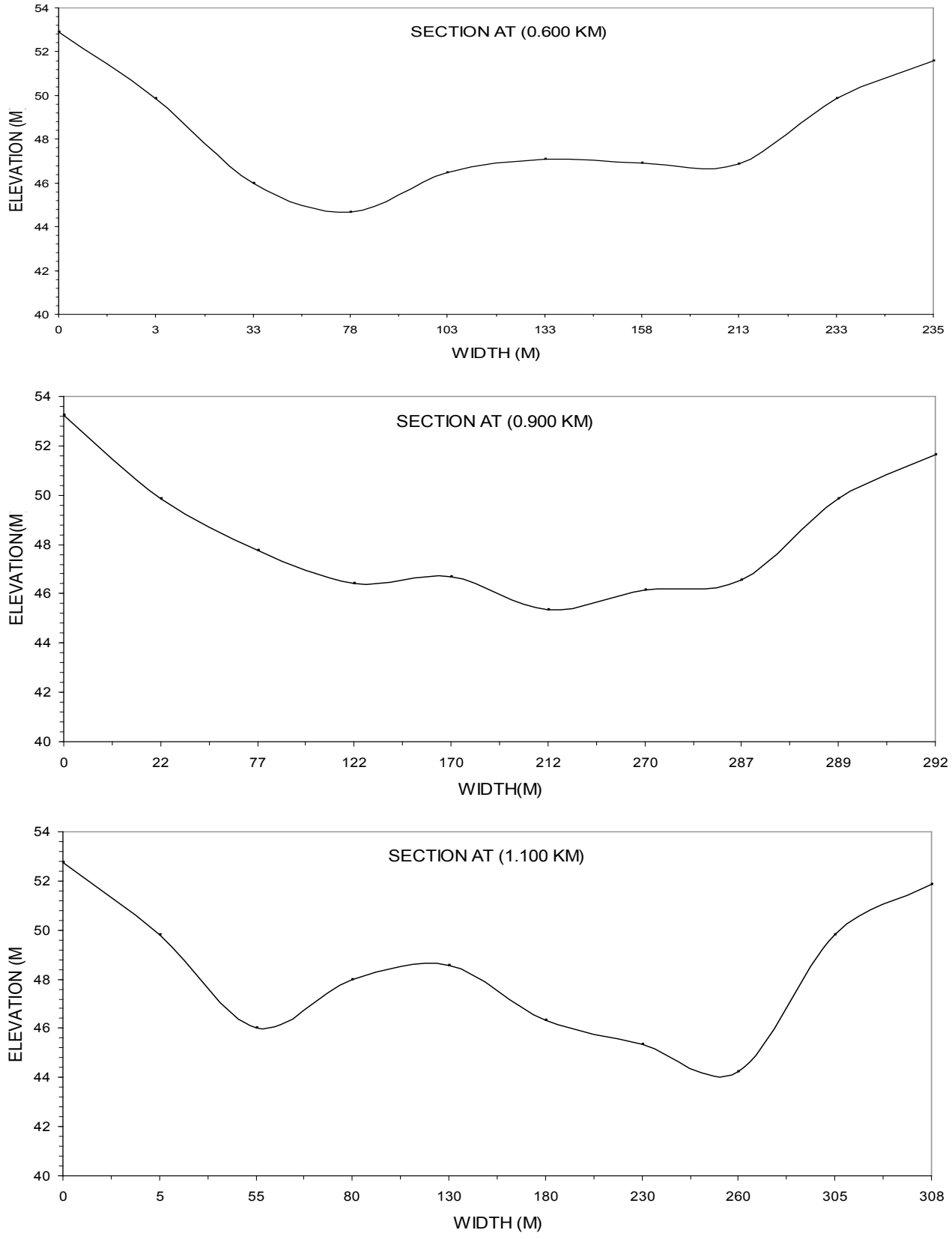

FIG. (4.6-B) INITIAL BED ELEVATION FOR EUPHRATES RIVER

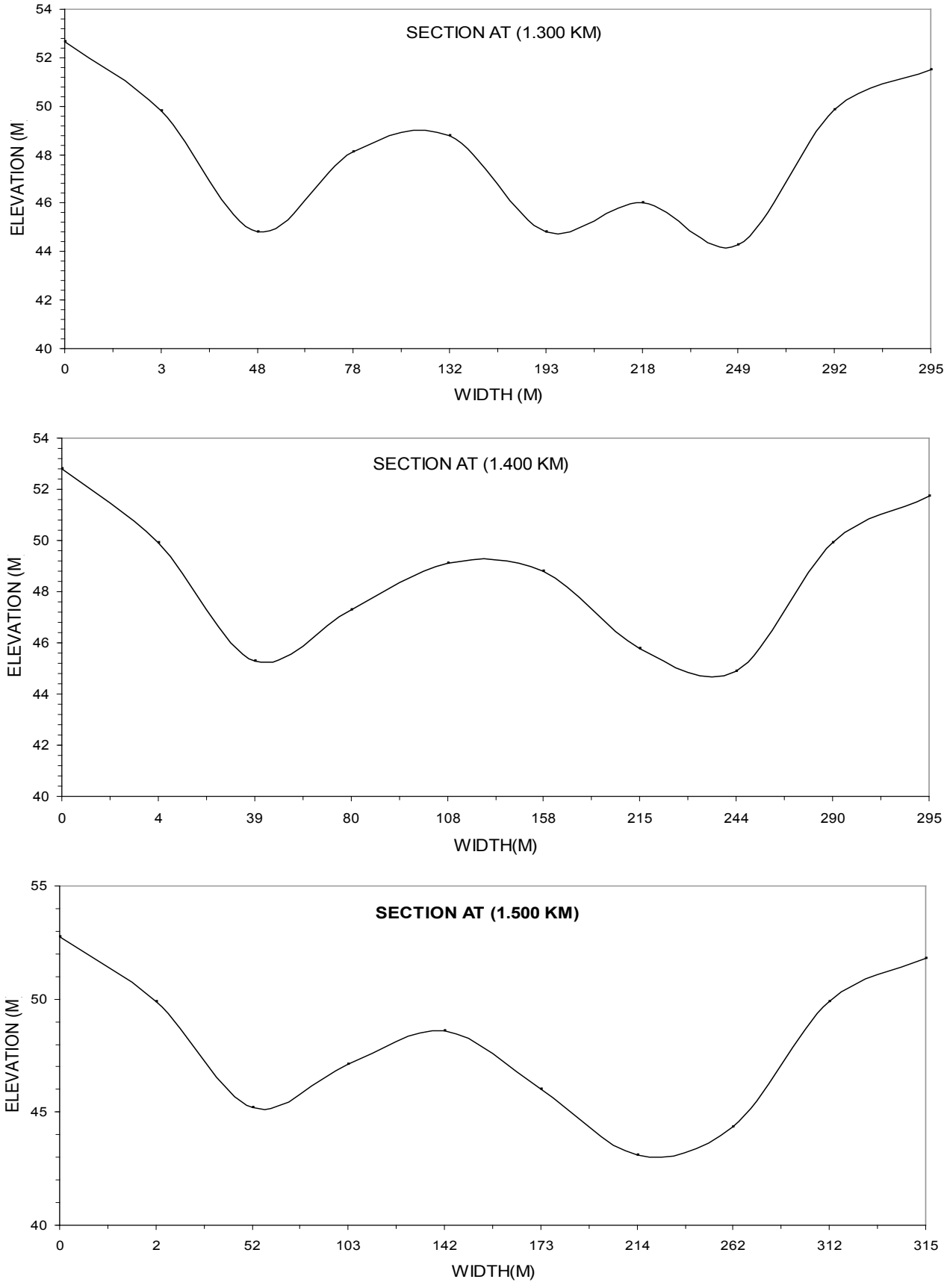

FIG. (4.6-C) INITIAL BED ELEVATION FOR EUPHRATES RIVER

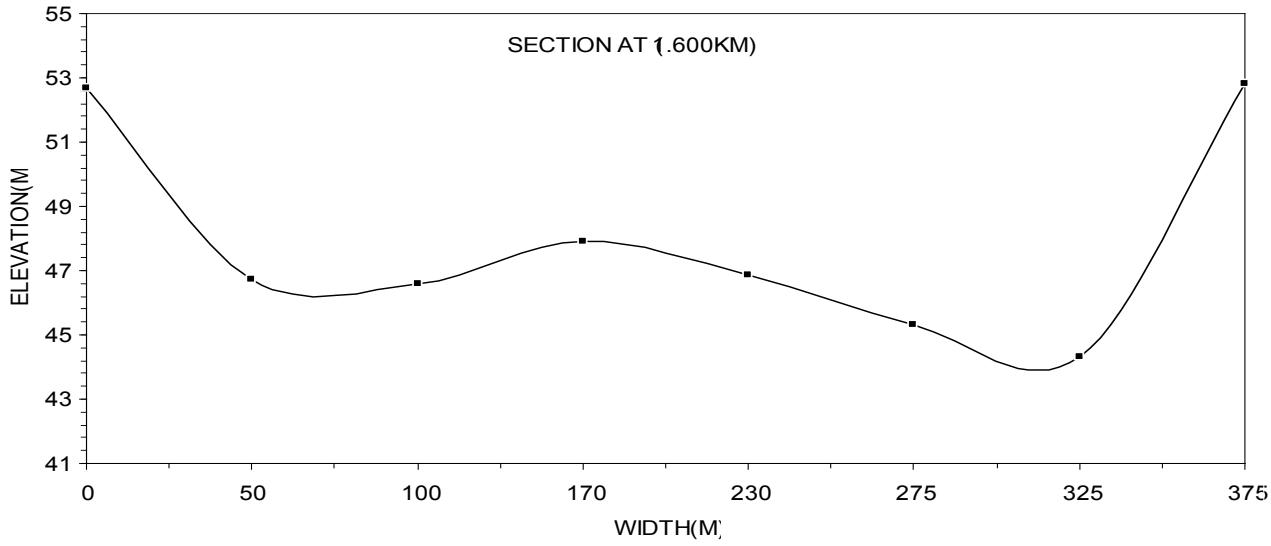

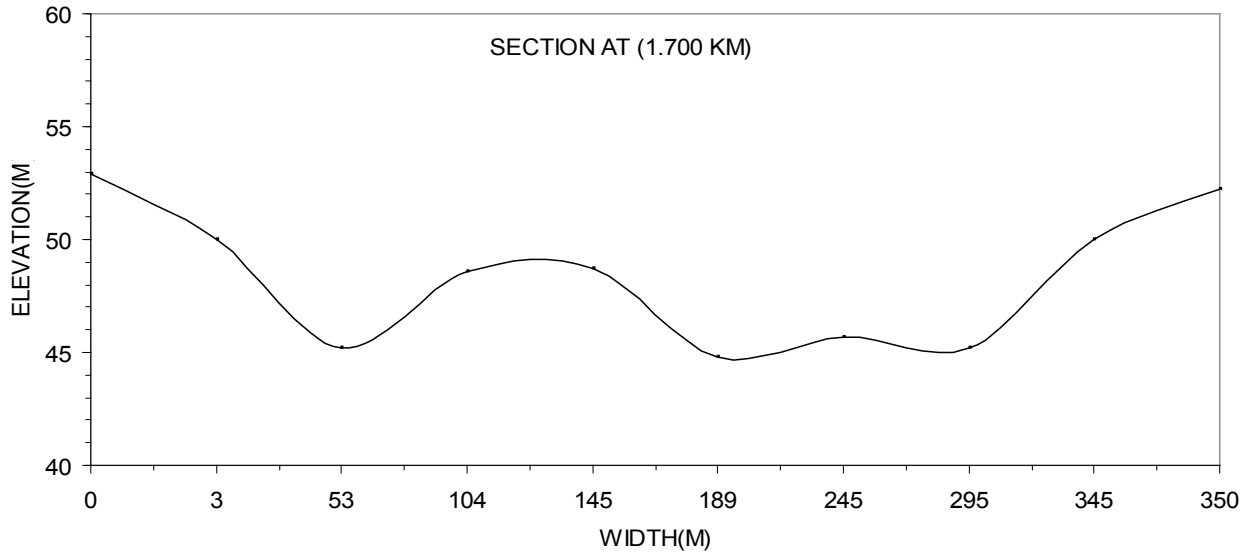

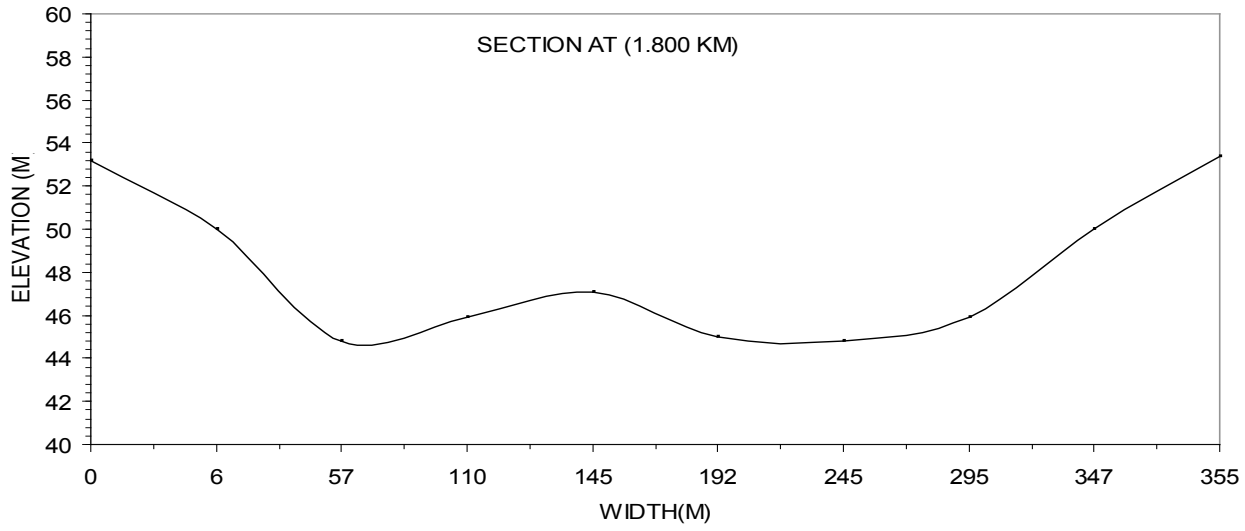

FIG. (4.6-D) INITIAL BED ELEVATION FOR EUPHRATES RIVER

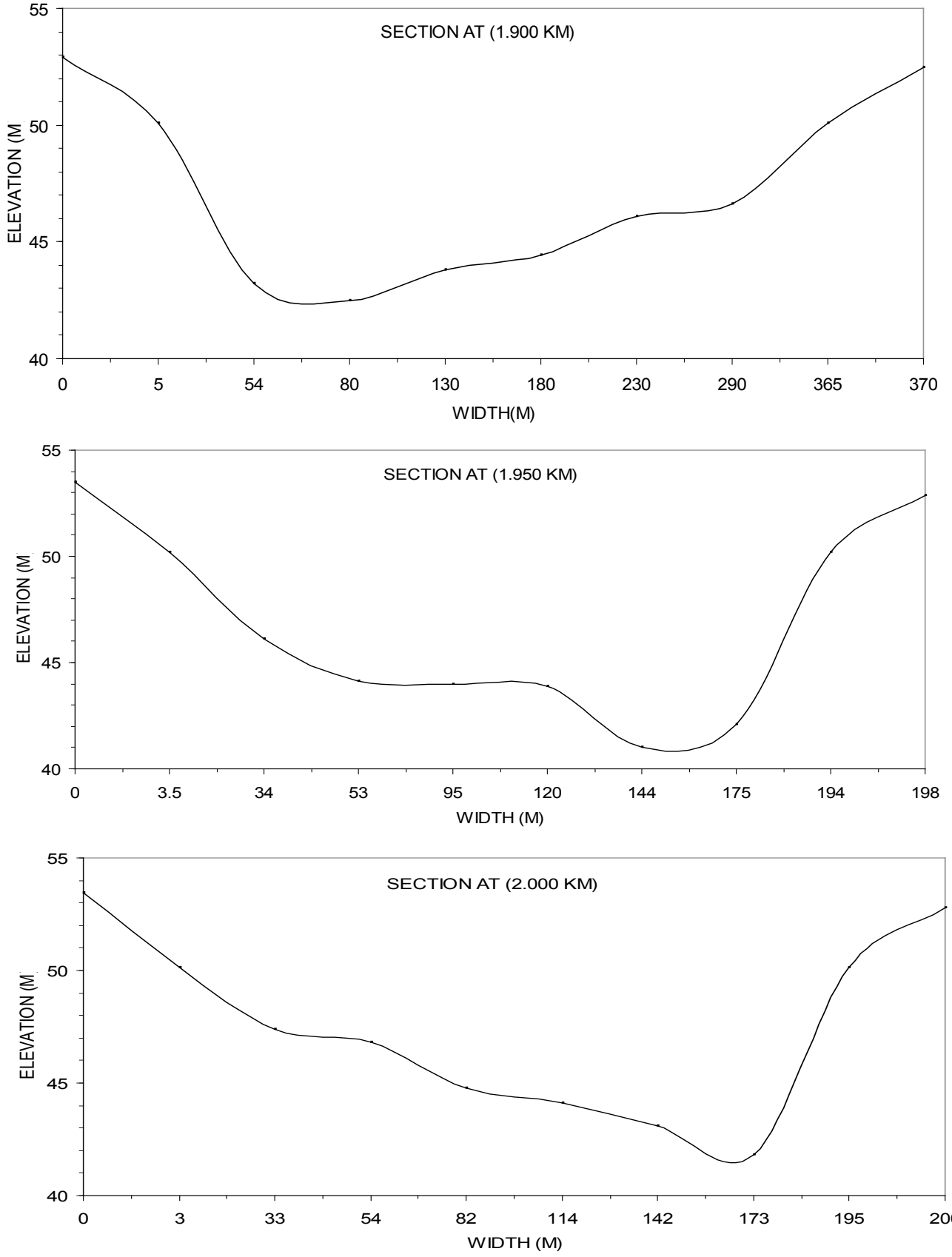

FIG. (4.6-E) INITIAL BED ELEVATION FOR EUFRATES RIVER UPSTREAM BOUNDARY CONDITION

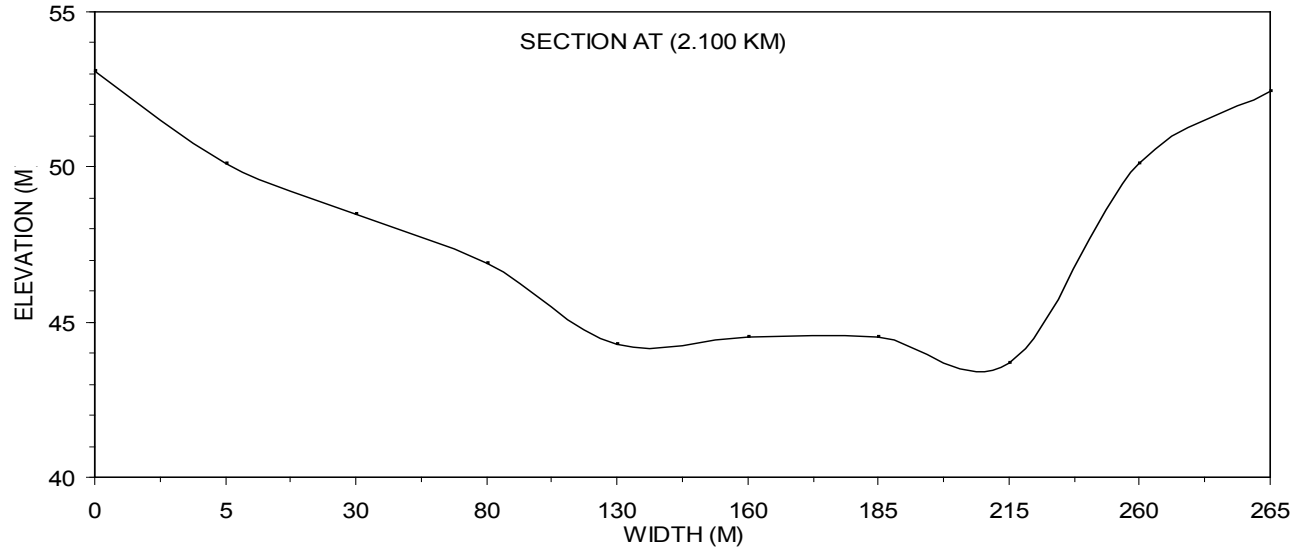

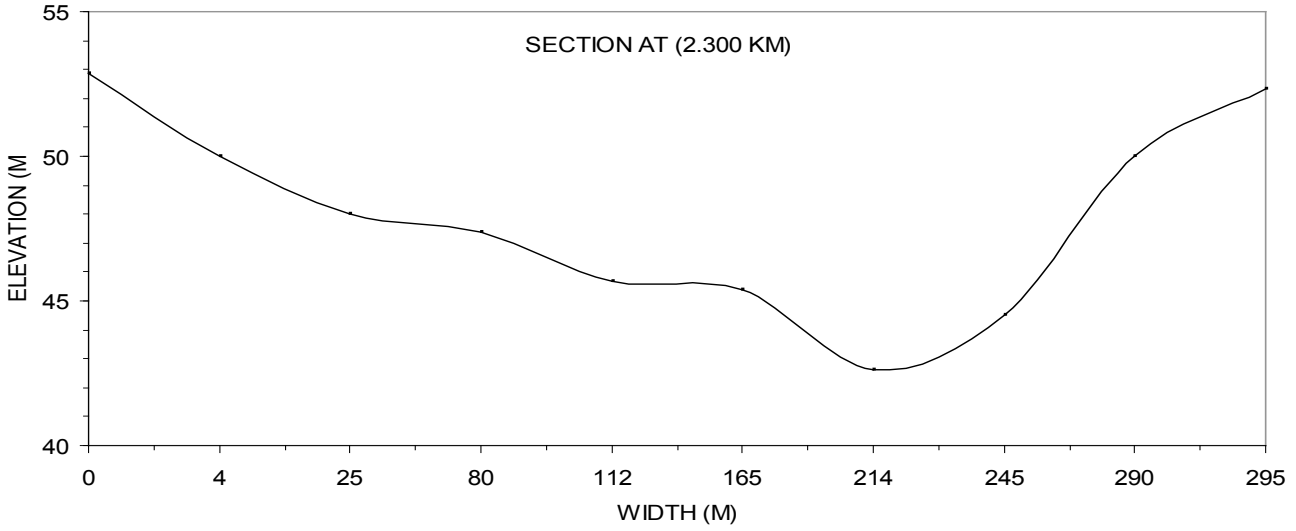

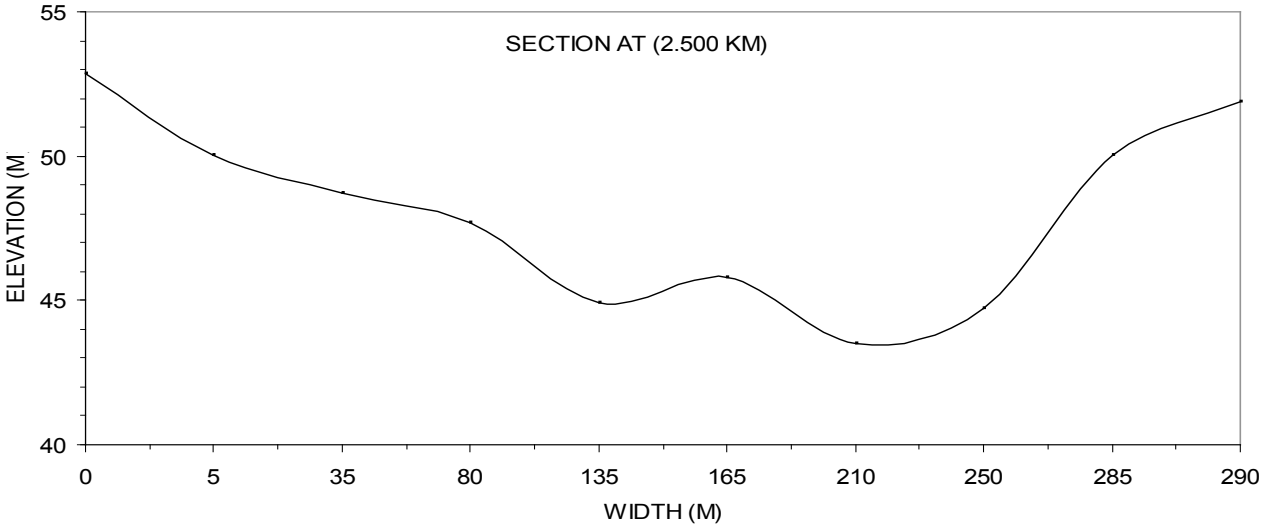

FIG. (4.6-F) INITIAL BED ELEVATION FOR EUPHRATES RIVER

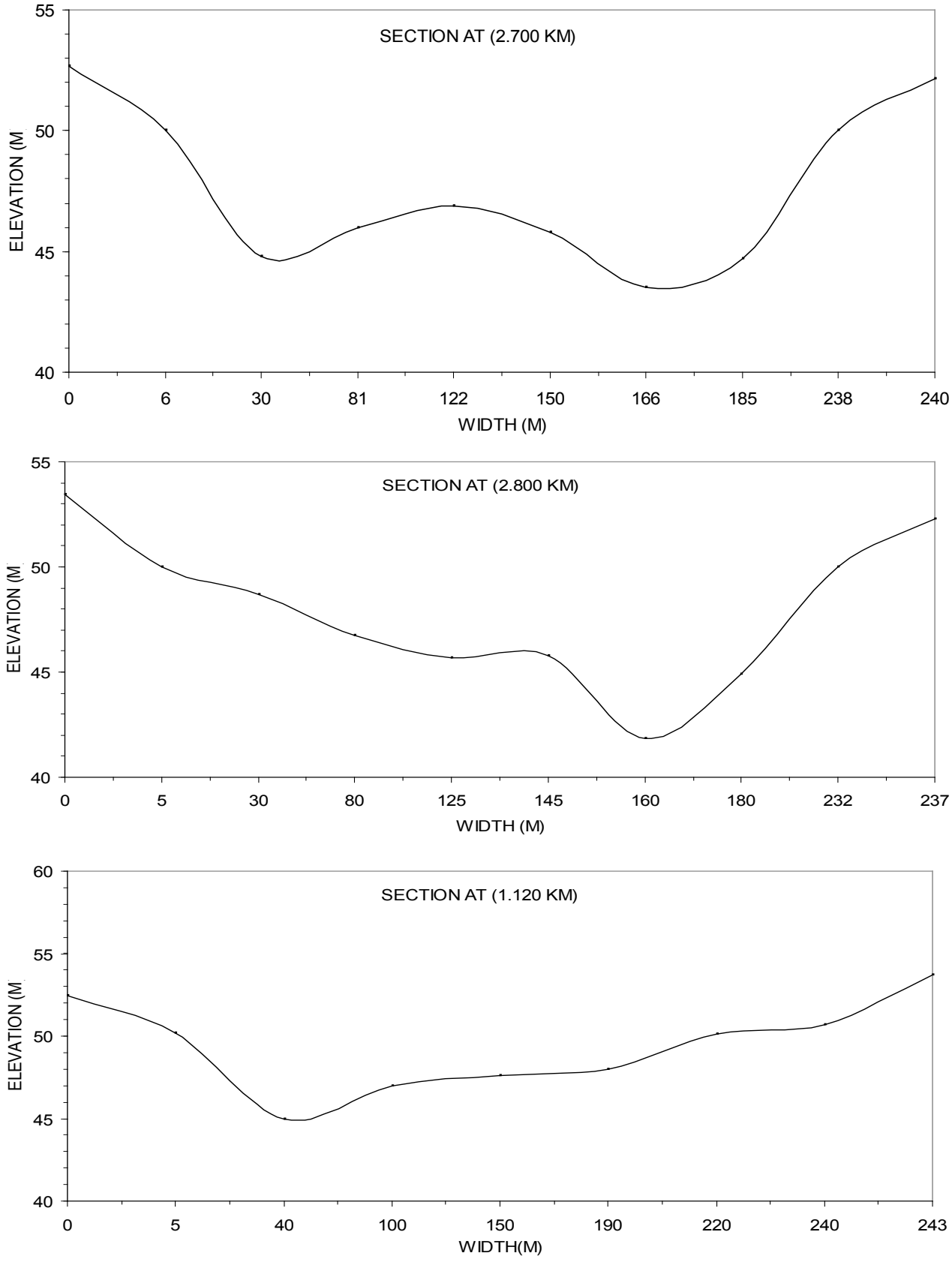

FIG. (4.6-G) INITIAL BED ELEVATION FOR EUPHRATES RIVER

4.4.2 Description of Input Data

Discharge hydrographic and water level surface (stage hydrograph) were taken from the head office of AL-Ramadi Barrage as shown in fig. (4.7-A), (4.7-B) and fig. (4.8-A), (4.8-B) respectively.

The velocity in X- and Y- directions at each section in initial condition can be obtained from discharge as following(see appendix B): -

$q=Q/B$ Where:

q= The discharge per meter width of river

B= The width of river

Q= The discharge

$V=q/h\ av.$

Where

V= is the velocity at longitudinal direction of channel

h av.=average depth of section of river.

$u=V\ Cos(\theta)$

$v=V\ Sin(\theta)$

$\theta=Tan^{-1}(y/x)$

The depth of water at each node in initial conditions can be obtained from the stage hydrograph and the cross-sections of the study region of river. Boundary conditions of hydrodynamic model is flow velocity at upstream of study region, it can be found by using discharge hydrograph. Depth of water as a downstream boundary conditions of study region, can be found from stage hydrograph.

No boundary conditions are needed to solve the morphological model. The mean particle size (d_{50}) which was set to (0.1138 mm) and the density of sediment was (2660kg/m^3) and the porosity of sediment was (λ=0.45)for sand bed river. (Khalaf 1988)

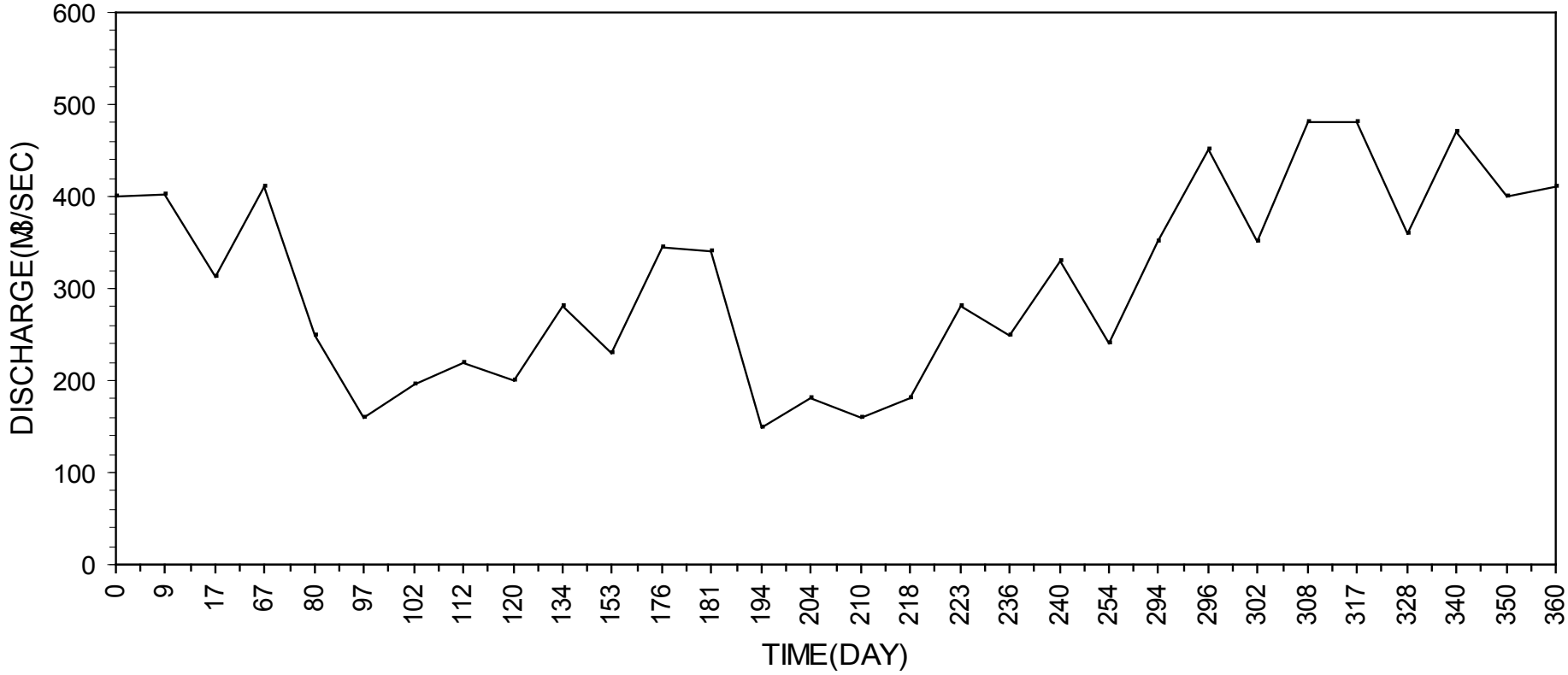

FIG. (4.7-A) DISHARGE HYDROGRAPH UPSTREAM BOUNDARY CONDITION

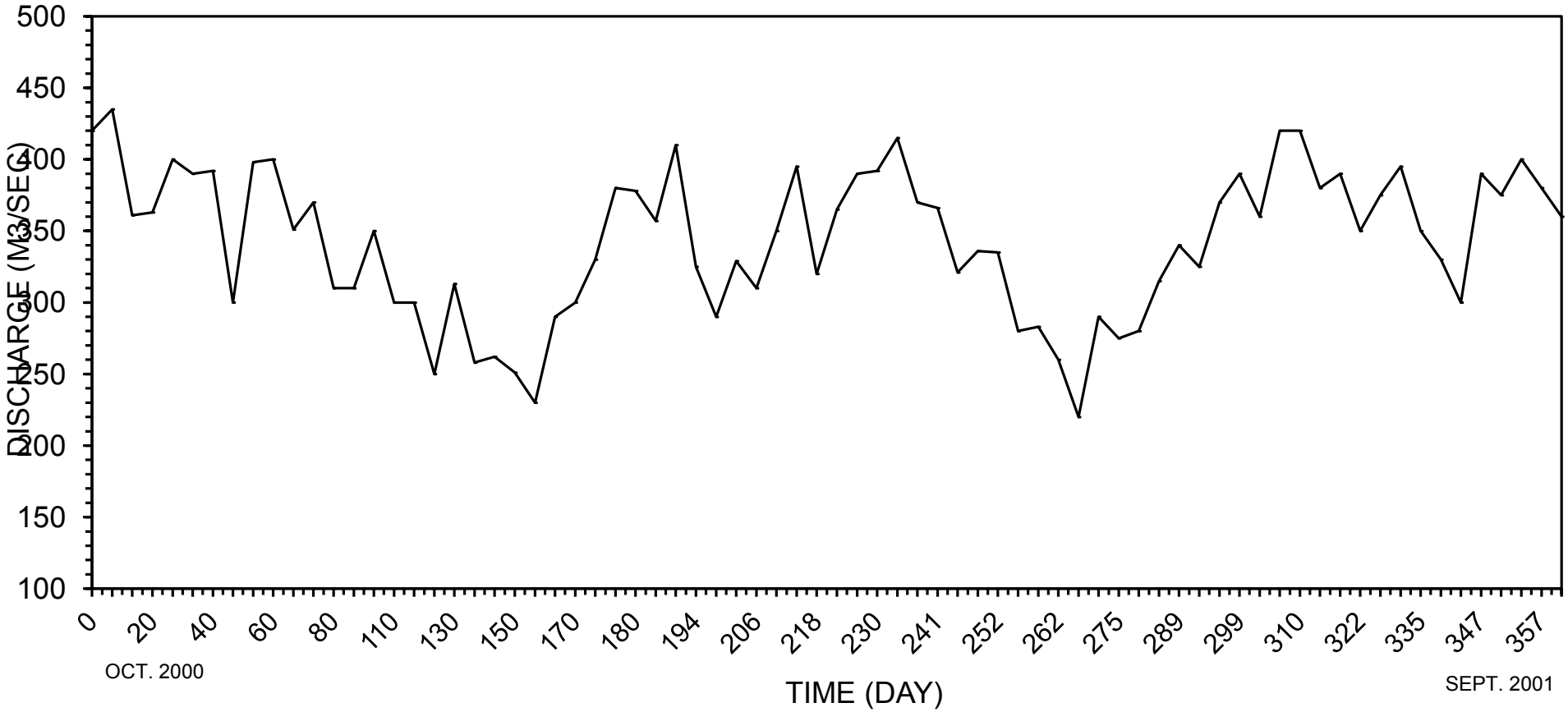

FIG.(4.7-B) DISCHARGE HYDROGRAPH UP STREAM BOUNDARY CONDITION

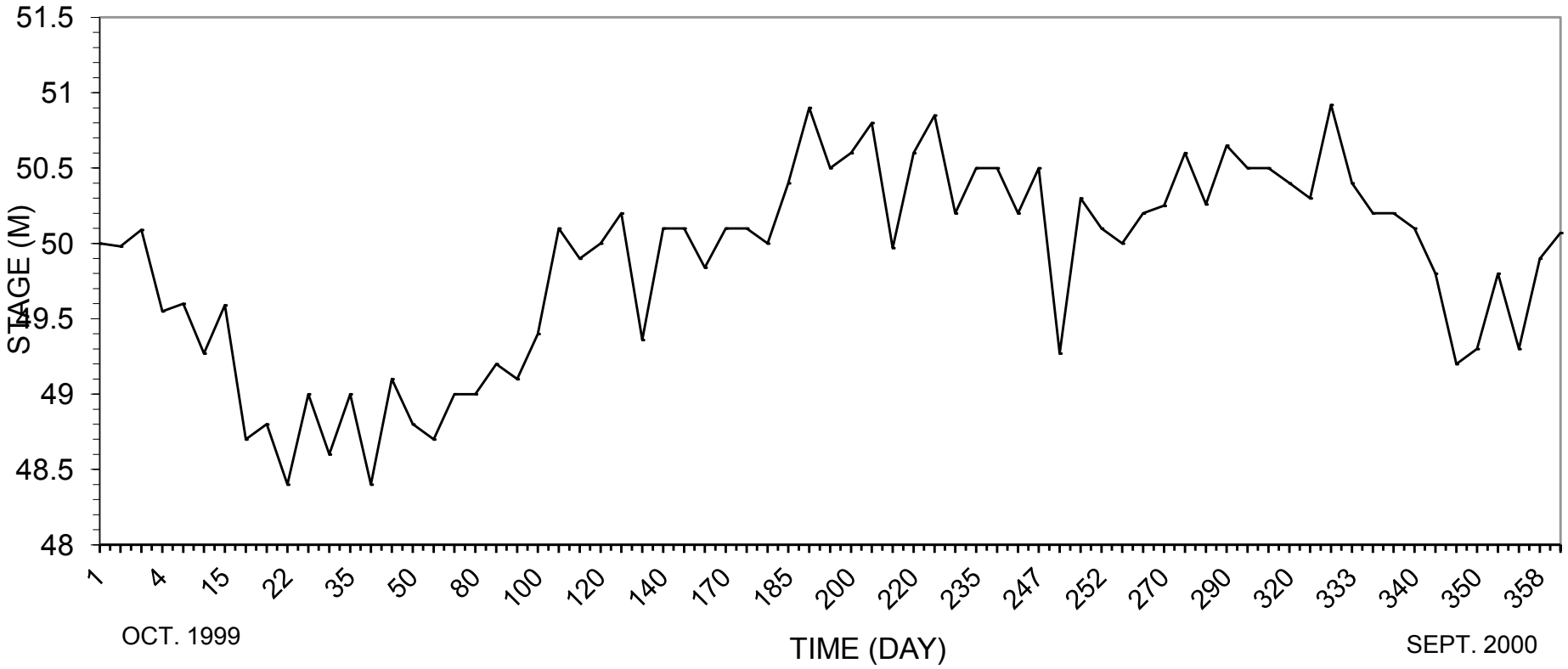

FIG(4.8-A) STAGE HYDROGRAPH UPSTREAM RAMADI BARRAGE (DOWN STREAM BOUNDARY CONDITION)

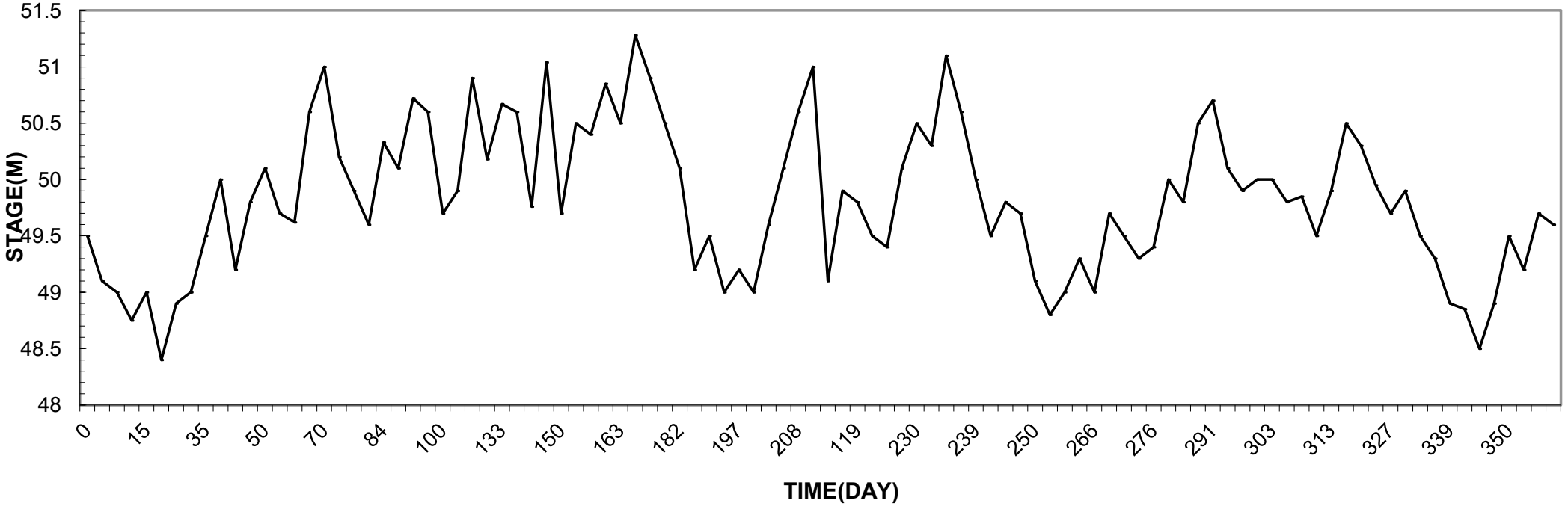

FIG. (4.8-B) STAGE HYDROGRAPH UPSTREAM RAMADI BARRAGE (DOWN STREAM BOUNDARY CONDITION)

4.4.3 Model calibration

An important step in calibration process is the determination of the appropriate values of the parameters that control the numerical computation operation. These parameters are Manning roughness coefficient (n) and the weighting factor (α). It has an effect on the accuracy and stability of numerical model.

The iteration process, which involved to solve the system of equations is effected in calibrating of the numerical model, therefore, it is necessary to specify tolerance limits for the values of variables within which iteration process is terminated. The iteration is usually terminated in hydrodynamic model if the changes in stage and velocity values in two consecutive iteration are within (± 5%).

4.4.3.1 Effect of Weighting Factor (α) and Manning Roughness Coefficient (n)

The weighting factor (α) and Manning coefficient of friction (n) have an effect on the accuracy and stability of the numerical model. The weighting factor (α) have a different values ranged between (0) and (1).

Mohammed (1994) and AL-Eoubaidy et.al. (1997) have used different values of Manning coefficient ranged between (0.027 and 0.034) to the calibration of numerical model of Euphrates river. For the purpose of model calibration in present study, the stage hydrograph measured at node (19) in section at 0.600 km from upstream boundary condition are used. Eleven reading for the period of twenty days between (10/3/2001) to (30/3/2001) are used for this purpose.

A series of computation are performed and repeated with each value of weighting factor which conducted with five values of Manning coefficient (0.027, 0.028, 0.03, 0.033, 0.034), the result of simulation model with these

values of weighting factor and Manning coefficient are compared with observed stage hydrograph measured at the above specified section.

Figures (4.9), (4.10), (4.11), (4.12), (4.13) and (4.14) present comparison between observed and calculated stage values using different values of (n).

Table (4.1) shows the mean square error (mse) of results with each value of (n) used at each spesified α . It was used as an indicator of results accuracy with respect to stage. Table (4.1) present that the smallest (mse) at (n=0.03 and α=0.7) .

4.4.4 Model Verification

Verification of hydrodynamic and morphological models expresses the real tests of numerical solution to estimate the flow and bed elevations variations by employing a set of observation. For the purpose of the simulation model verification, the stage hydrograph along twenty days started from (5/8/2001) to (25/8/2001) at node no. (27) at section 0.900 km upstream boundary condition are used.

The hydrodynamic model was run used values of weighting factor (α) and Manning coefficient (n) which resulted from calibrating part, the values used are (α =0.7 and n=0.03). The calculated and observed stage is presented in figure (4.15) which shows good agreement between observed and calculated values.

The final result of full solution of set of hydrodynamic and morphological models to Euphrates river in study reach after two year can be shown in figure (4.16-A), (4.16-B), (4.16-C) for bed level configurations.

The velocity fields for entire reach are shown in figure (4.17) where arrows can show the directions and magnitude of the velocities.

Figure (4.18-A), (4.18-B), (4.18-C) shows the bed level of Euphrates river study reach after (3) years.

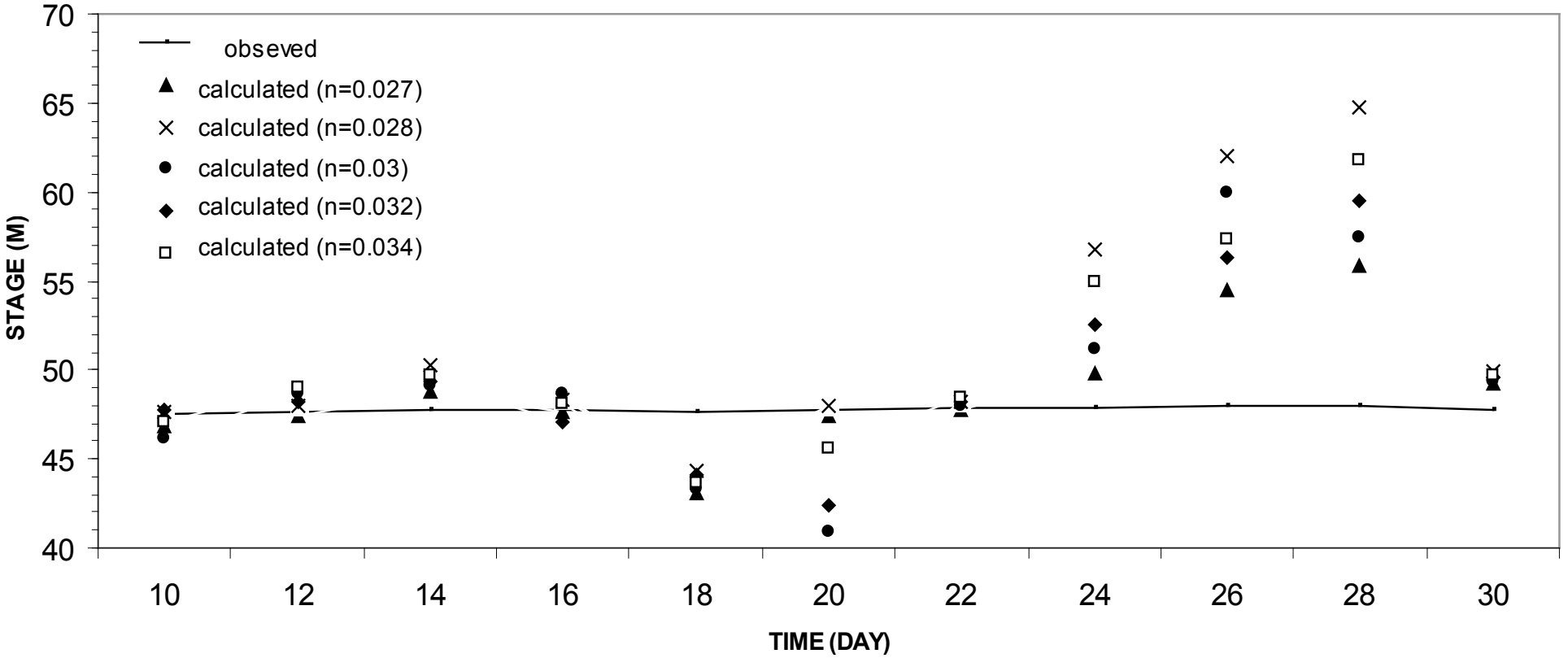

FIG. (4.9) OBSERVED AND CALCULATED STAGE HYDROGRAPH AT NODE NO. (19) IN SECTION AT (0.600 KM) UPSTREAM BOUNDARY CONDITION WITH α=0

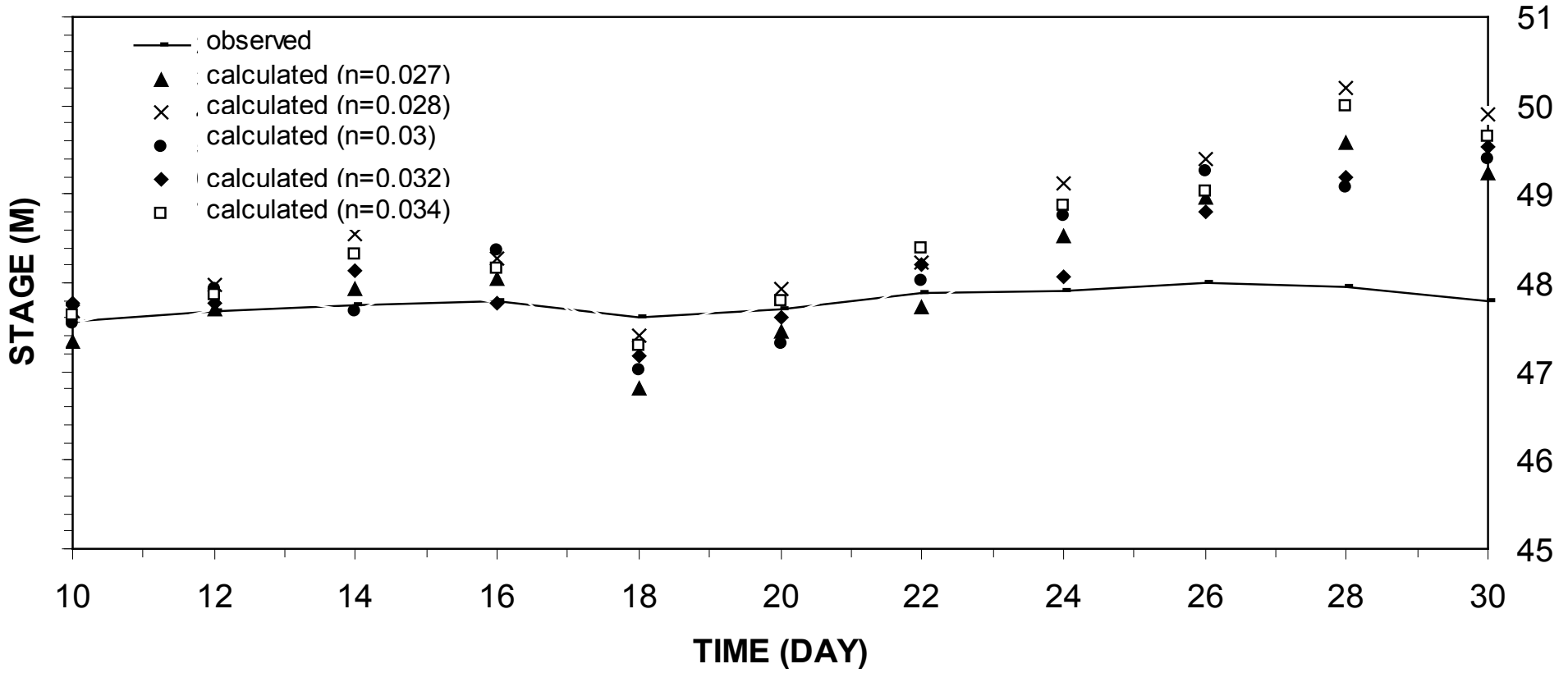

FIG. (4.10) OBSERVED AND CALCULATED STAGE HYDROGRAPH AT NODE NO. (19) IN SECTION AT (0.600 KM) UPSTREAM BOUNDARY CONDITION WITH α=0.5

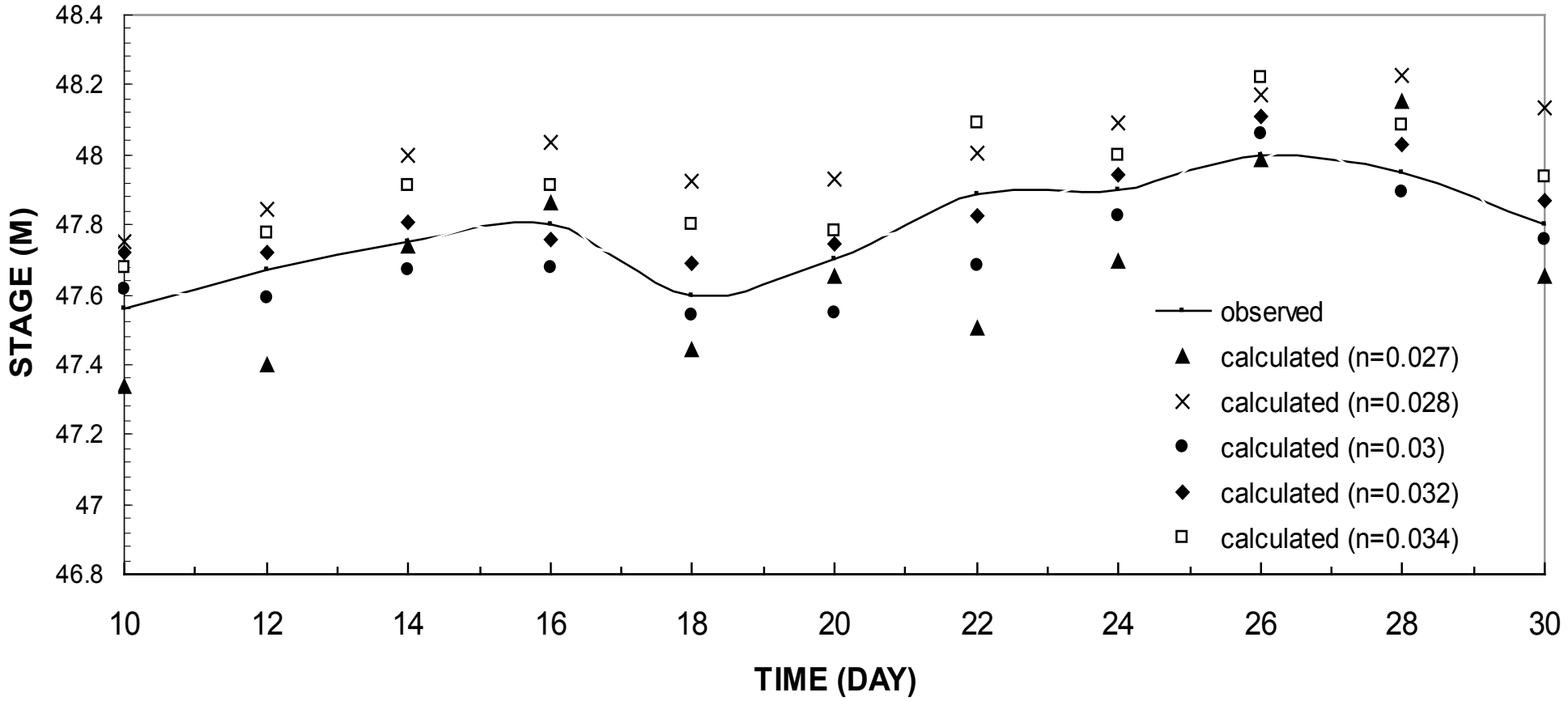

FIG. (4.11) OBSERVED AND CALCULATED STAGE HYDROGRAPH AT NODE NO. (19) IN SECTION AT (0.600 KM) UPSTREAM BOUNDARY CONDITION WITH α=0.67

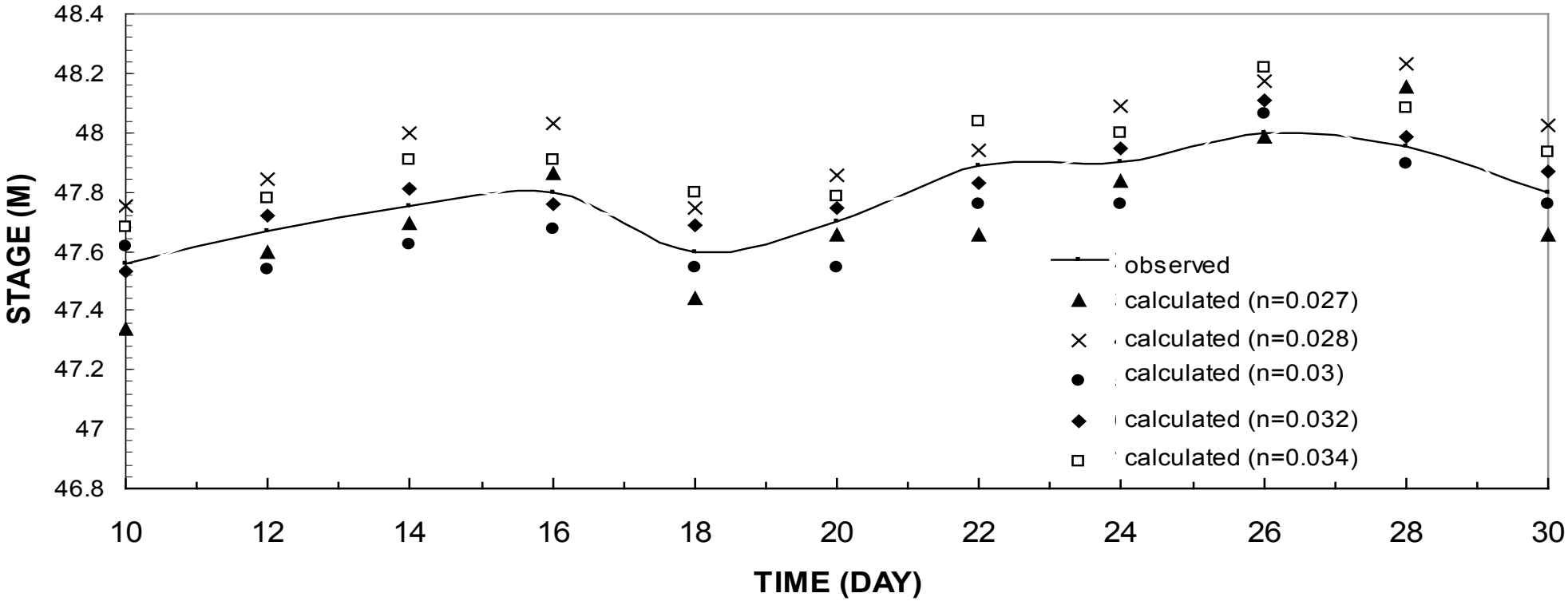

FIG. (4.12) OBSERVED AND CALCULATED STAGE HYDROGRAPH AT NODE NO. (19) IN SECTION AT (0.600 KM) UPSTREAM BOUNDARY CONDITION WITH α=0.7

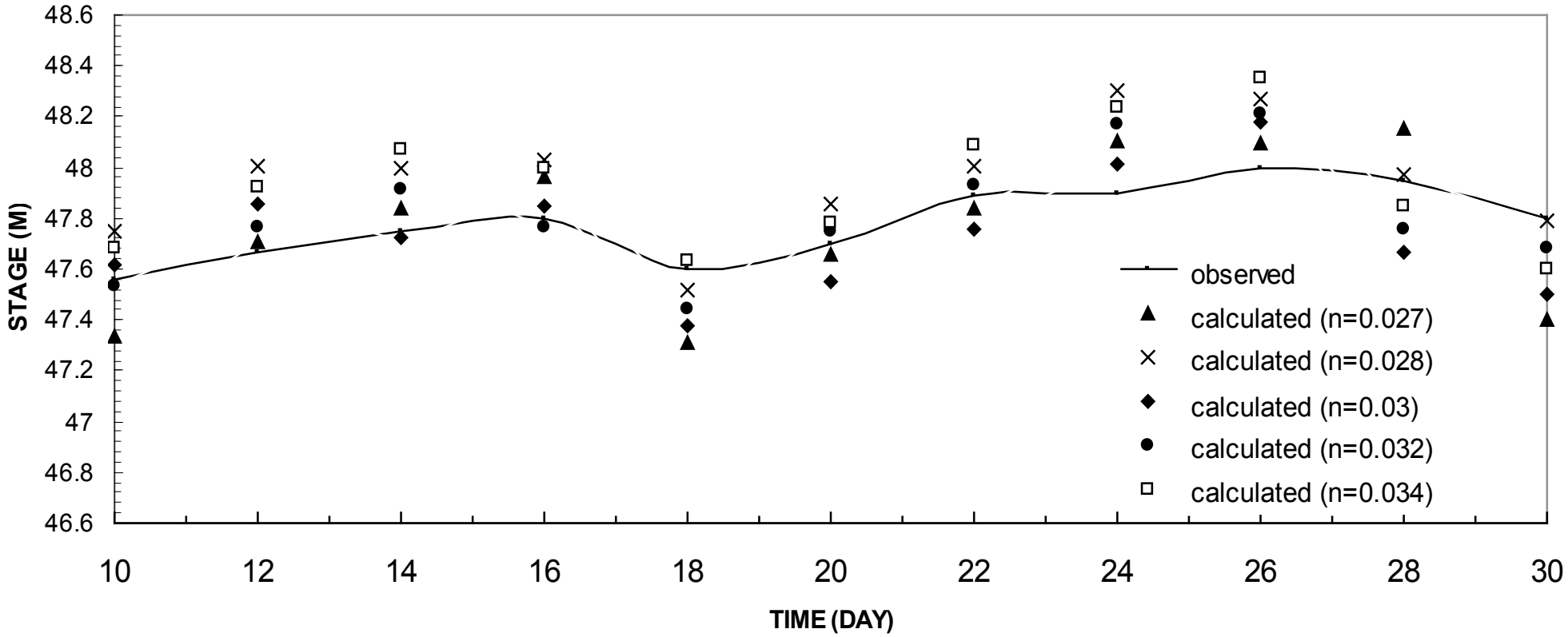

FIG. (4.13) OBSERVED AND CALCULATED STAGE HYDROGRAPH AT NODE NO. (19) IN SECTION AT (0.600 KM) UPSTREAM BOUNDARY CONDITION WITH α=0.8

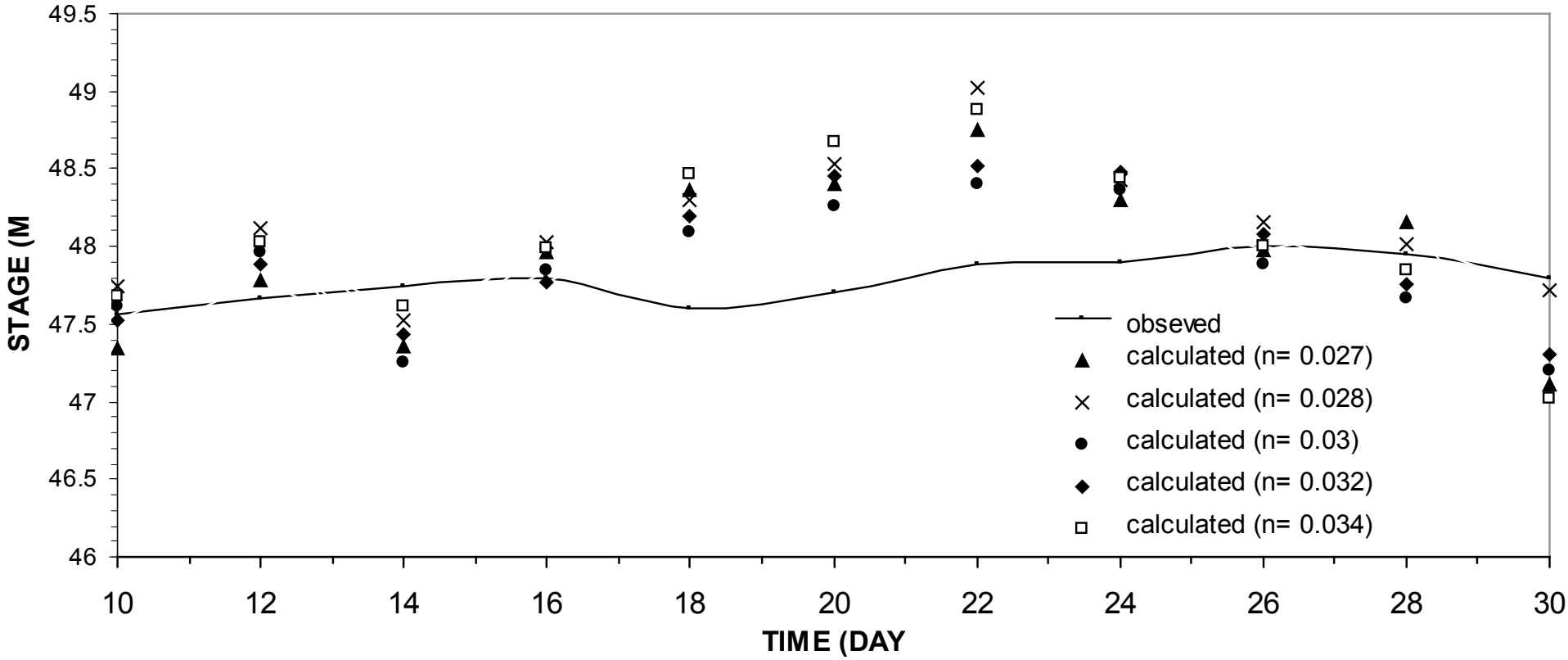

FIG. (4.14) OBSERVED AND CALCULATED STAGE HYDROGRAPH AT NODE NO. (19) IN SECTION AT (0.600 KM) UPSTREAM BOUNDARY CONDITION WITH α=1

Δt (hrs)	weighting factor (α)	Manning Roughness Coefficient (n)	mse
24	0	0.027	52.5
		0.028	32.6
		0.03	24.6
		0.032	28.72
		0.034	11.9
24	0.5	0.027	1.27
		0.028	0.95
		0.03	0.518
		0.032	0.63
		0.034	0.626
24	0.67	0.027	0.055
		0.028	0.022
		0.03	0.0065
		0.032	0.01
		0.034	0.036
24	0.7	0.027	0.038
		0.028	0.02
		0.03	0.0038
		0.032	0.0113
		0.034	0.019
24	0.8	0.027	0.049
		0.028	0.05
		0.03	0.021
		0.032	0.0312
		0.034	0.038
24	1	0.027	0.281
		0.028	0.344
		0.03	0.14
		0.032	0.165
		0.034	0.248

TABLE (4.1) EFFECT OF MANNING ROUGHNESS COEFFECIENT (n) AND WEIGHTING FACTOR (α) IN HYDRODYNAMIC MODEL CALCULATION

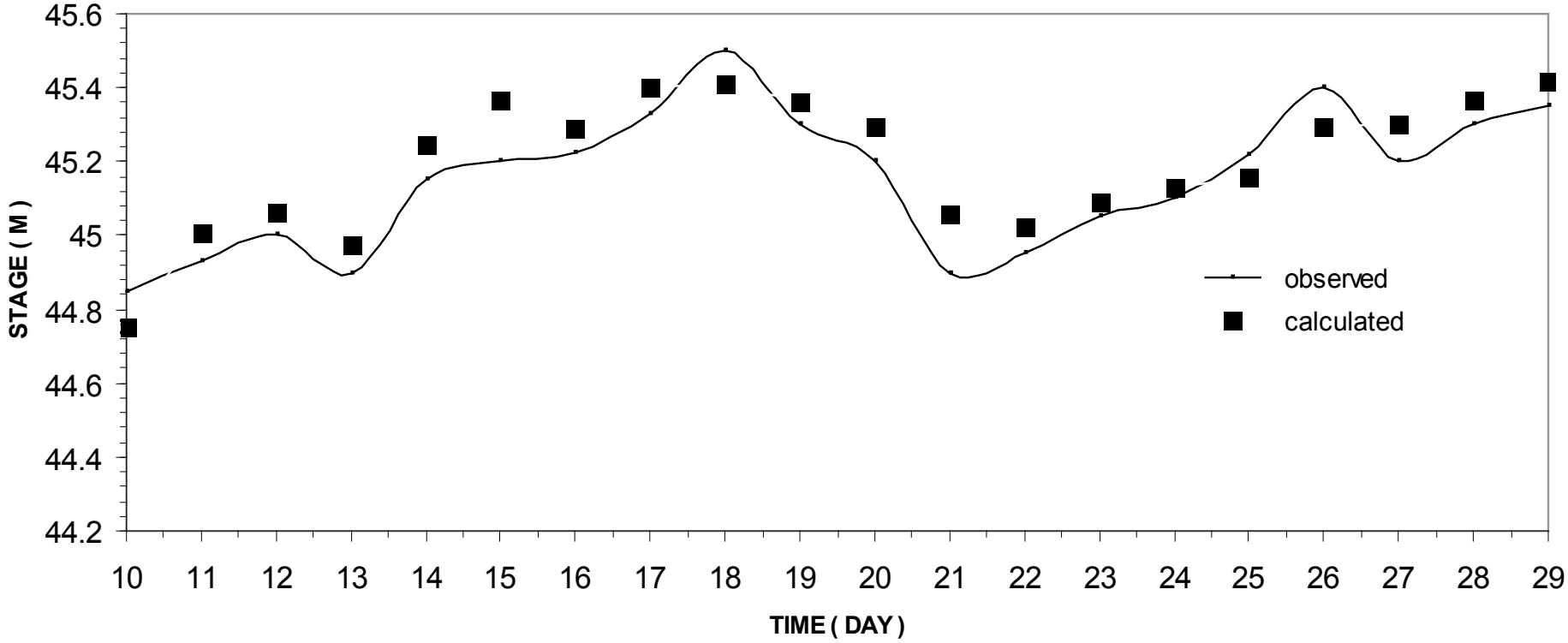

FIG. (4.15) OBSERVED AND CALCULATED STAGE HYDROGRAPH AT NODE NO. (27) IN SECTION AT (0.900 KM) UPSTREAM BOUNDARY CONDITION

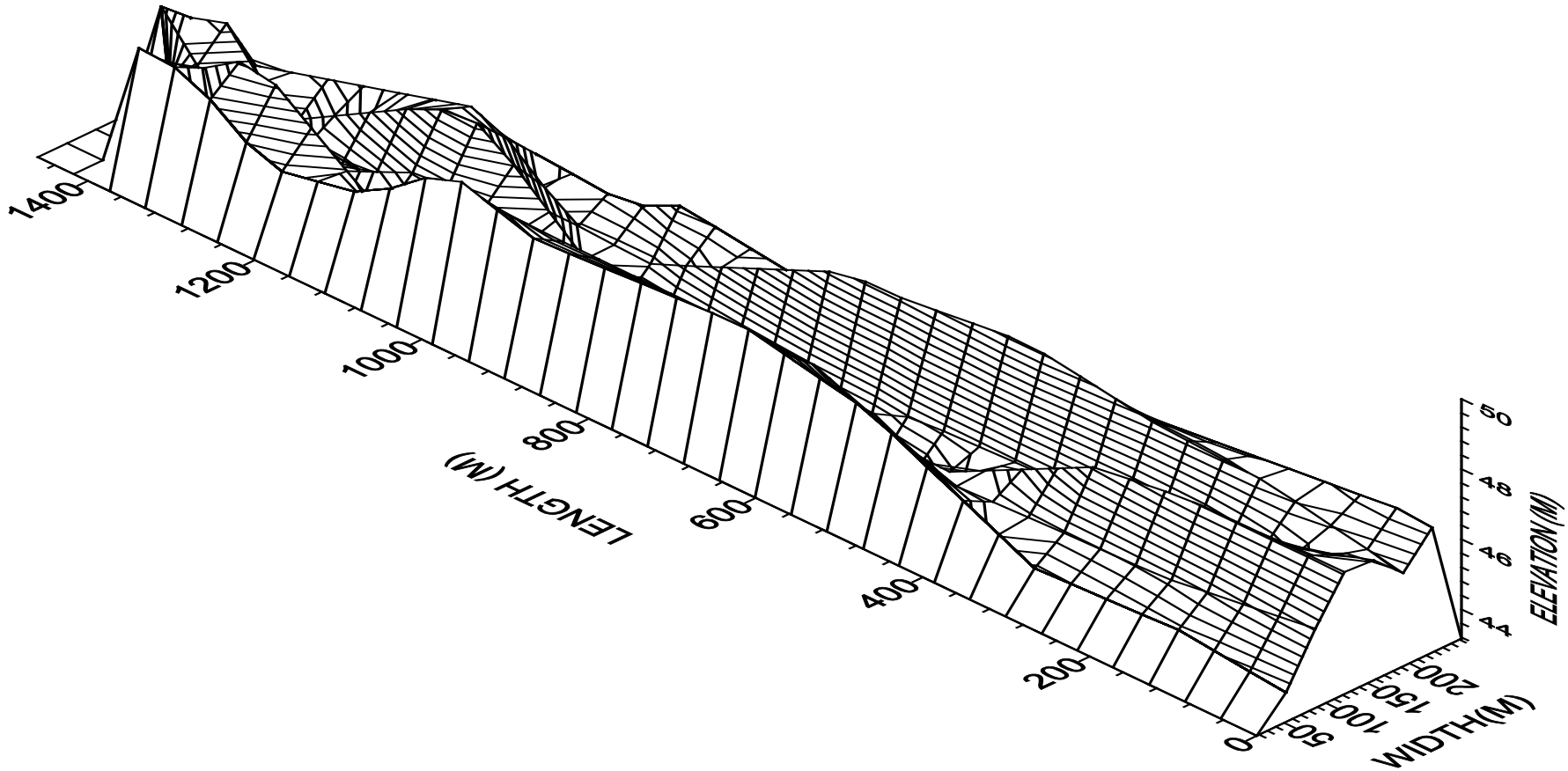

FIG. (4.16-A) BED TOPOGRAPHY OF EUPHRATES RIVER FOR STUDY REACH FROM (0.00 KM) TO (1.400 KM) AFTER (2) YEARS.(REGION I)

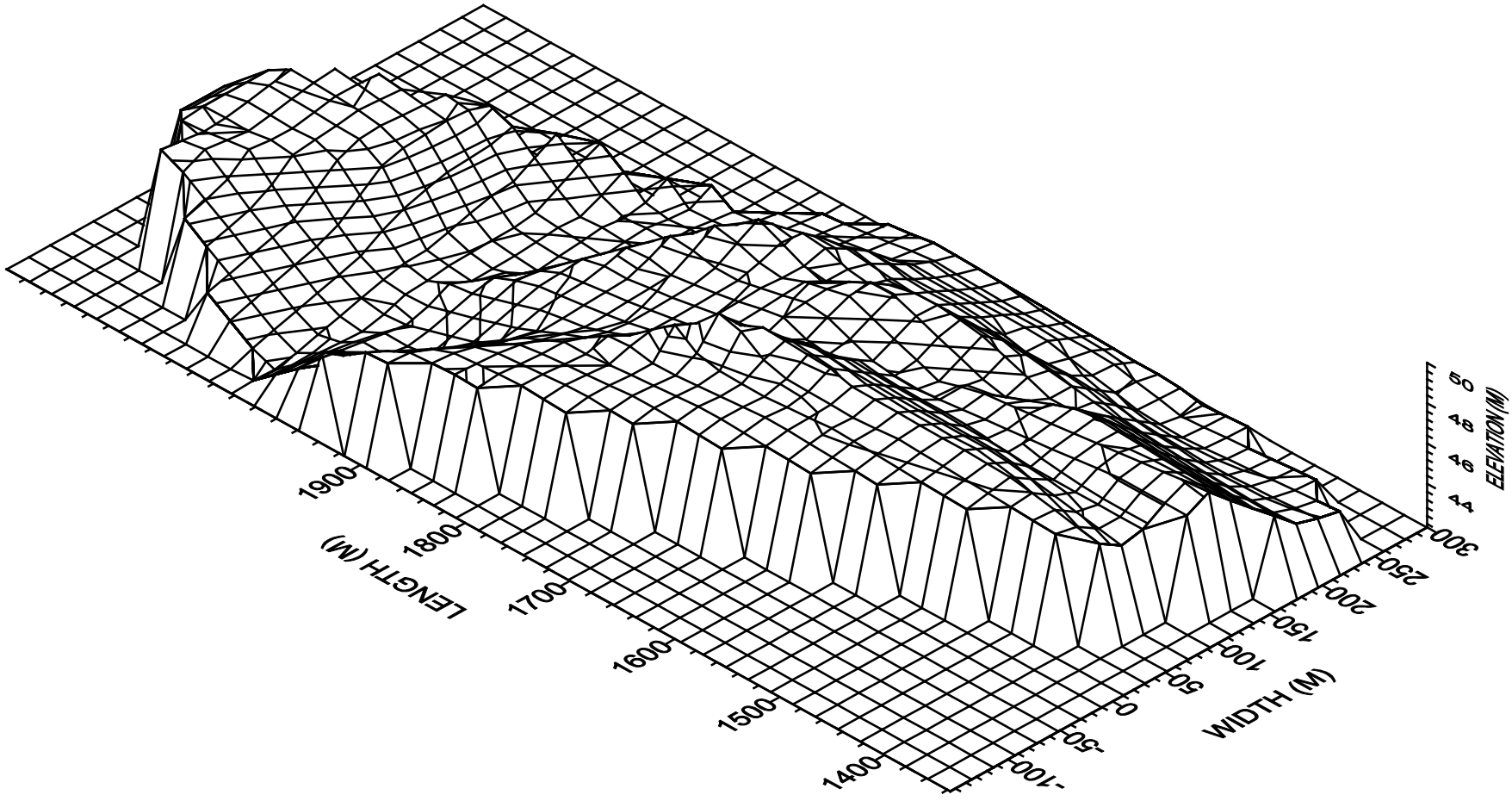

FIG. (4.16-B) BED TOPOGRAPHY OF EUPHRATES RIVER FOR STUDY REACH FROM (1.400 KM) TO (1.950 KM) AFTER (2) YEARS. (REGION II)

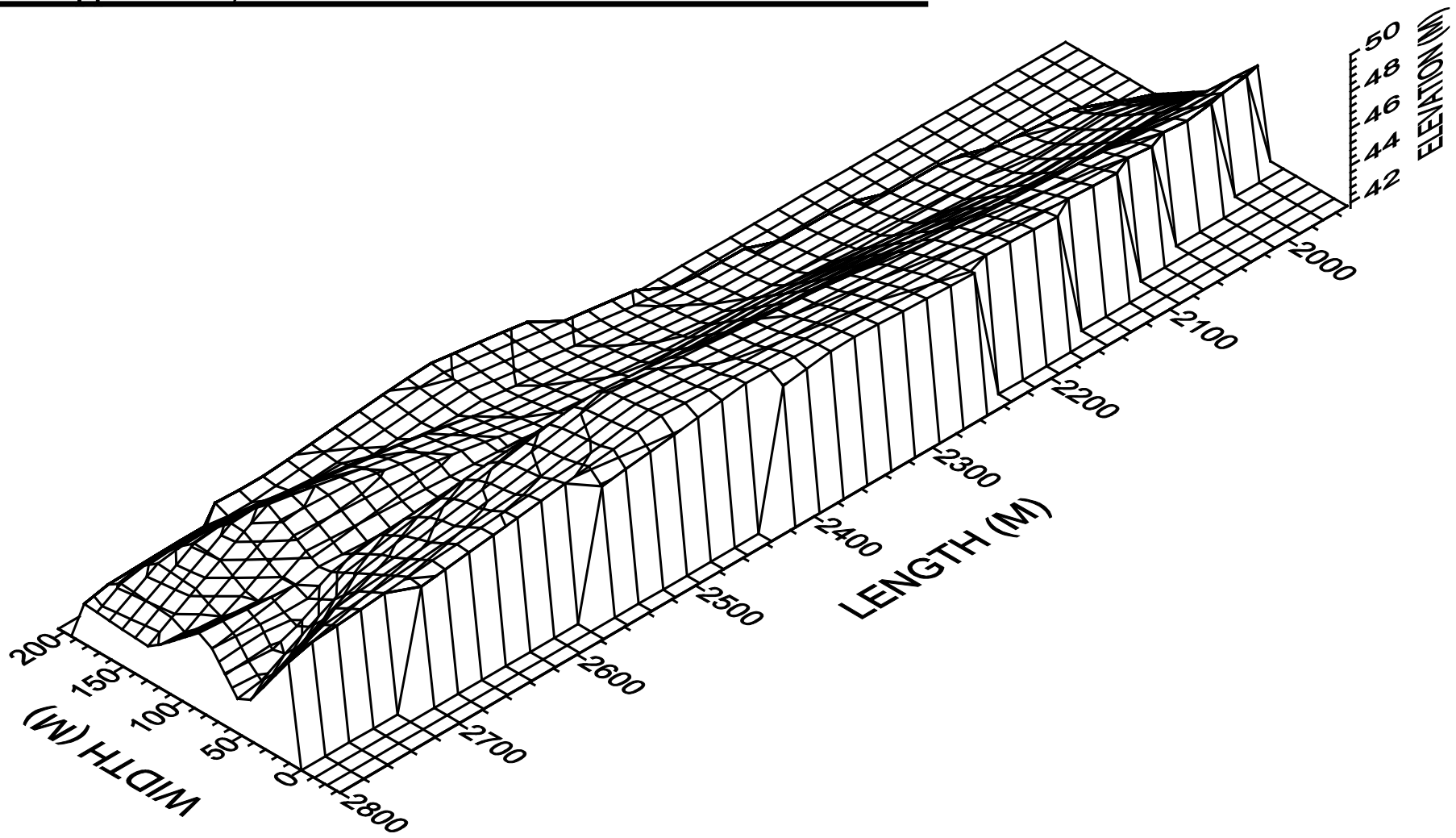

FIG. (4.16-C) BED TOPOGRAPHY OF EUPHRATES RIVER FOR STUDY REACH FROM (1.950 KM) TO (2.800 KM) AFTER (2) YEARS. (REGION III)

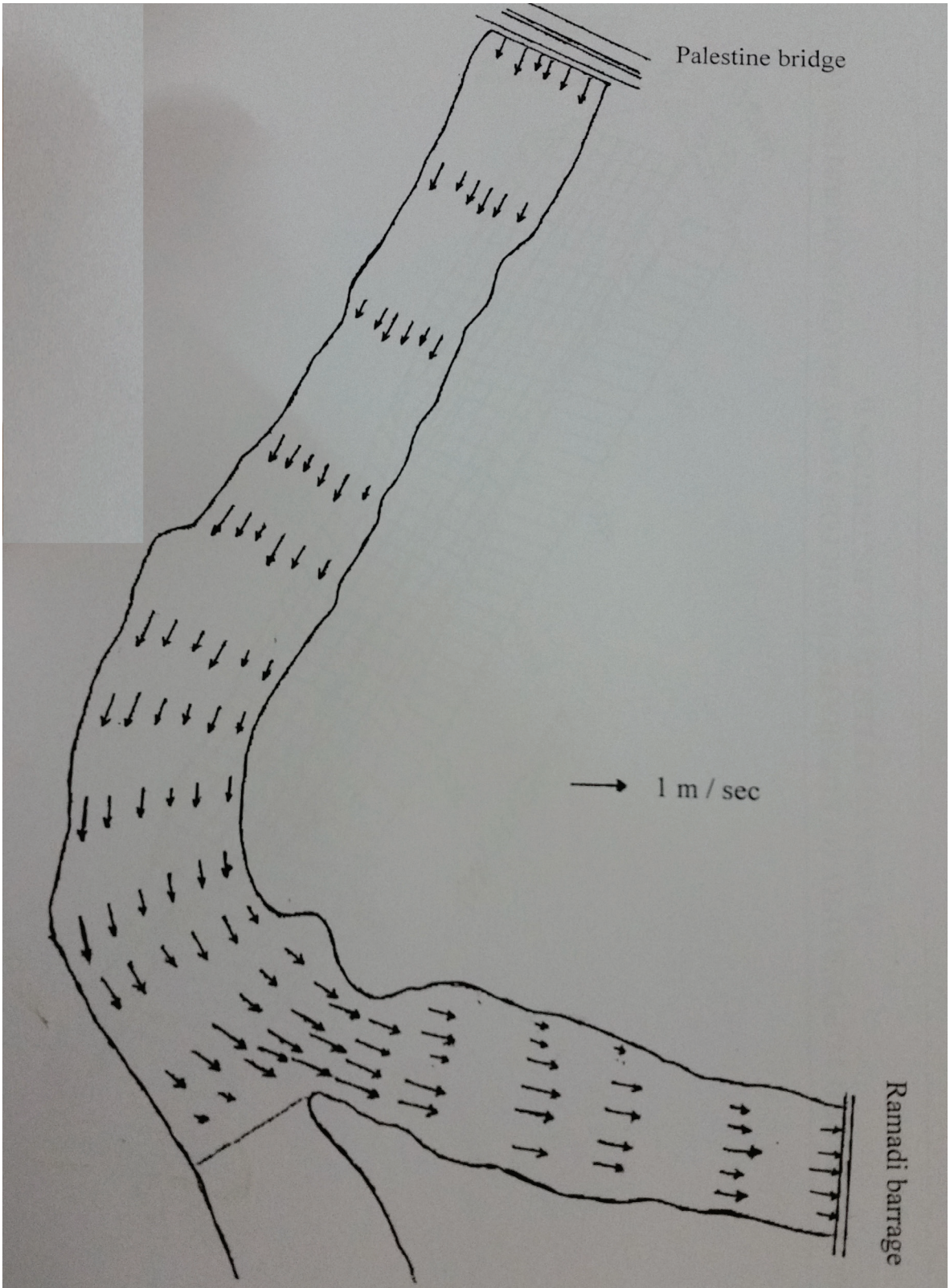

FIG. (4.17) VELOCITY FIELD OF EUPHRATES RIVER FOR STUDY REACH AFTER (2) YEARS.

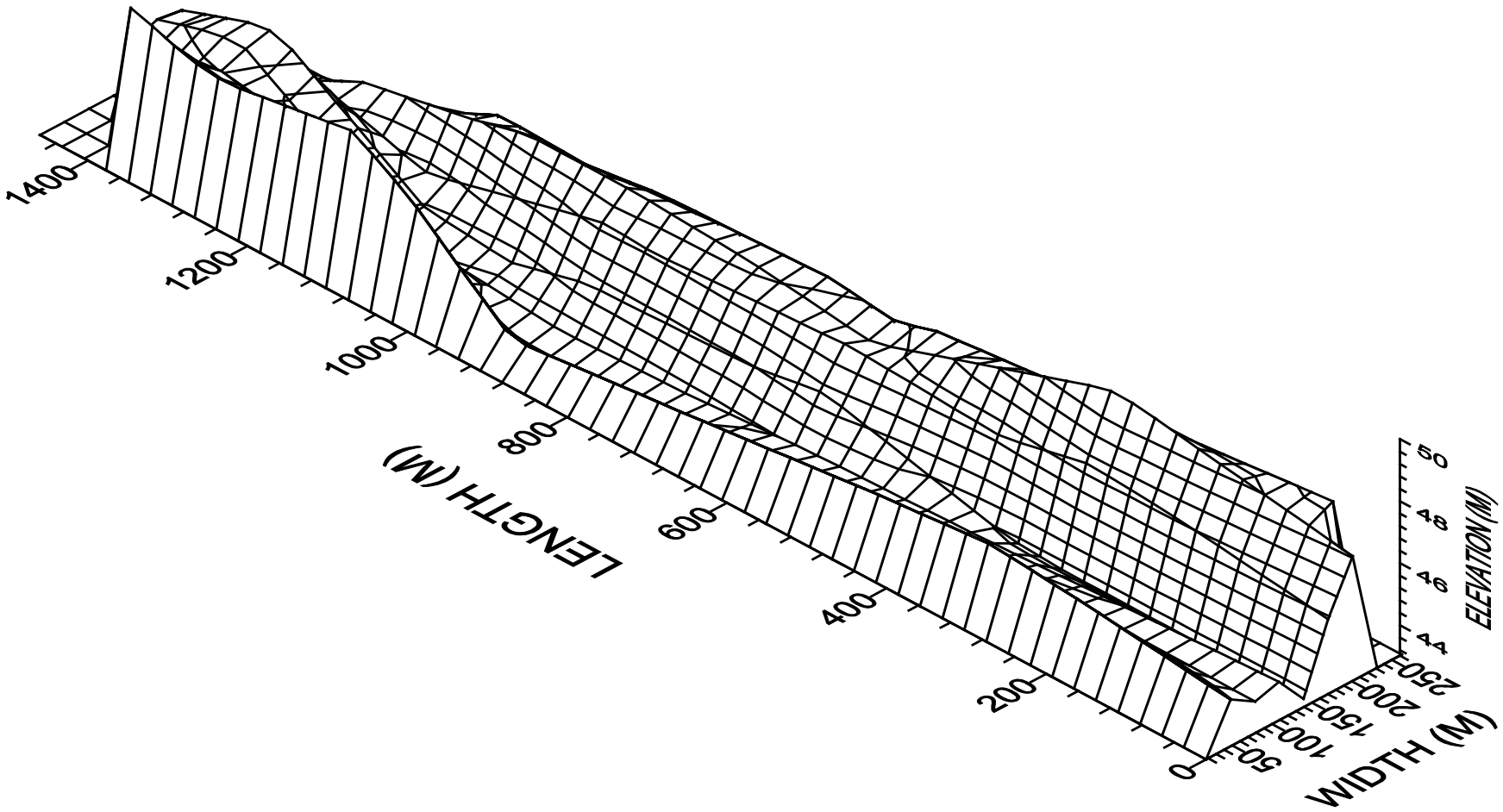

FIG. (4.18-A) BED TOPOGRAPHY OF EUPHRATES RIVER FOR STUDY REACH FROM (0.00 KM) TO (1.400 KM) AFTER (3) YEARS. (REGION I)

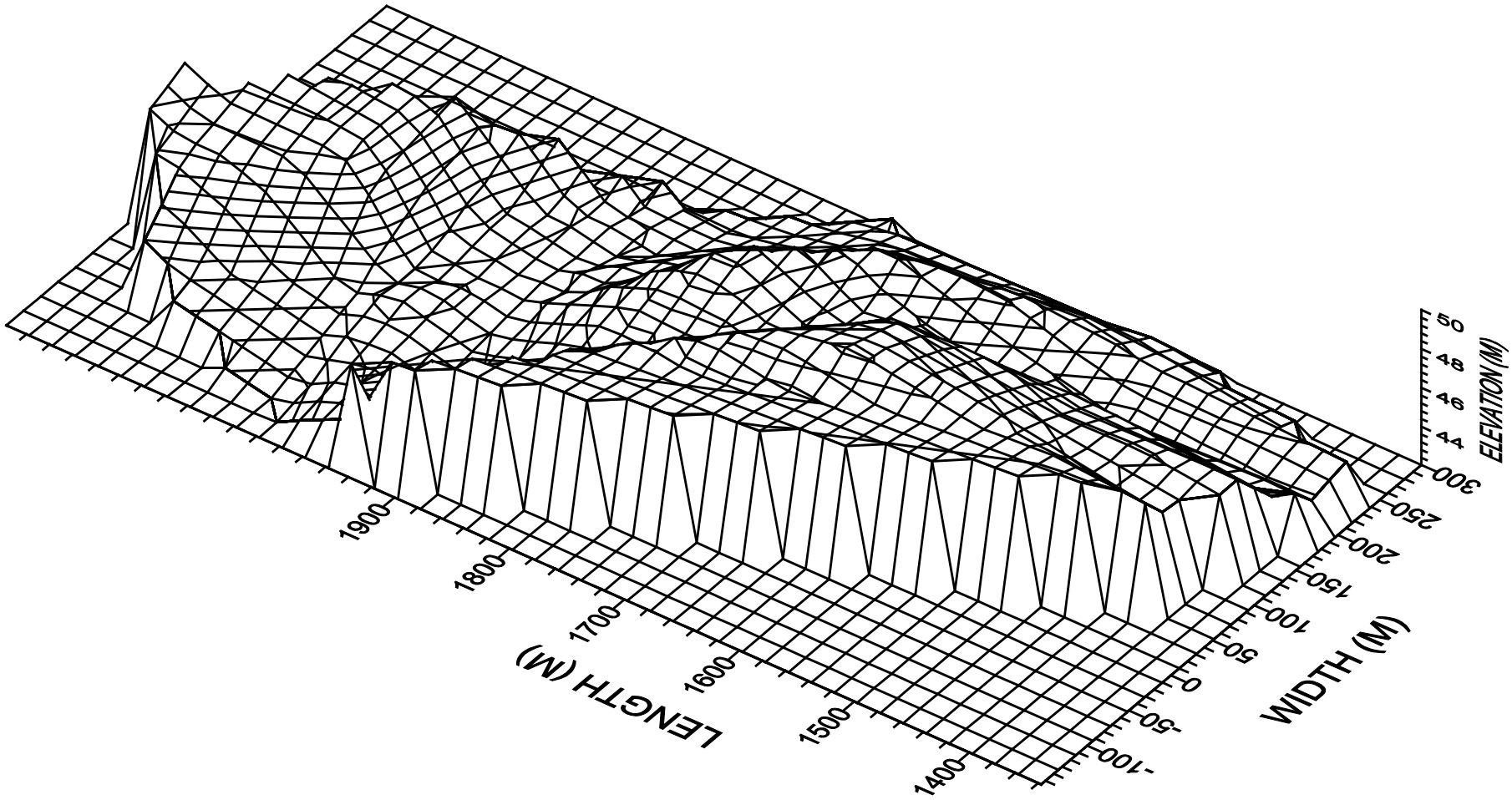

FIG. (4.18-B) BED TOPOGRAPHY OF EUPHRATES RIVER FOR STUDY REACH FROM (1.400 KM) TO (1.950 KM) AFTER (3) YEARS. (REGION II)

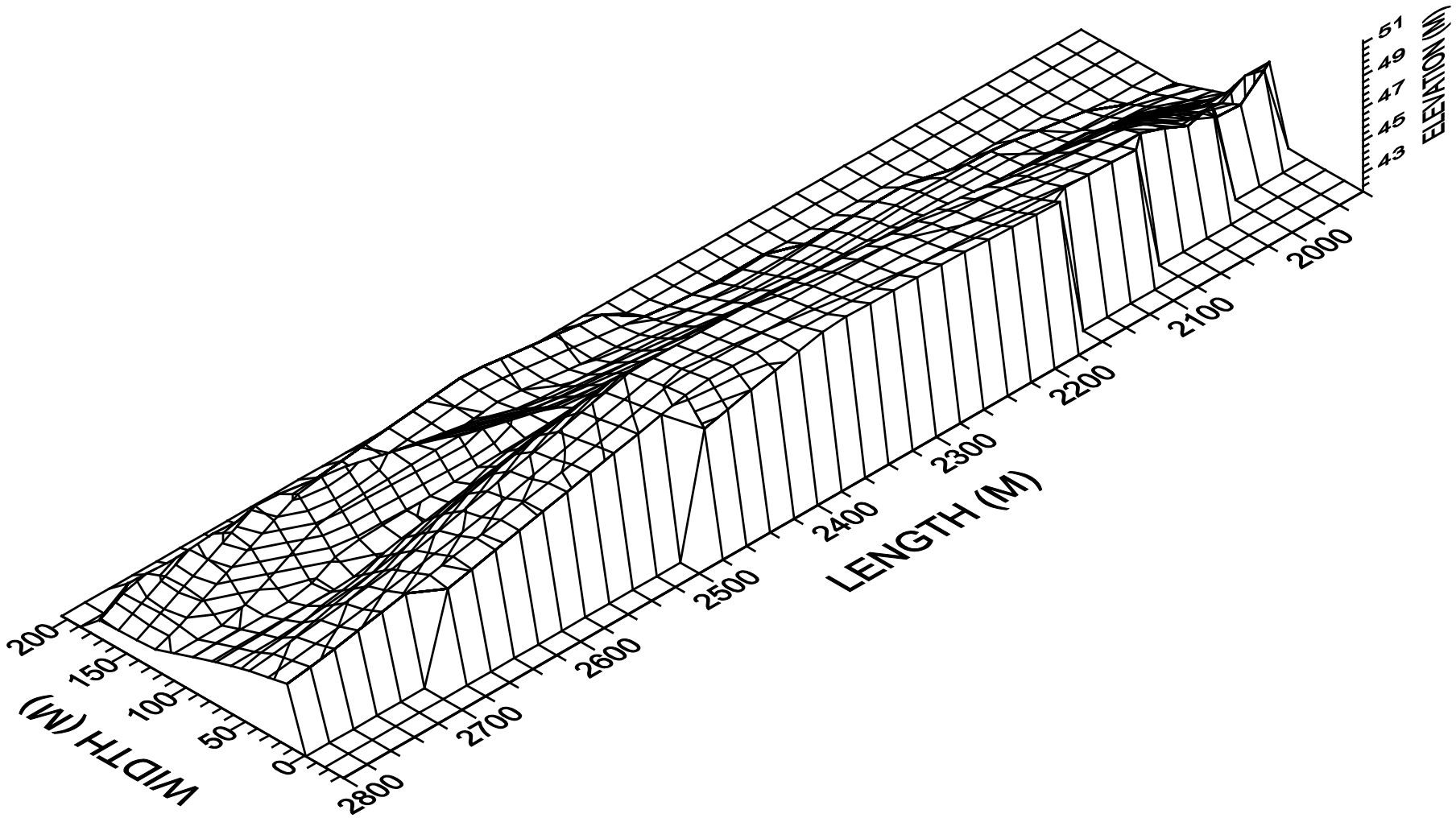

FIG. (4.18-C) BED TOPOGRAPHY OF EUPHRATES RIVER FOR STUDY REACH FROM (1.950 KM) TO (2.800 KM) AFTER (3) YEARS. (REGION III)

The variation in bed elevation of Euphrates river in initial condition and after two and three years can be shown in figures (4.19-A), (4.19-B), (4.19-C), (4.19-D), (4.19-E), (4.19-F) and (4.19-G).

4.5 Discussion

Figures (4.9), (4.10), (4.11), (4.12), (4.13) and (4.14) which present the comparison between observed and calculated stage values at different (n) values. These figures indicate fairly deviation of computed results from corresponding observed values except for the values (α =0 and α =1) there are evident divergence between the observed and calculated value of stage.

Table (4.1) shows the mean square error (mse) of results with each value of (n) used at each spesified α . It was used as an indicator of results accuracy with respect to stage. It is clear from table (4.1) that some values of (mse) are very high due to an error in the gathered data for the observed discharge in section at 0.600 km upstream boundary condition and we used the balance equation for which.

Table (4.1) and figures (4.9), (4.10), (4.11), (4.12), (4.13), and (4.14) present that the smallest (mse) at (n=0.03).

Comparison between computed and observed stage for section at 0.600km from upstream boundary condition for (n=0.03) and ranged values for weighting factor between (0 and 1) are represented in table (4.1), this table shows that the weighting factor (α) value of (0.7) gives a closer results to observed values.

The changes in bed elevations of Euphrates river in study reach after two and three years shows that in the meandering reachs the scour will take place at the outer bank while the diposition will occur at the inner bank. It is clearly shown in figure (4.18-C) that the increase in deposition between section at (2.000 kms) to section at (2.500 kms) makes an island along the left bank of the river.

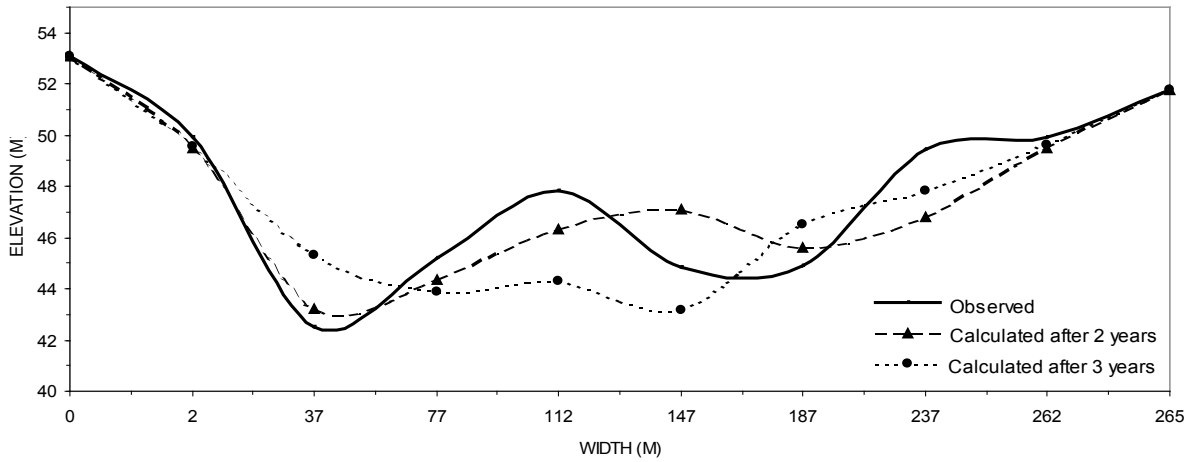

COMPARED BETWEEN INITIAL AND CALCULATED SECTION AT (0.00 KM) FROM UPSTREAM BOUNDARY CONDITION

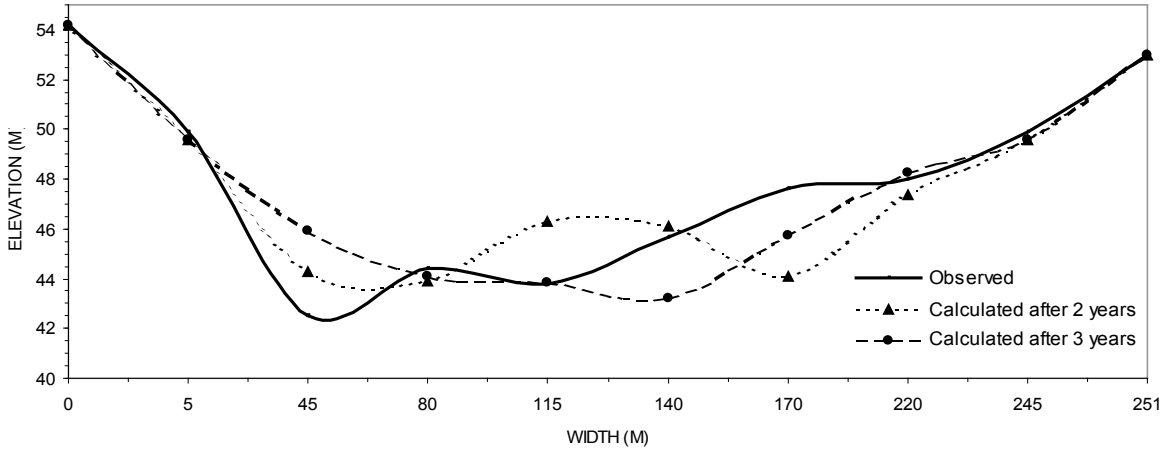

COMPARED BETWEEN INITIAL AND CALCULATED FOR SECTION AT (0.300 KM) FROM UPSTREAM BOUNDARY CONDITION

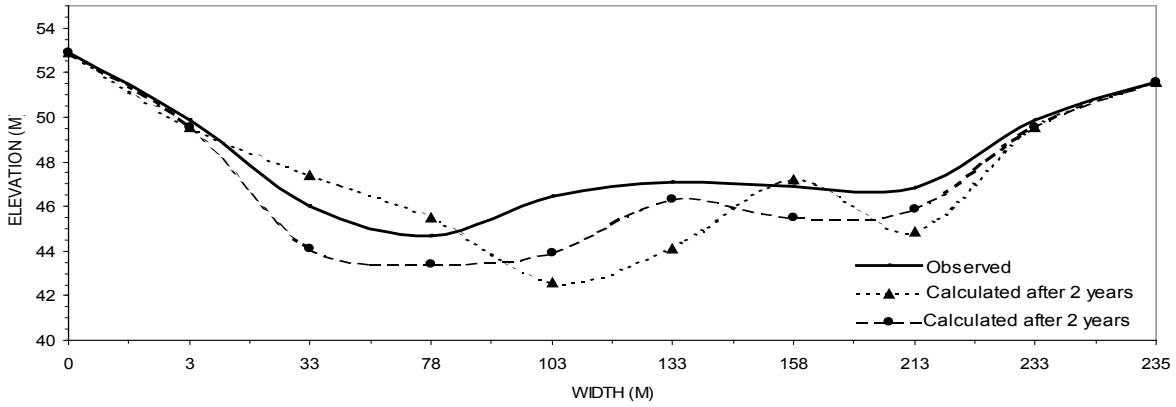

COMPARED BETWEEN INITIAL AND CALCULATED FOR SECTION AT (0.600 KM) FROM UPSTREAM BOUNDARY CONDITION

FIG. (4.19-A) COMPARISON BETWEEN INITIAL AND CALCULATED SECTION AFTER (2) AND (3) YEARS FOR DIFFERENT REACHS

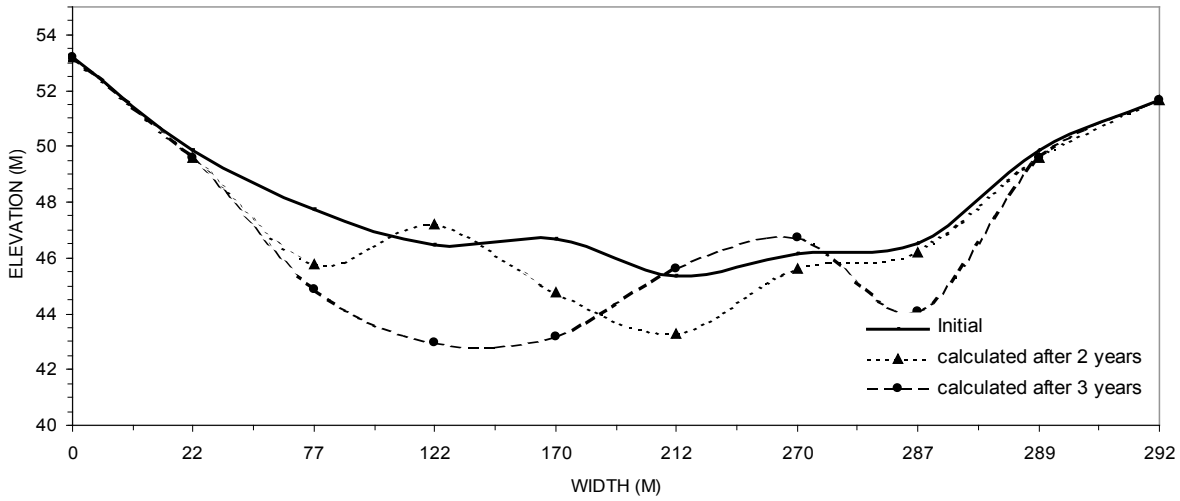

COMPARED BETWEEN INITIAL AND CALCULATED FOR SECTION AT (0.900 KM) FROM UPSTREAM BOUNDARY CONDITION

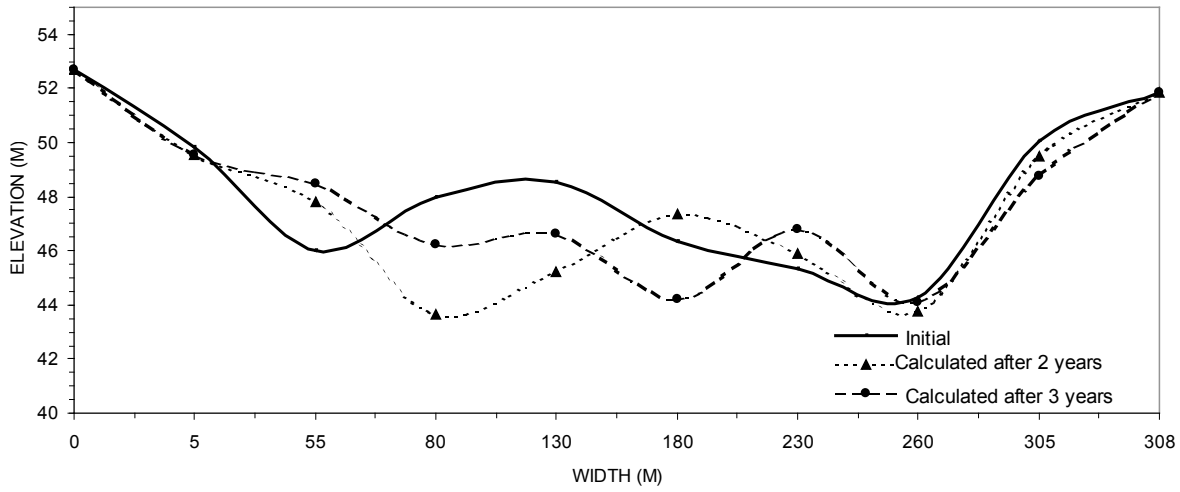

COMPARED BETWEEN INITIAL AND CALCULATED SECTION FOR SECTION AT (1.100 KM) FROM UPSTREAM BOUNDARY CONDITION

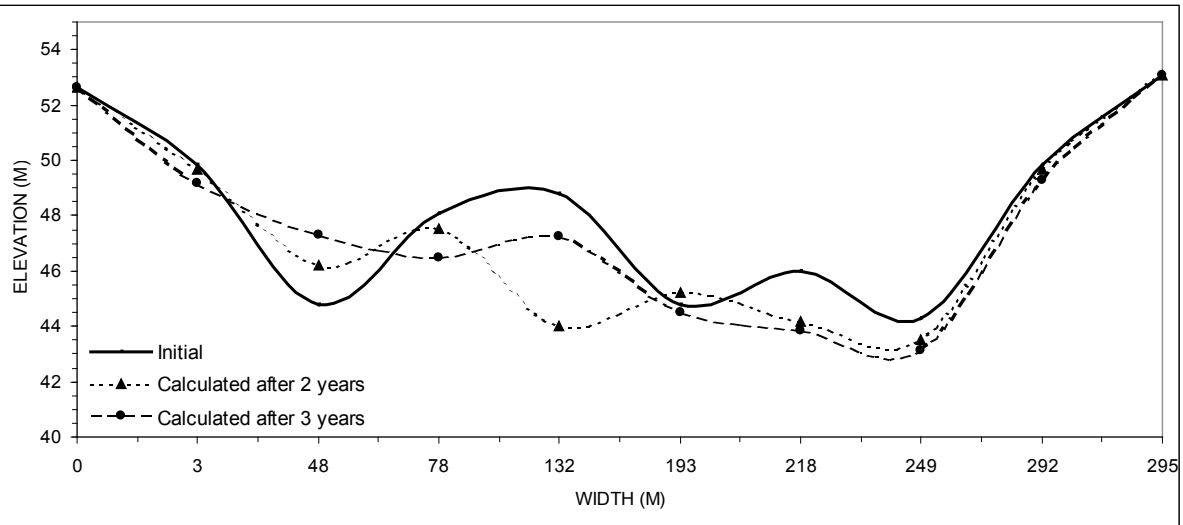

COMPARED BETWEEN INITIAL AND CALCULATED FOR SECTION AT(1.300 KM) FROM UPSTREAM BOUNDARY CONDITION

FIG. (4.19-B) COMPARISON BETWEEN INITIAL AND CALCULATED SECTION AFTER (2) AND (3) YEARS FOR DIFFERENT REACHS

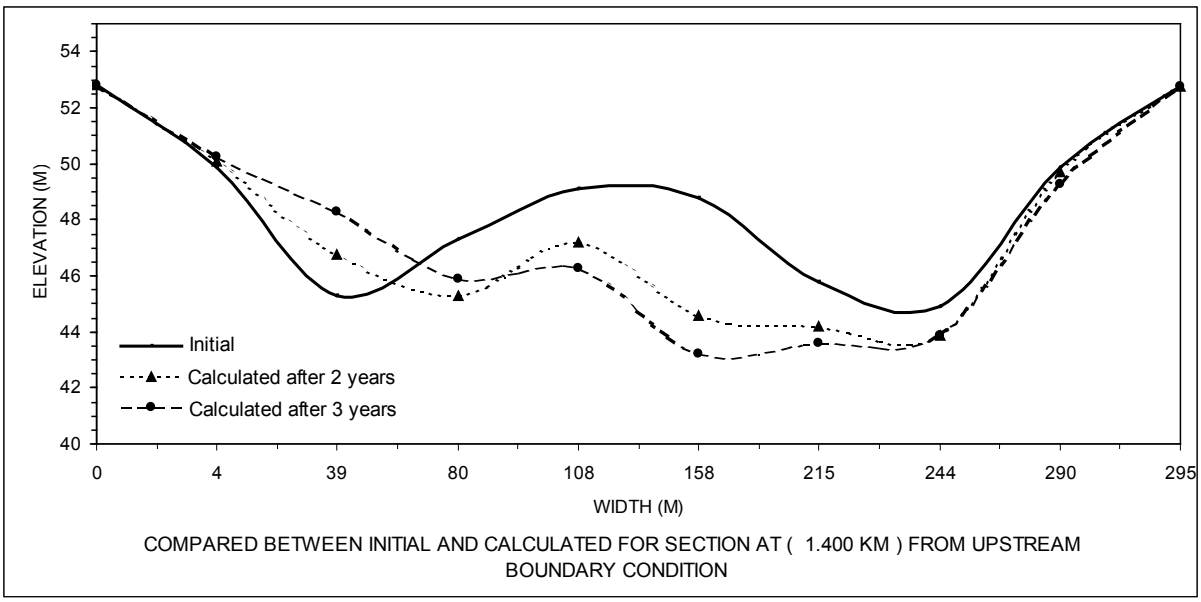

COMPARED BETWEEN INITIAL AND CALCULATED FOR SECTION AT (1.400 KM) FROM UPSTREAM BOUNDARY CONDITION

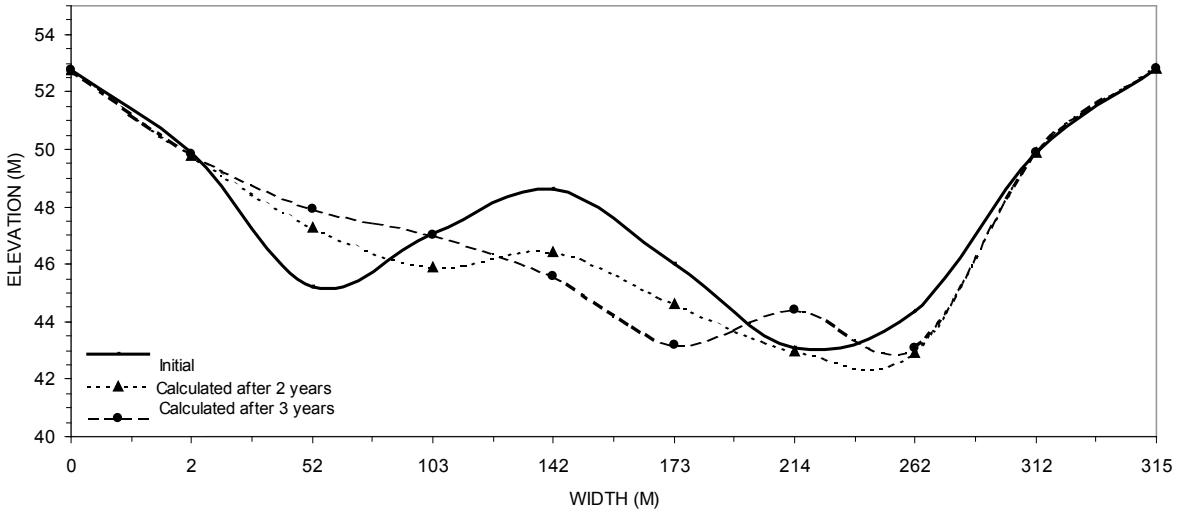

COMPARED BETWEEN INITIAL AND CALCULATED FOR SECTION (1.500 KM) FROM UPSTREAM BOUNDARY CONDITION

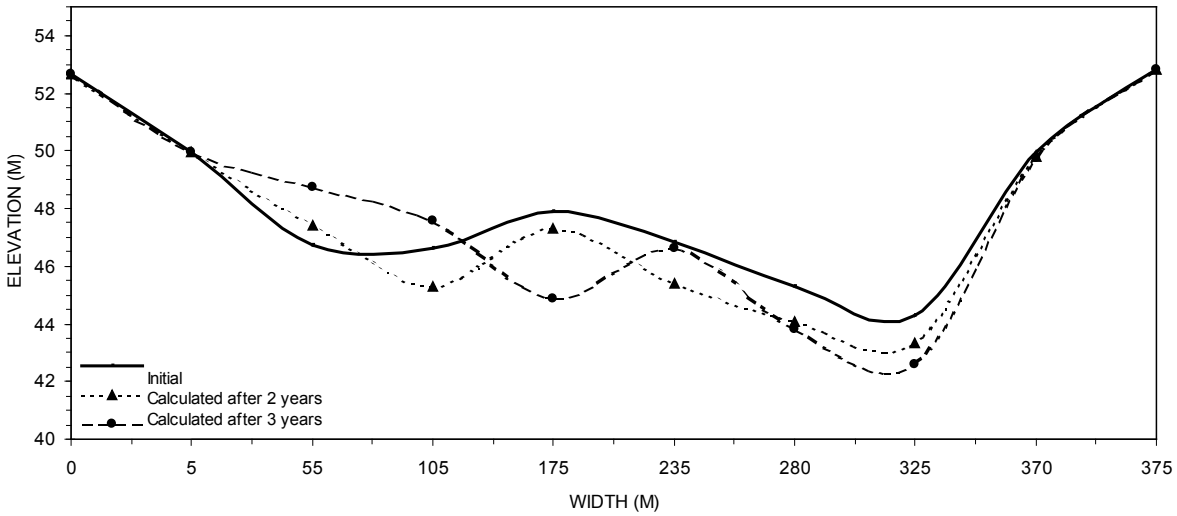

COMPARED BETWEEN INITIAL AND CALCULATED FOR SECTION AT (1.600 KM) FROM UPSTREAM BOUNDARY CONDITION

FIG. (4.19-C) COMPARISON BETWEEN INITIAL AND CALCULATED SECTION AFTER (2) AND (3) YEARS FOR DIFFERENT REACHS

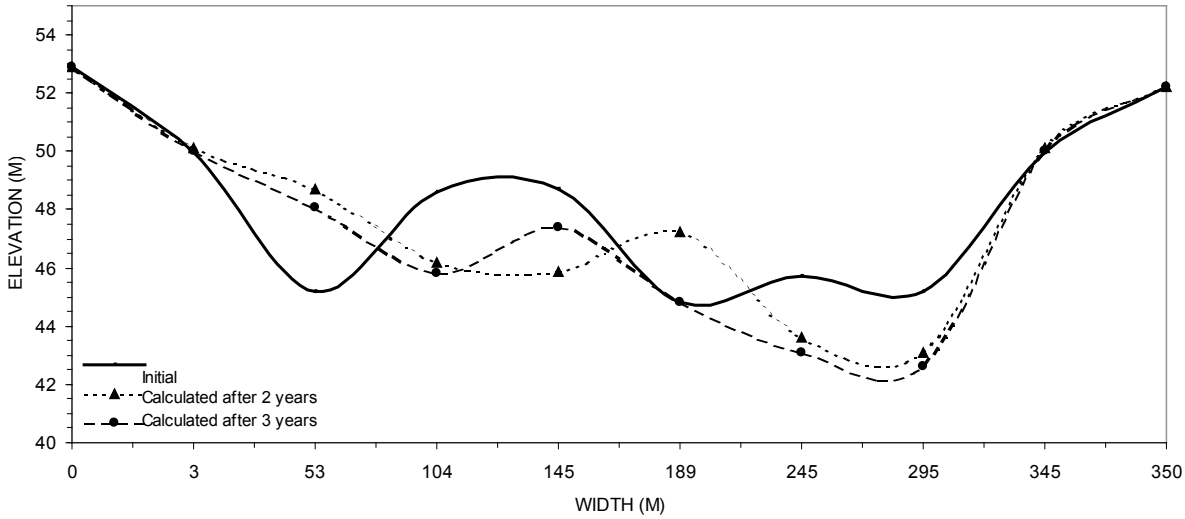

COMPARED BETWEEN INITIAL AND CALCULATED FOR SECTION AT (1.700 KM) FROM UPSTREAM BOUNDARY CONDITION

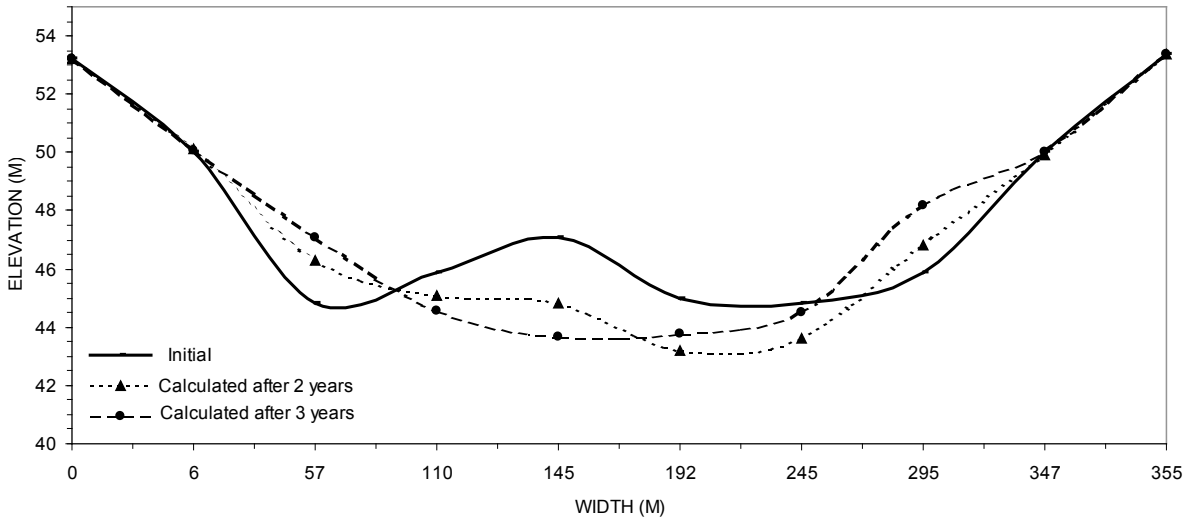

COMPARED BETWEEN INITIAL AND CALCULATED FOR SECTION AT (1.800 KM) FROM UPSTREAM BOUNDARY CONDITION

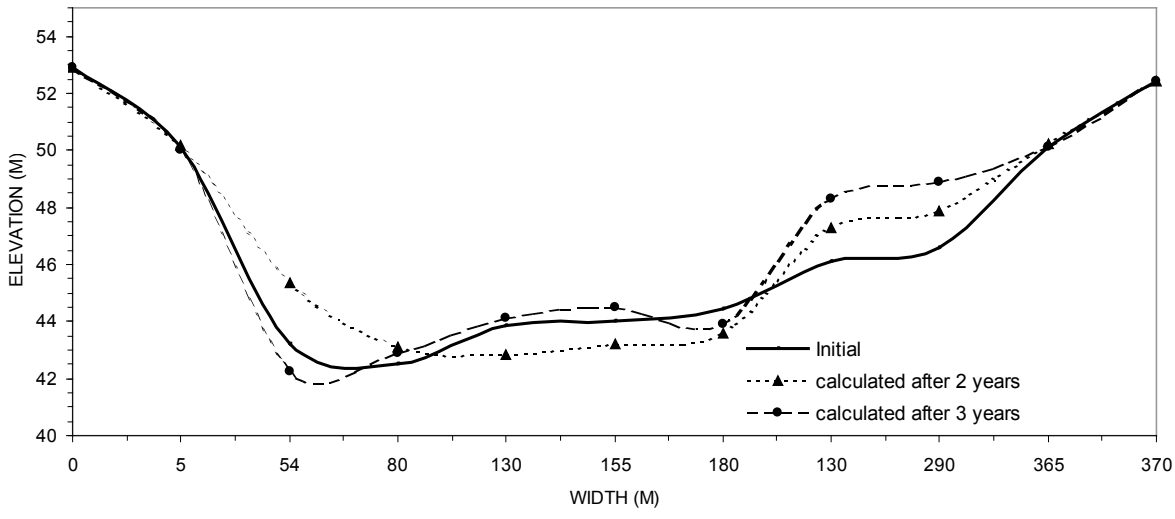

COMPARED BETWEEN INITIAL AND CALCULATED FOR SECTION AT (1.900 KM) FROM UPSTREAM BOUNDARY CONDITION

FIG. (4.19-D) COMPARISON BETWEEN INITIAL AND CALCULATED SECTION AFTER (2) AND (3) YEARS FOR DIFFERENT REACHS

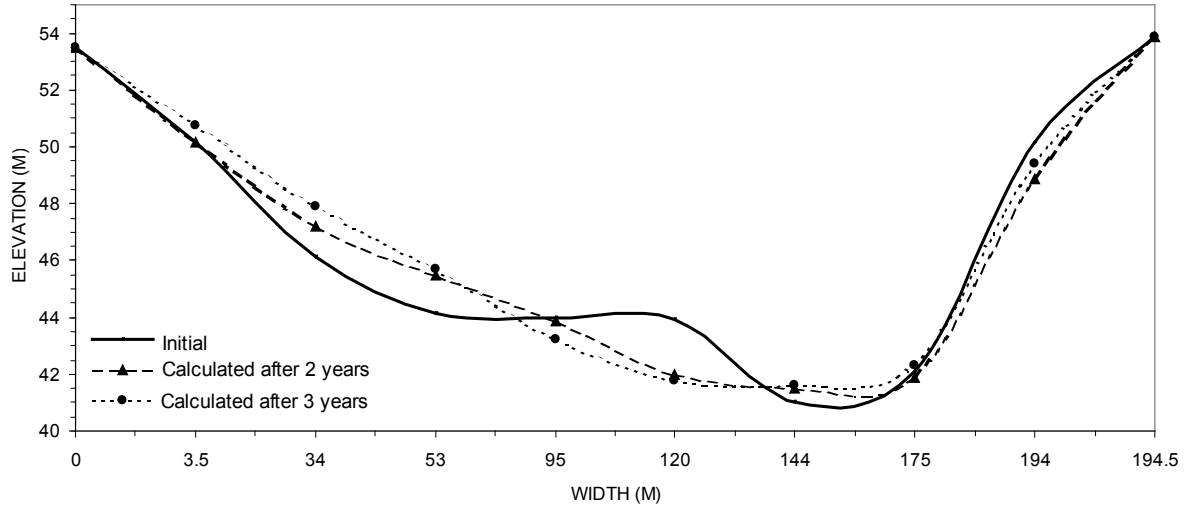

COMPARED BETWEEN INITIAL AND CALCULATED FOR SECTION AT (1.950 KM) FROM UPSTREAM BOUNDARY CONDITION

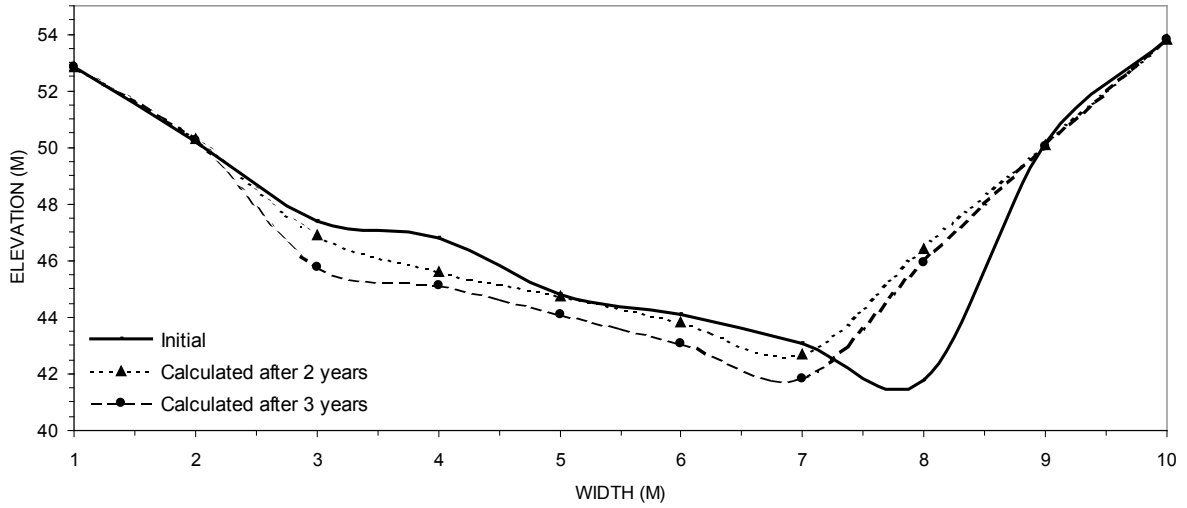

COMPARED BETWEEN INITIAL AND CALCULATED FOR SECTION AT (2.000 KM) FROM UPSTREAM BOUNDARY CONDITION

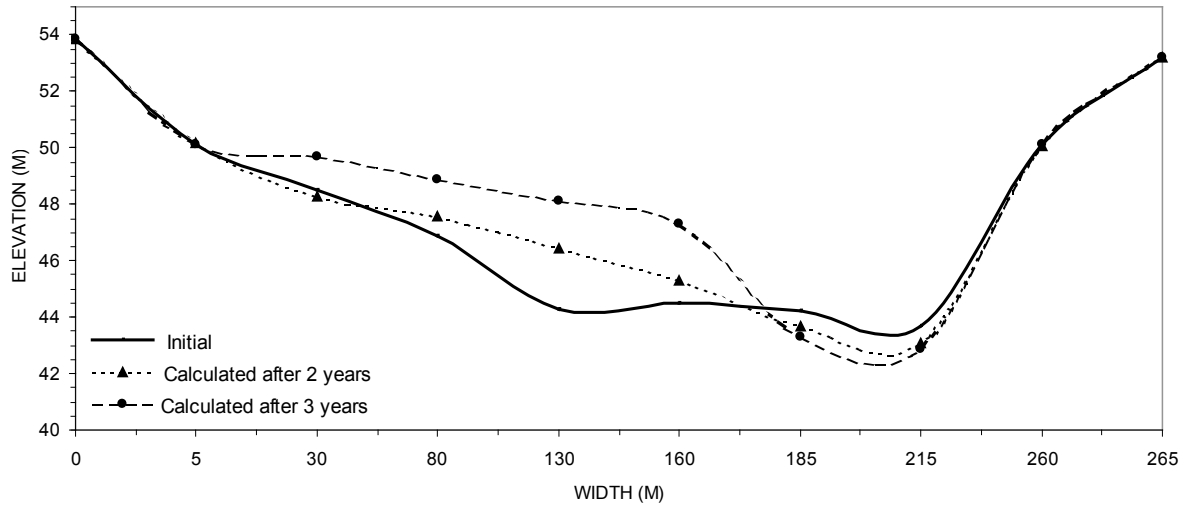

COMPARED BETWEEN INITIAL AND CALCULATED FOR SECTION AT (2.100 KM) FROM UPSTREAM BOUNDARY BCONDITION

FIG. (4.19-E) COMPARISON BETWEEN INITIAL AND CALCULATED SECTION AFTER (2) AND (3) YEARS FOR DIFFERENT REACHS

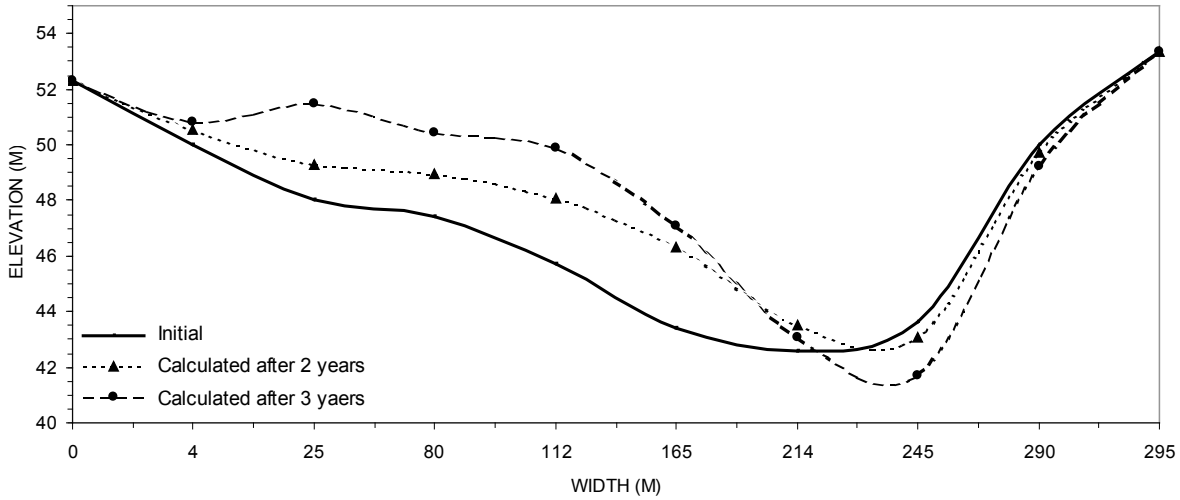

COMPARED BETWEEN INITIAL AND CALCULATED FOR SECTION AT (2.300 KM) FROM UPSTREAM BOUNDARY CONDITION

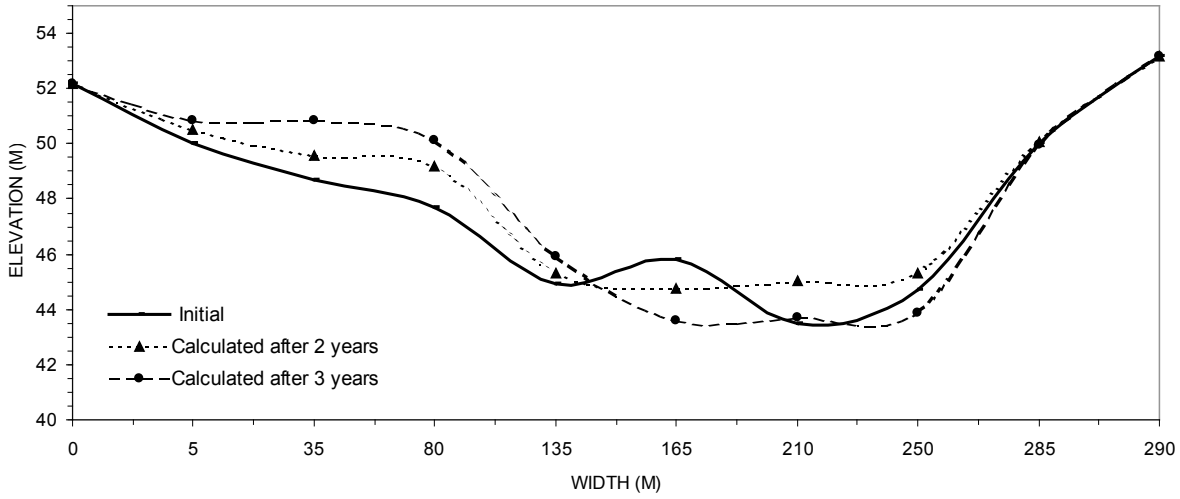

COMPARED BETWEEN INITIAL AND CALCULATED FOR SECTION AT (2.500 KM) FROM UPSTREAM BOUNDARY CONDITION

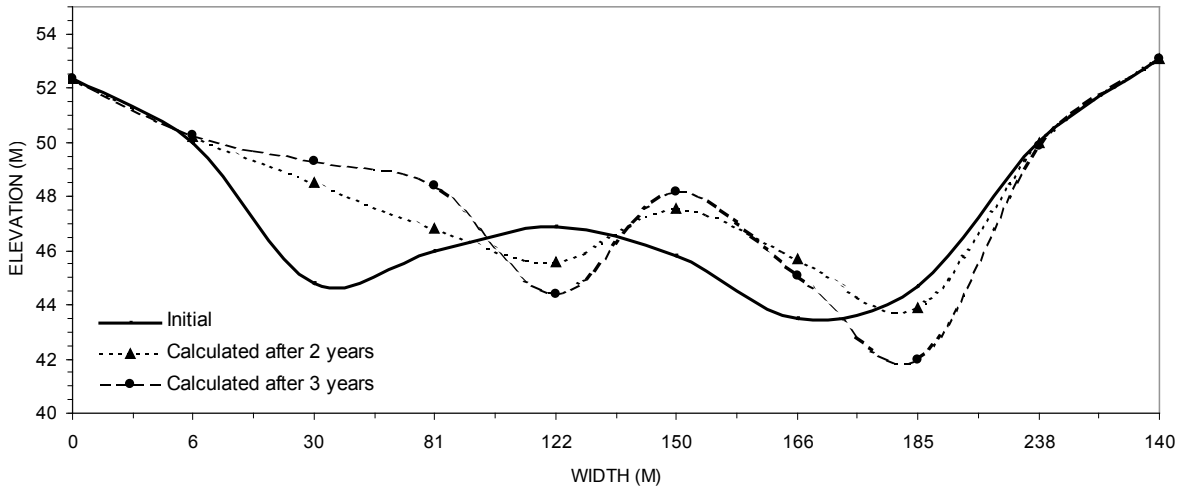

COMPARED BETWEEN INITIAL AND CALCULATED FOR SECTION AT (2.700 KM) FROM UPSTREAM BOUNDARY CONDITION

FIG. (4.19-F) COMPARISON BETWEEN INITIAL AND CALCULATED SECTION AFTER (2) AND (3) YEARS FOR DIFFERENT REACHS

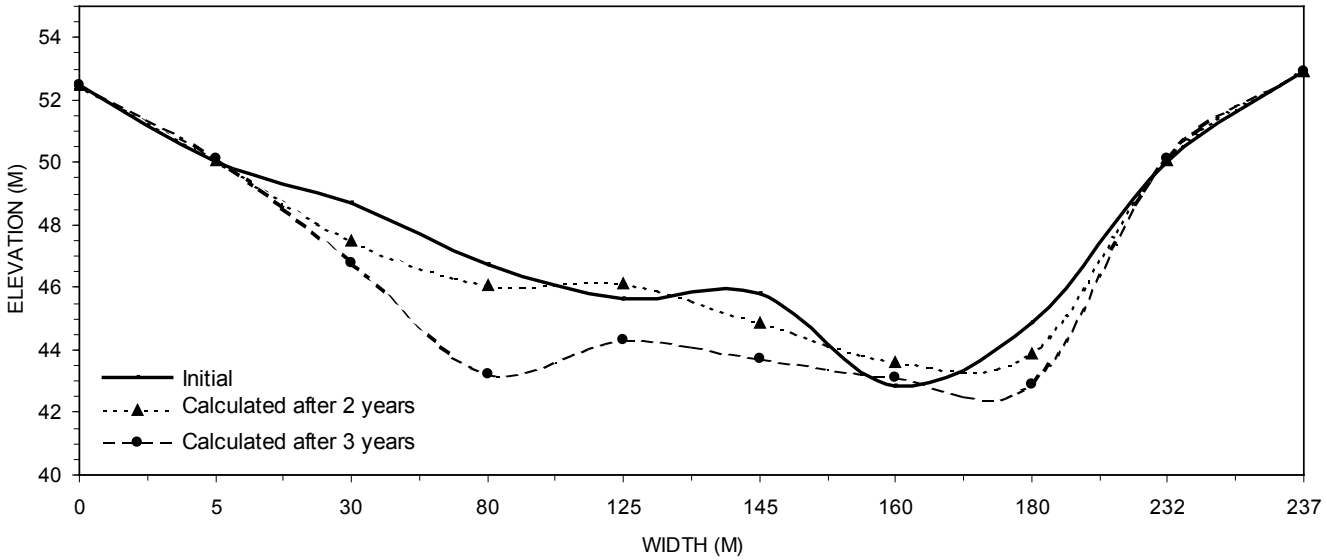

COMPARED BETWEEN INITIAL AND CALCULATED FOR SECTION AT (2.800 KM) FROM UPSTREAM BOUNDARY CONDITION

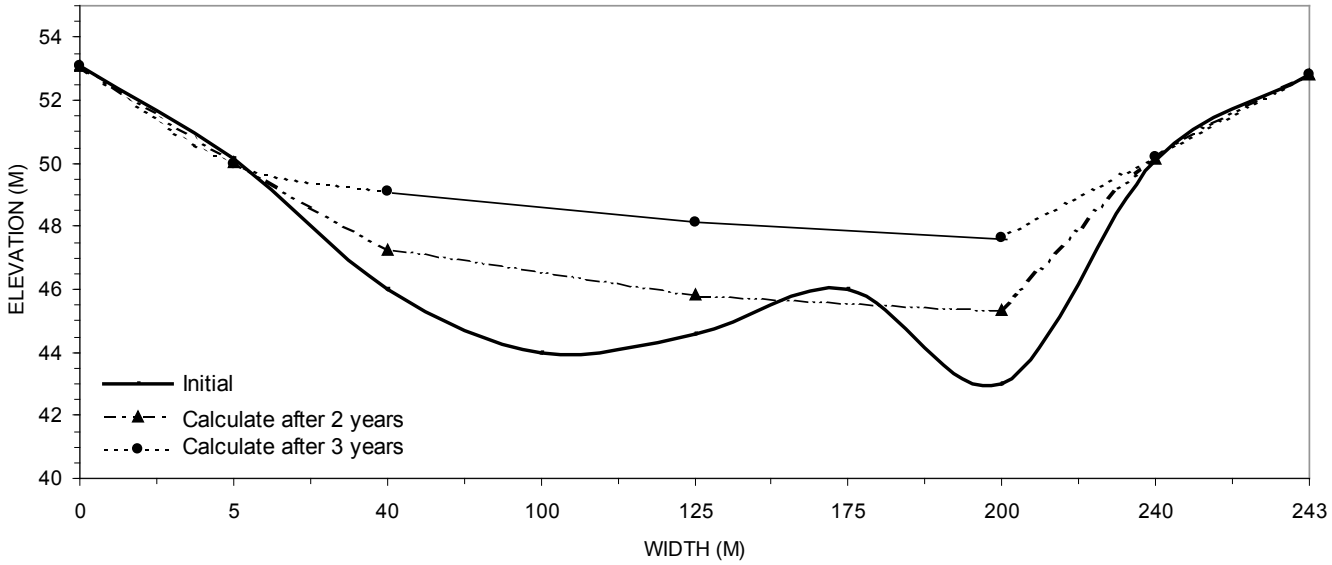

COMPARED BETWEEN INITIAL AND CALCULATED FOR SECTION AT AL-WARRAR RIVER (2.120 KM) FROM UPSTREAM BOUNDARY CONDITION

FIG. (4.19-G) COMPARISON BETWEEN INITIAL AND CALCULATED SECTION AFTER (2) AND (3) YEARS FOR DIFFERENT REACHS

The velocity fields for entire reach after operating the models for two years are shown in figure (4.17), we can see from this figure the velocity has maximam value at the outer bank of the bend and minimum value at the inner bank of the bend along transverse direction. The velocity varied along stream direction according to the reduction or expansion of river width.

The future run of the models show a high rate of morphological changes in river bed elevations in different locations of the river reach under study.

In section at 1.400 km upstream boundary conditions shown in fig.(4.19-C), we can see that the bed elevation of the River at node no. 53 has been scoured from 48.8m at initial condition to reach 44.9m after run of the models for two years and 43.4m after run of the models for three years.

CHAPTER FIVE

Conclusions and Recommendations

Chapter Five

Conclusions and Recommendations

5.1 General

A mathematical model was developed to simulate the two – dimensional hydrodynamic depth averaged equations. A second developed model was the morphological model based on dynamic equation of sediment continuity equation and the output of hydrodynamic model.

The finite element technique was used for the solution of the above two models by using triangular element with three nodes for the space discretization. The computer programms related to above two models were constructed using Fortran power station under windows version.

The programme was run on computer Pentium 3 of microprocessor with 650 MHz clock speed. The results of the models are tested by analytical solution and by observed data.

The models were applied to the Euphrates river within Ramadi city for 2.8 kms upstream Ramadi Barrage.

5.2 Conclusions

In view of the discussion of numerical results of the above models, the following conclusions may be drawn:

1. The two dimensional depth – averaged hydrodynamic model and two-dimensional morphological model were developed and applied successfully by using the finite element technique.
2. All values of weighting factor (α) in the range between (0.5) and (0.9) for hydrodynamic model led to stable and accurate solution but a good agreement was obtained when a weighting factor of (0.7) was used.

3. Calibration of the hydrodynamic model indicates that the value of Manning roughness (n) equal to (0.03) gives a good agreement when used for the operation of the hydrodynamic model for the river reach under study.

4. Application of coupled hydrodynamic and morphological model show that the rivers tend to scour at the inner bank and deposit in outer bank between section at 1.900 km to section at 2.500 which are a natural tendency in river bend.

5. From the distribution of velocity filed that obtained from models can be observed that the high velocity occur in outer bank than that noticed in inner bank particularly in river bend region.

6. The future run of the models show a high rate of morphological changes in river bed elevations in different locations of the river reach under study.

5.3 Recommendations

1. The model should be applied to specific reach of Euphrates river with comprehensive data collection program for the calibration and verification purposes.

2. Actual data of bed profile and median bed material size (d_{50}) are needed for further applications of present model.

3. The model can be improved by accounting for variable width of the River.

4. The trends of bed level variation along the flow direction and the variables encountered in controlling this phenomena need a further future study.

REFERENCES

1. Abed, B. S., 1998 *" Development of Dynamic Water Quality Model for Tigris River within Baghdad City"*, Ph. D., Thesis , College of Eng., University of Baghdad.
2. Al – Ani, U. H., 2001 "*Two Dimensional FEM Model For The Flow Of Euphrates River At Falluja Regulator",* M.Sc., Thesis, College Of Engineering, University Of AL-Anbar
3. Al – Eoubaidy, K. A., And Salman,I. D.,1997 *"Numerical Method Of Computing Flow Profiles With Lateral Outflow In Euphrates River ",*The Scientific Journal Of Tikrit University, Vol. 4, No. 2,Pp. 41-51.
4. Al – Eoubaidy, K. A, 1999 *"Water Quality Model in Euphrates River (Case Study)",*Ph. D., Thesis, College of Engineering, University of Baghdad.
5. Bathe, K. J., 1996 *" Finite Element Procedure" ,* Prentic- Hall International, Inc.
6. Chandrupatla, T. R., and Belegundu, A. D., 1997 *" Introduction to Finite Elements in Engineering"* Prentice-Hall of India, New Delhi,2nd Edition
7. Chaudhry, M. H. 1987 "*Applied Hydraulic Transients*" 2nd Edition, Van Nostrand Reinhold Company, Newyork, N.Y.
8. Engelund, F., 1974 *" Flow and Bed Topography in Channel Bends",* J. Hydr. Div., Vol.100, No.8.
9. Ghailan, A. H., 1982 *" Studies on Numerical River Flow Analysis for Systematical Water Use" ,* Ph. D.,Thesis, Kyoto University, Kyoto.
10. Gartling, P. K., Nickell, R. E., and Janner, R. I., 1977 *" A Finite Element Converge Study for Accelerating Flow Problems'* , Int. Jour. Num. Math. In Eng., Vol.11, PP.1155-1174.
11. Howard, H. C., 1985 *" Water and Sediment Routing Through Curved Channels" ,* J. Hydr. Eng., Vol.111, No.4, PP.644-657.

12. Ippen, A. T., 1966 " *Estuary and Coastline Hydrodynamics*" ,McGraw-Hill Book Company Inc., New York, N.Y.

13. Ikeda, S. and Nishmura, T. 1985 " *Bed Topography in Bends of Sand-Silt Rivers*", J. Hydr. Eng., ASCE, Vol.111, No.11, PP.1397-1411.

14. Jin, X., and Karnenburg, C., 1993 "*Quasi- 3D Numerical Modeling of Shallow Water Circulation*", J. Hydr. Eng., Vol.119, No.4, PP.458-471.

15. Khalaf, R. M., 1988 " *Modeling Sediment Transport Load in Tigris River within Baghdad City*", M.Sc. Thesis College of Engineering, University of Baghdad.

16. Khalaf, R. M., 1999 " *Two Dimensional Depth-Averaged Hydrodynamic, Transport-Dispersion and Morphological Models*", Ph. D., Thesis, College of Engineering, University of Baghdad.

17. Kashif AL-Ghitaa, B., 1959 "*Forecasting The Peak Levels For The Euphrates*", Irrigation Directorate General, Baghdad.

18. Kikkawa, H., Ikeda, S. And Kitagawa, A. 1976 "*Flow And Bed Topography In Curved Open Channels*", J. Hydr. Div., Asce, Vol. 102, No.9, Pp. 1317-1342.

19. Kreyszig, E., 1988 " *Advanced Engineering Mathematics* " 6th edition, John Wiley, New York.

20. Mohammed, A. Y., 1994 " *The Hypothetical Failure of Sammarra Embankment Dam*" Flood Wave Studies, Confidential Report Rafidain Company for Dams Construction, Ministry of Irrigation.

21. Mahmood, K., And Yevjevich, V., 1975 " *Unsteady Flow In Open Channels*" Water Resources Publications, Fort Collins, Colorado, USA.

22. Majeed, O., 1994 " *Development of Two Dimensional Hydrodynamic and Morphological Mathematical Model*", Ph. D. Thesis, College of Engineering, University of Baghdad.

23. Odgaard, A.J., 1989 " *River Meander Model Development* " , J. Hydr. Eng., Vol.115, No.11, pp. 1433-1449.

24. Odgaard, A.J., 1989 " *River Meander Model Applications*" J. Hydr. Eng., Vol.115, No.11, pp. 1451-1463.

25. Petersen, M. S., 1986 " *River Engineering*" Prentice Hall, Englewood Cliffs, New Jersey.

References

26. Rao, S. S., 1989 *"The Finite Element Method in Engineering"* Pergamon Press, Oxford.

27. Sharhan, F.A., 1986 *"The Finite Element Modeling of Unsteady Flow Around Obstructions",* M.Sc. Thesis, College of Eng., University of Baghdad.

28. Shimizu, Y., and Itakura, T., 1989 *" Calculation of Bed Variation in Alluvial Channels" ,* J. Hydr. Eng., Vol.115, No.3, pp.367-383.

29. Su, T. Y. And Wang, S. Y., 1980 "*Depth-Averaged Models Of River Flows*" Finite Element In Water Resources Vol.3, University of Mississippi Press., USA.

APPENDIX A

A.1 Finite Element Formulation for Continuity Equation :

The continuity equation for two-dimensional flow field can be written as:

$$\frac{\partial h}{\partial t}+\frac{\partial (uh)}{\partial x}+\frac{\partial (vh)}{\partial y}=0 \quad \ldots\ldots\ldots\ldots\ldots\ldots\ldots\ldots\ldots\ldots(A.1)$$

By using the weighted residual approach, the functional from for equation (A.1) is: -

$$\iint N\ [\frac{\partial h}{\partial t}+\frac{\partial (uh)}{\partial x}+\frac{\partial (vh)}{\partial y}]\ dx\ dy=0 \ldots\ldots\ldots\ldots\ldots(A.2)$$

The finite element solution is started by discretizing the field flow domain into a triangular elements with three node at each element. By using a suitable interpolation function that called a shape function as follows can approximate the field variable over each element: -

$$h=\sum_{i=1}^{n} Nihi \qquad U=\sum_{i=1}^{n} Niui \qquad V=\sum_{i=1}^{n} Nivi \quad \ldots\ldots\ldots\ldots(A.3)$$

Where: -

hi,ui,vi= the field variables at node:-

n= total number of element nodes.

Ni= a set of interpolation (or shape) functions written in terms of coordinates system associated with n discrete values within or on the boundary of an element (Khalaf, 1999).

By applying the standard Galerkin residual method the equation (A.2) can be written as: -

$$\iint NN^{t}\frac{\partial h}{\partial t}+\iint \overline{U}N\frac{\partial h}{\partial x}dxdy+\iint \overline{V}N\frac{\partial h}{\partial y}dxdy+\iint \overline{h}N\frac{\partial u}{\partial x}dxdy+\iint \overline{h}N\frac{\partial v}{\partial y}dxdy=0 \ \ldots.(A.4)$$

By using green's theorem the final equation will be,

$$\iint NN^t \frac{\partial h}{\partial t} + \left[-\bar{u}\iint \frac{\partial N}{\partial x} N^t dxdy - \bar{V}\iint \frac{\partial N}{\partial y} N^t dxdy \right] h$$

$$+ \left[-\bar{h}\iint \frac{\partial N}{\partial x} N^t dxdy \right] u + \left[-\bar{h}\iint \frac{\partial N}{\partial x} N^t dxdy \right] V$$

$$+ \left[\bar{u}\int NN^t dy + \bar{V}\int NN^t dx \right] h + \left[\bar{h}\int NN^t dy \right] u$$

$$+ \left[\bar{h}\int NN^t dx \right] V = 0 \quad \text{...(A.5)}$$

A.2 Finite Element Formulation For the Momentum Equations in (x, y) Directions

The momentum equations in (x, y) directions result from the application of Newton's second low, which can be written as: -

$$\frac{\partial U}{\partial t} + u\frac{\partial u}{\partial x} + V\frac{\partial u}{\partial y} + g\frac{\partial H}{\partial x} + Fu - E\left[\frac{\partial^2 u}{\partial x^2} + \frac{\partial^2 u}{\partial y^2} \right] = 0 \quad \text{....................(A.6)}$$

$$\frac{\partial V}{\partial t} + u\frac{\partial V}{\partial x} + V\frac{\partial V}{\partial y} + g\frac{\partial H}{\partial x} + FV - E\left[\frac{\partial^2 V}{\partial x^2} + \frac{\partial^2 V}{\partial y^2} \right] = 0 \quad \text{..................(A.7)}$$

The application of the Galerkin weighted residual approach to equation (A.6), (A.7) is made by simulating approach to equation (A.1), using the Galerkin weighted residual method principle and invoking of green's theorem leads finally to a matrix form of the equation (A.6) and (A.7) which can written as follows: -

$$\iint NN^t \frac{\partial u}{\partial t} + \left[-\bar{u}\iint \frac{\partial N}{\partial x} N^t dxdy - \bar{V}\iint \frac{\partial N}{\partial y} N^t dxdy + \bar{F}\iint NN^t dxdy \right.$$

$$\left. E\iint (\frac{\partial N}{\partial x})(\frac{\partial N^t}{\partial y}) + (\frac{\partial N}{\partial y}\frac{\partial N^t}{\partial y}) dxdy \right] u + \left[-g\iint \frac{\partial N}{\partial x} N^t dxdy \right] H + g\int NN^t dyH +$$

$$\left[\bar{u}\int NN^t dy + \bar{V}\int NN^t dx - E\int N^t \left[(\frac{\partial N}{\partial x})\ell_x + (\frac{\partial N}{\partial y})\ell_y \right] ds \right] u = 0 \quad \text{...(A.8)}$$

$$\iint \mathrm{NN^t}\frac{\partial \mathrm{V}}{\partial \mathrm{t}}+\left[-\bar{\mathrm{u}}\iint\frac{\partial \mathrm{N}}{\partial \mathrm{x}}\mathrm{N^t dxdy}-\bar{\mathrm{V}}\iint\frac{\partial \mathrm{N}}{\partial \mathrm{y}}\mathrm{N^t dxdy}+\bar{\mathrm{F}}\iint \mathrm{NN^t dxdy}\right. \quad +$$

$$\left. E\iint\left(\frac{\partial N}{\partial x}\cdot\frac{\partial N^t}{\partial x}\right)+\left(\frac{\partial N}{\partial y}\frac{\partial N^t}{\partial y}\right)dxdy\right]V+\left[\bar{u}\int NN^t dy+\bar{V}\int NN^t dx-E\int N^t\left[\left(\frac{\partial N}{\partial x}\right)\ell_x+\left(\frac{\partial N}{\partial y}\right)\ell_y\right]ds\right]v$$

$$= \iint g\frac{\partial N}{\partial x}N^t dxdyH-g\int NN^t dxH \quad \text{.....(A.9)}$$

A.3 Green Theorem

The Green theorem can be written for clockwise element numbering as (Kreyszig, 1988):

$$\iint_{\Omega} F\left(\nabla^2 g\right)dxdy=\oint_{\Gamma} F\frac{\partial g}{\partial n}ds-\iint_{\Omega}\left(\nabla F\right)\left(\nabla g\right)dxdy$$

and

$$\iint_{\Omega}\left(\nabla F\right)\left(\nabla g\right)dxdy=\oint_{\Gamma} g\frac{\partial F}{\partial n}ds-\iint_{\Omega} g\left(\nabla^2 F\right)dxdy$$

The theorm of integration by parts are:

$$\iint_{\Omega} F\frac{\partial g}{\partial x}dxdy=\oint_{\Gamma} Fgdy-\iint_{\Omega}\frac{\partial F}{\partial x}dxdy$$

and

$$\iint_{\Omega} F\frac{\partial g}{\partial y}dxdy=\oint_{\Gamma} Fgdx-\iint_{\Omega}\frac{\partial F}{\partial y}dxdy$$

APPENDIX C

C.1 Isoparametric Linear Triangular Element

The two types of coordinates system are shown in fig (C.1), Cartesian (Global) system and natural (Local) system. It is useful to employs a local system which is simple, unique and independent of the global system. Such system is known as an intrinsic system and its coordinates (ξ , η).

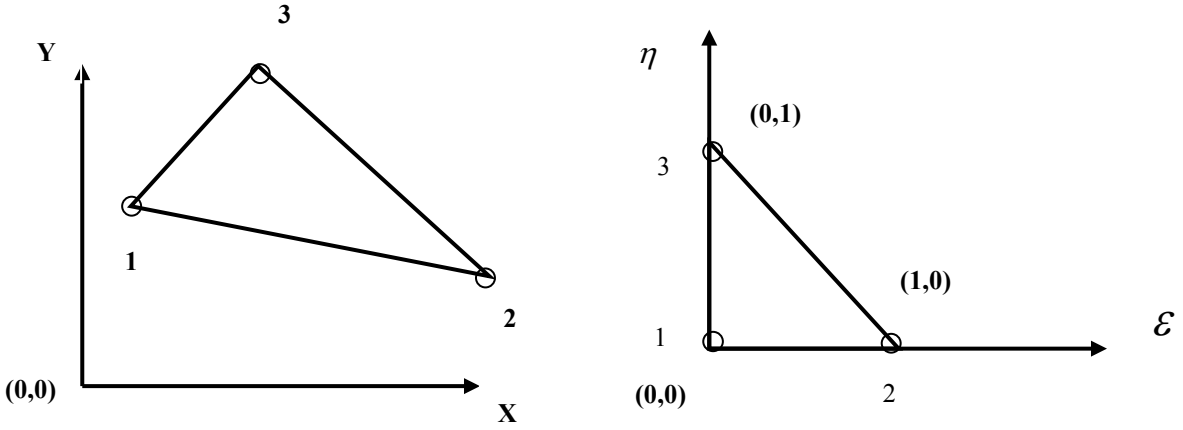

Cartesian (global) system

Natural (local) system

Fig (C.1) Types of coordinates system

The isoparametric concept allows any arbitrary geometry to be closely approximated, thereby minimizing any error associated with modeling the geometry and with out resorting to the use of a fine mesh along the boundaries. The interpolation of the element coordinates (x, y) and element displacement (u,v,h) using the same interpolation functions, which are defined in natural coordinates system (ξ , η), is the basis of the isoparametric finite element (Rao, 1989) .

Pair, (Chandrapulta 1997), represents the shape functions of isoparametric linear triangular element are represented by the pair ξ , η as follows: -

$N_1=\xi$, $N_2=\eta$, N3=1- ξ - η ……..…(C.1)

The derivatives of the shape function with respect to ξ and η which is needed in the element matrix can easily obtained from equation (C.1), and can be expressed in a matrix form as follows: -

$$\frac{\partial Ni}{\partial \xi} = [1 \quad 0 \quad -1]$$

$$\frac{\partial Ni}{\partial \eta} = [0 \quad 1 \quad -1] \text{ ..……..…(C.2)}$$

The matrix system has the derivatives of shape function with respect to the coordinates x and y, but the derivatives of shape function of the finite element must be for local coordinates ξ and η. In order to solve this difficulty it is necessary to obtain a relation ship between derivatives of the two sets of coordinates and this can be achieved through the normal chain rule of partial differentiation. For a two dimensional problem the derivatives are related by:

$$\frac{\partial Ni}{\partial \xi} = \frac{\partial N}{\partial x}.\frac{\partial x}{\partial \xi} + \frac{\partial N}{\partial y}.\frac{\partial y}{\partial \xi}$$

$$\frac{\partial N}{\partial \eta} = \frac{\partial N}{\partial x}.\frac{\partial x}{\partial \eta} + \frac{\partial N}{\partial y}.\frac{\partial y}{\partial \eta} \quad \text{……...(C.3)}$$

Which can be written matrix notation as (chandrupatla 1997): -

$$\begin{Bmatrix} \frac{\partial Ni}{\partial \xi} \\ \frac{\partial Ni}{\partial \eta} \end{Bmatrix} = \begin{bmatrix} \frac{\partial x}{\partial \xi} & \frac{\partial y}{\partial \xi} \\ \frac{\partial x}{\partial \eta} & \frac{\partial y}{\partial \eta} \end{bmatrix} \begin{bmatrix} \frac{\partial Ni}{\partial x} \\ \frac{\partial Ni}{\partial y} \end{bmatrix} = [J] \begin{Bmatrix} \frac{\partial Ni}{\partial x} \\ \frac{\partial Ni}{\partial y} \end{Bmatrix} \text{……..…..(C.4)}$$

Where [J] is the (2x2) square matrix, which is denoted as the Jacobain operator relating the natural coordinate derivatives to the local coordinate derivatives (Bathe 1996).

Now, to estimate the Jacobain matrix, must be represented the local coordinates x and y in terms of nodal coordinates by using the shape function of ξ and η, considering a general Two-dimensional element, the coordinate interpolation are (Chandraaputla, 1997): -

$X=N_1x_1+N_2X_2+N_3X_3$

$Y=N_1Y_1+N_2Y_2+N_3Y_3$ .....(C.5)

Then, for triangular element the Jacobain matrix can be calculated by differentiating equation (C.3) with respect to ξ and η coordinate and can be written as (Chandrupatla, 1997): -

$$[J]=\begin{bmatrix} x1-x3 & y1-y3 \\ x2-x3 & y1-y3 \end{bmatrix} \text{.....(C.6)}$$

From equation no. (C.4) the derivation of shape function with respect (x, y) can be obtained by: -

$$\begin{Bmatrix} \frac{\partial Ni}{\partial x} \\ \frac{\partial Ni}{\partial y} \end{Bmatrix} = [J]^{-1} \begin{bmatrix} \frac{\partial Ni}{\partial \varepsilon} \\ \frac{\partial Ni}{\partial \eta} \end{bmatrix} \text{.....(C.7)}$$

Where $[J]^{-1}$ is the inverse of Jacobain [j], given by: -

$$[J]^{-1} = \frac{1}{|\det j|} \begin{bmatrix} y2-y3 & y3-y1 \\ x3-x2 & x1-x3 \end{bmatrix} \text{.....(C.8)}$$

We should note that the system of matrices is function of the natural coordinates ξ, η. Therefor, The area integration extends over the natural coordinate area, and the area differential dA need also be written in terms of the natural coordinates, can be written as (Bathe, 1996): -

$dA= |\det j|\ .\ d\xi\ x\ \eta$ ..... (C.9)

In which dA= dx . dy

دراسة انتقال الرسوبيات في نهر الفرات مقدم سدة الرمادي

صادق عليوي سليمان الفهداوي
(بكالوريوس / هندسة مدنية)
كلية الهندسة / جامعة الانبار
إشراف الأستاذ المساعد الدكتور عبد الكريم حمزة غيلان

الخلاصة

استحوذ انتقال الرسوبيات الذي يحدث بسبب جريان الأنهار في القنوات الضحلة على اهتمام متزايد في الوقت الحاضر لان له تأثير مباشر على كثير من المشاكل الهندسية .

تم تطوير نموذجين للتنبؤ بتصرف الأنهار تحت ظروف جريان محددة . النموذج الأول هو النموذج الهيدروديناميكي وهو نموذج رياضي ثنائي البعد وموسط على العمق اعتمد في بنائه على معادلات حفظ الكتلة والزخم لحساب السرع والأعماق . أما النموذج الثاني فهو النموذج المورفولوجي الذي اعتمد في بنائه على معادلة حفظ الرسوبيات للتنبؤ بتغيرات منسوب قاع النهر بالاتجاهين .

استخدمت تقنية الحل بالعناصر المحددة وبطريقة البواقي الموزونة لغرض صياغة معادلات النموذجين . كما طبق اسلوب المعاودة بالحل (iteration) مع طريقة كاوس (Gauss) المطورة للحذف لحل المعادلات التفاضلية غير الخطية للنموذج الهيدروديناميكي ، في حين ان معادلات النموذج المورفولوجي هي معادلات خطية ليست بحاجة إلى أسلوب المعاودة بالحل تم تطبيق النموذج الهيدروديناميكي على قناة مثالية وتم تدقيق النتائج بالمقارنة مع الحل الرياضي الدقيق حيث أعطى النموذج الهيدروديناميكي توافق مقبول مع الحل الرياضي. أنجزت معايرة النموذج الهيدروديناميكي في منطقة الدراسة باستخدام المعلومات الحقلية .

تم ربط النموذجين معاً لغرض تطبيقهما على نهر الفرات في مدينة الرمادي وكانت النتائج مقبولة حيث إن تغير مناسيب قاع النهر يعكس الميل المتوقع للنهر في منطقة الانحناء من حيث حصول التآكل على الضفة الخارجية والترسيب على الضفة الداخلية .